NASA TECHNICAL MEMORANDUM

NASA TM X-2972

NASA TM X-2972

PRESSURE-ACTIVATED STABILITY BYPASS CONTROL VALVES TO INCREASE THE STABLE AIRFLOW RANGE OF A MACH 2.5 INLET WITH 40 PERCENT INTERNAL CONTRACTION

by Glenn A. Mitchell and Bobby W. Sanders

Lewis Research Center
Cleveland, Ohio 44135

NATIONAL AERONAUTICS AND SPACE ADMINISTRATION • WASHINGTON, D. C. MAY 1974

1. Report No.	2. Government Accession No.	3. Recipient's Catalog No.
NASA TM X-2972		

4. Title and Subtitle	5. Report Date
PRESSURE-ACTIVATED STABILITY-BYPASS-CONTROL VALVES TO INCREASE THE STABLE AIRFLOW RANGE OF A MACH 2.5 INLET WITH 40 PERCENT INTERNAL CONTRACTION	MAY 1974
	6. Performing Organization Code

7. Author(s)	8. Performing Organization Report No.
Glenn A. Mitchell and Bobby W. Sanders	E-7557
	10. Work Unit No. 501-24

9. Performing Organization Name and Address	11. Contract or Grant No.
Lewis Research Center National Aeronautics and Space Administration Cleveland, Ohio 44135	

12. Sponsoring Agency Name and Address	13. Type of Report and Period Covered
National Aeronautics and Space Administration Washington, D.C. 20546	Technical Memorandum
	14. Sponsoring Agency Code

15. Supplementary Notes

16. Abstract

The throat of a Mach 2.5 inlet with a coldpipe termination was fitted with a stability-bypass system. The inlet stable airflow range provided by various stability-bypass entrance configurations in alternate combination with several stability-bypass exit controls was determined for both steady-state conditions and internal transient pulses. Transient results were also obtained for the inlet with a choke point at the diffuser exit. Unstart angles of attack were determined for the various stability-bypass entrance configurations. The response of the inlet-coldpipe system to internal and external oscillating disturbances was determined. Poppet valves at the stability-bypass exit provided an inlet stable airflow range of 28 percent or greater at all static and transient conditions.

17. Key Words (Suggested by Author(s))		18. Distribution Statement
Air intakes	Throat bypass	Unclassified - unlimited
Supersonic-cruise inlets	Stability bypass	
Shock stability		
Inlet bleed		CAT. 01

19. Security Classif. (of this report)	20. Security Classif. (of this page)	21. No. of Pages	22. Price*
Unclassified	Unclassified	98	$4.00

* For sale by the National Technical Information Service, Springfield, Virginia 22151

CONTENTS

PRESSURE-ACTIVATED STABILITY-BYPASS-CONTROL VALVES TO INCREASE THE STABLE AIRFLOW RANGE OF A MACH 2.5 INLET WITH 40 PERCENT INTERNAL CONTRACTION

by Glenn A. Mitchell and Bobby W. Sanders

Lewis Research Center

SUMMARY

The throat of a Mach 2.5 mixed-compression inlet with 40 percent internal contraction was fitted with a stability-bypass system that was designed to provide the inlet with a large stable airflow operating range. Airflow entered the stability-bypass system through either a distributed porous surface, distributed "educated" slots, or a forward-slanted slot. Bypass airflow was controlled at the bypass exit by either poppet valves, vortex valves, or fixed exits. Combinations of these stability-bypass entrance configurations and exit controls were evaluated, by using the inlet with a long coldpipe, to determine the inlet stable airflow range resulting from steady-state conditions and internal transients. Transient data are presented in terms of the reciprocal of the pulse period. These pseudofrequencies varied from 1 to 40 pseudohertz. Each internal transient was generated by a single sine wave pulse of the overboard-bypass doors. Transient stable airflow ranges were also determined for the inlet with a choke point at the compressor face; and for the inlet with various stability-bypass plenum volumes, bypass exit areas, and inlet pressure recoveries. Unstart angles of attack were determined for the various configuration combinations. The dynamic response of the inlet-coldpipe combination was obtained for both internal and external sinusodially oscillating disturbances. The test was conducted in the Lewis 10- by 10-Foot Supersonic Wind Tunnel at a Mach number of 2.5.

Stability-bypass systems provided the inlet with a large stable airflow range from an inlet operating point having nominal throat airflow removal for boundary-layer control and a total-pressure recovery of 0.90. During steady-state operation the use of the poppet valves allowed inlet airflow to be reduced as much as 28 percent without causing unstart. Vortex valves allowed an 11 percent reduction in airflow, and a small comparable stability-bypass exit area allowed only a 5 percent reduction. The poppet valves were the only stability-bypass exit control that provided the inlet with a large stable air-

flow range at all the internal transient pulse pseudofrequencies from 1 to 40 pseudohertz. Airflow stability ranges were above 33 percent for the porous stability-bypass entrance configurations with the poppet valves and an inlet-coldpipe system. Terminating the inlet with a choke plate rather than a coldpipe reduced the transient stable operating range at the higher transient pseudofrequencies. Despite these reductions, a porous stability-bypass entrance configuration with poppet valves obtained a transient stable airflow range above 30 percent over the 1- to 40-pseudohertz range.

INTRODUCTION

At flight speeds above Mach 2.0 an inlet having a mixture of internal and external compression offers optimum performance by supplying the engine with airflow at a high pressure level while maintaining minimum drag. Optimum internal performance for this type of inlet is provided by maintaining the terminal shock at the inlet throat. This operation provides the highest pressure recovery and minimizes distortion at the engine entrance. However, mixed-compression inlets suffer from an undesirable airflow characteristic known as unstart, which may occur when the terminal shock is placed too near the inlet throat. A slight airflow transient can cause the terminal shock to move forward of the throat, where it is unstable and is abruptly expelled ahead of the inlet cowling. This shock expulsion, or unstart, causes a large rapid reduction in mass flow and pressure recovery and a large drag increase. Inlet buzz, compressor stall, and/or combustor blowout may also occur. Obviously, an inlet unstart is extremely undesirable because of the effects not only on the propulsion system itself, but also on the aerodynamic qualities of the aircraft. If an inlet unstart does occur, complex mechanical variations of the inlet geometry are required to reestablish initial design operating conditions.

Both external airflow transients (such as atmospheric turbulence) and internal airflow changes (such as a reduction in engine airflow demand) can cause the inlet to unstart. For an internal airflow change the inlet should provide a margin in corrected airflow below the value for optimum performance without incurring unstart. This margin is defined as the stable airflow operating range. Conventional mixed-compression inlets can be designed to have a limited stable range that is provided by the capacity of the performance bleed system to bleed increased airflow as the terminal shock moves upstream into the throat bleed region. With performance bleed exit areas that are fixed, this stable range may not be adequate to absorb many of the airflow transients that are encountered by a typical supersonic propulsion system. An increased stable airflow range is currently provided for these inlets by operating them supercritically, with a resultant loss in performance. Since any loss in inlet performance is reflected directly as a loss in thrust and efficiency of the propulsion system, supercritical operation

should be avoided.

To provide the necessary system stability without compromising steady-state performance (i.e., pressure recovery and distortion), the inlet can be redesigned by replacing the throat bleed system with a stability-bypass system capable of removing large amounts of airflow. This system prevents unstarts by removing airflow from the inlet throat to compensate for reductions in the diffuser exit airflow demand. Reference 1 has indicated that large increases in bypass airflow may be provided without prohibitive amounts of airflow removal during normal operation if the bypass exit area can be controlled to maintain a relatively constant pressure in the bypass plenum. (Reference 1 calls the throat airflow removal system a bleed system rather than a bypass system.) This bypass-exit-area variation might be provided either by an active control that senses the shock position with pressure taps and regulates the bypass exit area, or by pressure-activated valves at the bypass exit which increase bypass flow in response to a small pressure rise in the bypass plenum induced by forward shock movement.

An experimental test program was conducted in the Lewis 10- by 10-Foot Supersonic Wind Tunnel to evaluate the effectiveness of several different types of stability-bypass systems. The investigation was conducted with a Mach 2.5 mixed-compression inlet having 40 percent of the design supersonic area contraction occurring internally. Bypass airflow was removed on the cowl side of the inlet throat through several alternate stability-bypass entrance configurations. These configurations used either a distributed porous surface, distributed educated slots, or a forward-slanted slot on the cowl side of the inlet throat. The open bypass areas were designed to remove approximately 20 to 30 percent of the inlet capture mass flow during minimum stable operation if a nearly constant bypass plenum pressure was maintained. The airflow through the stability bypass was alternately controlled by various stability-bypass exit controls such as poppet valves, vortex valves, and remotely actuated variable-area choked-plug assemblies. The latter was used to simulate various fixed bypass exit areas.

Some selected results from this test are reported in reference 2 and 3 and show that stability-bypass exit controls can operate automatically to provide large stable margins for the inlet. Additional results from this test are reported in reference 4, wherein choked plug assemblies were used as bypass exit controls and were manually positioned to establish the performance of many stability-bypass entrance configurations. Some of the better bypass entrance configurations of each type were selected from reference 4 for use with more sophisticated bypass exit controls, that is, pressure-activated valves. Inlet stability limits for these combinations are reported herein for steady-state conditions and for transient internal airflow disturbances. These transient stability limits were determined for an inlet-coldpipe combination. The transients simulated distrubance pseudofrequences to 40 pseudohertz and were produced by a single pulse of the diffuser exit, overboard bypass doors. Transient stability limits for the

inlet with a choke point at the compressor face were determined for a single stability-bypass entrance configuration. Transient stability limits were also determined for various stability-bypass plenum volumes, stability-bypass fixed exit areas, and inlet pressure recoveries. Inlet unstart angle of attack was determined for combinations of stability-bypass entrance configurations and stability-bypass exit controls.

In order to obtain a comprehensive picture of the dynamic response of the inlet used in this test, it would be necessary to obtain inlet dynamics with the inlet coupled to an operating turbojet engine, as well as coupled to a coldpipe with internal volume variations. Such a comprehensive dynamics test is reported in reference 5 for a mixed-compression inlet almost identical in size to the inlet of this test. During the current test a limited amount of dynamic response data was obtained with a single configuration, a large-volume inlet-coldpipe combination. This configuration was subjected both to a symmetrical internal disturbance (by oscillating the inlet's overboard bypass exit area at frequencies to 140 Hz) and to an external disturbance at frequencies to 15 hertz. Some comparisons are made with the data of reference 5. All data were obtained at a free-stream Mach number of 2.5 and a Reynolds number, based on the inlet-cowl-lip diameter, of 3.88×10^6.

U. S. customary units were used in the design of the test model and for the recording and computing of experimental data. These units were converted to the International System of Units for presentation in this report.

APPARATUS AND PROCEDURE

Inlet Model

The inlet used in this investigation was a Mach 2.5 axisymmetric, mixed-compression type with 40 percent of the design supersonic area contraction occurring internally. The inlet capture area of 0.1757 square meter sized the inlet to match the airflow requirement of the J85-GE-13 engine at Mach 2.5 and a free-stream temperature of 390 K. The inlet was attached to a cylindrical nacelle 0.635 meter in diameter in which the J85-GE-13 engine or a coldpipe with a choked-plug assembly could be installed. For this study, only the coldpipe was used. Figure 1 shows the test model installed in the wind tunnel test section.

Some of the basic inlet design details are presented in figure 2. Local theoretical airflow conditions on the cowl and centerbody, inlet contours, and diffuser area variation are shown for the inlet design Mach number and spike position. The inlet featured a bicone centerbody which utilized half-angle cones of 10° and 18.5° to provide the external compression (fig. 3). In concept, the two-cone design would require that the contraction ratio be varied by collapsing the second cone. But to simplify the mechanical

design of the test inlet, the contraction ratio was varied by translating the centerbody rather than by collapsing the second cone. The internal oblique shock generated by the cowl lip was theoretically cancelled at the centerbody impingement point by a turn of the surface. The remaining compression of the flow to a throat Mach number of 1.3 was isentropic and was distributed over a distance of 0.4 of the inlet capture radius, or 0.0946 meter.

The subsonic diffuser consisted of an initial throat region 4 hydraulic radii in length with a 1° equivalent conical expansion, followed by the main subsonic diffuser. The diffuser just downstream of the throat was mated to an existing subsonic diffuser (ref. 6). Control of the diffuser-centerbody boundary layer was provided by vortex generators installed at inlet station 3 (fig. 3). Details of the vortex generator design are shown in figure 4. The overall inlet length at design, cone tip to compressor face, was 7.88 cowl-lip radii. Internal surface coordinates of the inlet in terms of the cowl-lip radius are presented in table I. A more complete disucssion of the inlet design characteristics is presented in reference 7.

In addition to the normally rather long coldpipe at the end of the diffuser, a choke plate could be placed at the diffuser exit (fig. 3). The plate was used during the transient and dynamics portion of the test to more closely simulate the volume of an inlet-engine combination. The plate reduced the inlet-coldpipe volume from 0.42 cubic meter to 0.16 cubic meter (table II).

Bleed regions were located in the throat region of the inlet on the cowl and centerbody surfaces. When used, the bleed flow from the forward-cowl location was dumped directly overboard, as shown in figure 5. Stability-bypass flow (used to give the inlet a large stable range) was removed through the stability-bypass entrance located on the cowl side of the throat region. Figures 3 and 5 illustrate the ducting of the bypass flow through the cowling to the location of the pressure-activated valves and on to the pipes housing the choked-plug assemblies. Centerbody bleed flow was ducted through hollow support struts to the centerbody bleed pipes (fig. 3). Both the cowl stability-bypass flow and the centerbody bleed flow utilized two coldpipe choked-plug assemblies. The remotely actuated plugs that were used to vary these bypass and bleed flows, as well as the main-duct flow, are shown in figure 1(b).

When the choked-plug assemblies were controlling the stability-bypass flow by forming a choked exit at the rear end of the pipes, one type of pressure-activated valve (the poppet valve) was in the bypass flow circuit. The valves were in place in the chamber shown in figure 5 but were set in the open position so as not to interfere with the rear choke point. When the pressure-activated valves (either poppet or vortex valves) were used to control the bypass flow, the choke point moved forward so that the effective exit was at the valve location and the bypass choked-plug assemblies were set wide open to prevent choking at the end of the pipes. Valve control of the bypass flow resulted in a small effective bypass plenum volume of about 0.01 to 0.02 cubic meter,

which was almost equal to the main-duct volume of 0.42 cubic meter (table II).

The aft portion of the subsonic diffuser incorporated two remotely controlled bypass systems: a high-response overboard system, and a low-speed ejector bypass for engine and nozzle cooling airflow. For steady-state data taking, both bypasses were closed. The high-response system contained six equally spaced doors. These were operated in unison to obtain data on the effect of symmetrical internal transient and sinusoidal disturbances to the inlet airflow. The cascades placed at the entrance of the bypass cavity (fig. 3) were found to minimize a resonant condition in the bypass cavity. A discussion of the resonance that resulted from the open cavity is presented in reference 8.

The photographs and sketches of the test model that have been presented thus far have revealed a bulky external profile. The bulky cowl was used to facilitate the major changes made to the cowl stability bypass and associated ducting during the test, and hence was not representative of flight-type hardware. The sketch in figure 6 shows how a stability-bypass system can be packaged within the low-external-cowl-drag profile essential for supersonic flight.

Stability-Bypass Entrance and Bleed Region Configurations

The various bypass entrance configurations tested are shown in figure 7. For two of these configurations the stability-bypass entrance was a porous surface created by distributed holes (fig. 7(a)). A forward-slanted slot (fig. 7(b) and distributed "educated" slots (fig. 7(c)) were also used for stability-bypass entrances ("education" is defined later in this section). These four configurations represent the better bypass entrance configurations of each type developed in reference 4. The distributed porous configuration I, the forward-slanted slot, and the distributed educated stability-bypass entrance configurations were designed to provide a bypass mass-flow ratio of about 0.20 at the inlet minimum stable condition. Increasing the distributed porous bypass entrance area from that provided by configuration I to that provided by configuration II increased the bypass flow capacity to a mass-flow ratio of about 0.30. The bypass entrance for the distributed porous configuration II extended over the same axial cowl region as the distributed educated bypass entrance area. The airflow capacities of the two configurations varied because the nominal porosities varied, the porosity being 40 percent for the porous-hole configuration and 25 percent for the educated-slot configuration.

The centerbody bleed region variations are shown in figure 7(a). These represent the centerbody bleed configurations used in reference 4 that allowed the terminal shock to remain stable when ahead of the inlet throat. They do not represent an optimum centerbody bleed configuration in terms of inlet performance, that is, pressure recovery. The centerbody bleed hole pattern used with distributed porous configuration I was

also used with the forward-slanted-slot and distributed educated stability-bypass entrance configurations.

The hole regions of porosity, on both the centerbody and cowl, were composed by staggering the holes in adjacent circumferential rows to achieve a more uniform open-area distribution. The hole pattern is shown photographically in figure 8(a). Holes were 0.318 centimeter in diameter and were drilled normal to the local inlet surface. The nominal porosity of 40 percent was achieved by locating the holes on 0.476-centimeter centers. The nominal thickness of the metal surfaces in the bleed regions was equal to the bleed hole diameter.

As illustrated in figure 7(a), the porous pattern and the amount of open bleed or bypass area were varied by filling selected holes. A schematic representation of the forward-centerbody bleed region with part of the holes filled is shown. Filling the forward eight rows of holes of the stability-bypass entrance created the distributed porous configuration I, with eight open rows aft of the inlet throat and seven open rows forward.

The forward-slanted-slot configuration is presented in figure 7(b). The slot was flush with the local inlet surface and was slanted away from the surface at a 20° angle. The upstream corner was sharp and the downstream lip, prior to rounding, was located at the inlet geometric throat. Slot height was 1.36 centimeters. Porous forward-cowl bleed was provided for the forward-slanted-slot configuration by having alternate holes in three bleed rows open. In concept, a slanted slot offers a bypass configuration superior to the porous surface because it provides a higher plenum pressure recovery.

The distributed educated configuration, figure 7(c), was an approximation of the ideal rearward-slanted-hole concept. In this concept the rear slant, or "education," theoretically limits the amount of airflow through holes when the flow is supersonic over an area perforated with holes. When the flow over such a perforated area is subsonic, the airflow through the holes is relatively unaffected by the slant, and a flow coefficient is achieved that is nearly that of holes drilled normal to the surface. Because of the practical difficulty of drilling slanted holes in the cowl surface, a number of circumferential slots rather than many holes were used to form the distributed educated configuration. These slots are shown photographically in figure 8(b). To "educate" these slots, the downstream edge was relieved to obtain a 10° angle with the local surface. The slot width was 0.318 centimeter with 1.27 centimeters between adjacent slots.

Pressure-Activated Valves

Control of the stability-bypass airflow was provided by 16 pressure-activated valves that were located circumferentially within the inlet cowl. The valves were placed at the exit of the small stability-bypass plenum (fig. 5). Two types of valves were investigated:

a poppet valve and a vortex valve. The poppet valves installed in the inlet cowl are shown in figure 9(a), and details of valve mechanical design in figure 9(b). The valve was essentially a floating piston with a trapped volume having a preset internal pressure on one side of the piston. The piston was activated by differential pressure. The internal pressure, inside the valve, was controlled during the test by connection to an external supply. (In a flight situation a suitable internal pressure could be found by a probe on the inlet or airplane and a pressure regulator could be used if necessary.) The internal pressure was set to just close the valve during normal inlet operation, that is, with the inlet operating at a high pressure recovery near critical with the terminal shock at the aft edge of the stability-bypass entrance. Under these conditions, a perturbation of the inlet terminal shock forward over the stability-bypass entrance would increase the pressure in the bypass plenum above the internal pressure and cause the valve to open and allow bypass flow to occur.

The poppet valve was simply designed with the single intent of demonstrating the feasibility of the concept of constant-pressure control in a stability-bypass plenum. The design allowed the valve to open fully with an increase in pressure on the valve face (stability-bypass total pressure P_{sb}) of only 20 percent. The actual valve performance, as determined on a static test stand, is shown in figure 9(c) in nondimensional form. A reference pressure $P_{sb,ref}$ was chosen as the pressure that occurred when the flow choked at the valve attachment bulkhead opening. The reference mass flow $m_{pv,ref}$ was the theoretical flow through the bulkhead opening at this reference pressure (flow coefficient of 1.0). The valve characteristic was indeed quite sensitive to pressure until the flow choked at the valve attachment opening. This choke point was reached with a 25 percent increase in initial operating pressure.

In a flight situation it is probable that many of the perturbations of the inlet shock into the throat region would be quite rapid. It therefore was necessary for the poppet valve to be fast acting in order to absorb such transients. The movable valve head assembly was therefore designed to minimize its weight (fig. 9(b)). For the designed valve head weight of 0.20 kilogram, it was calculated that the valve natural frequency was about 12 hertz at the pressure levels encountered during the test.

The vortex valves are shown in figure 10(a), and details of valve design appear in figure 10(b). This valve was developed during the study reported in reference 9. It required a small amount of flow for control purposes, amounting to less than 1 percent of inlet capture mass flow. (During the test, this flow was supplied by an external source; but in a flight situation, the flow might be supplied by suitably located inlet performance bleed.) The externally supplied flow was called the tangential control airflow and was directed into the valve central chamber tangentially to create a swirling or vortex flow (fig. 10(b)). Flow exited from the central chamber through the center hole located in each exit wall. The two radial entries into the central chamber of the valve were the ports for the stability-bypass flow. During inlet critical or supercritical

operation, the pressure gradient of the vortex flow insulated the relatively high bypass plenum pressure (inlet throat pressure) from the low valve exit pressure and prevented flow through the radial passageways. When an internal transient perturbed the terminal shock forward into the inlet throat and over the stability-bypass entrance, the resulting throat pressure rise was communicated to the radial valve ports through the bypass plenum. A breakdown of the vortex resulted, allowing bypass flow to exit through the center holes in the valve chamber.

The condition of no stability-bypass airflow (no radial flow) was referred to in reference 9 as "cutoff." This condition is represented by the leftmost point of the valve performance curve from reference 9, reproduced in figure 10(c). Note that a proper pressure ratio was required to produce the cutoff condition. This was supplied during the test by regulation of the external tangential flow source. The mass flow shown at cutoff was wholly from the tangential control flow. The reference mass flow used in figure 10(c) represented the maximum theoretical flow (flow coefficient of 1.0) possible through the valve exit holes at the tangential control pressure level. Also shown in figure 10(c) is the expected stability-bypass total-pressure range. The maximum amount of bypass flow is thus limited by the pressure rise across the terminal shock.

The important valve mass-flow parameter may be thought to be the gain in mass flow from cutoff to maximum flow. In fact, by proper tailoring of the tangential flow entry size, the valve characteristic curve and the inlet operating limits as shown in figure 10(c) may be varied from that shown and matched so that the minimum inlet pressure level produced at supercritical conditions would exactly match cutoff. Based on the physical size of the present valve, this would yield a minimum valve flow of 0.005 of the inlet capture mass flow and a maximum of 0.035. The valve gain ratio is then 7, and by enlarging the valves it would seem possible to obtain a stability-bypass flow of 14 percent by using a 2 percent tangential flow as performance bleed. Unfortunately, this ideal cannot be achieved because of the small size of the valve exit holes in relation to the size of the valve chamber. The diameter ratio of 4 is a design parameter affecting valve performance. Thus, the valves cannot be physically enlarged to handle large bypass flows and still be installed within the confines of a typical inlet cowl.

Instrumentation

Static-pressure distributions along the top centerline of the inlet cowl and centerbody were measured by the axially located static-pressure instrumentation presented in tables III and IV. The main-duct total-pressure instrumentation as illustrated in figure 11 was used to determine the local flow profiles in the subsonic diffuser. The axial location of these total-pressure rakes is shown in figure 3. Overall inlet total-pressure recovery and distortion were determined from the six 10-tube total-pressure

rakes that were located at the diffuser exit, inlet station 5. Each rake consisted of six equal-area-weighted tubes, with additional tubes added at each side of the extreme equal-area-weighted tubes in positions corresponding to an 18-tube area-weighted rake. The main-duct airflow, as well as the cowl stability-bypass and centerbody bleed airflow, was determined by measurements from the coldpipe choked-exit-plug assemblies shown in figure 1(b). When the stability bypass was controlled by pressure-activated valves (with the cowl plugs fully open), the stability-bypass mass flow was determined by the subtraction method.

Bleed flow through the forward-cowl bleed was determined from measured total and static pressures (fig. 12) and the bleed exit area. Stability-bypass total pressure was obtained from two total-pressure rakes that were located in the bypass plenum just forward of the valve attachment bulkhead (fig. 12). Pressures from these rakes were averaged to obtain the stability-bypass recovery. Centerbody bleed and overboard-bypass total pressures were each measured by a single probe, as indicated in figure 12. The overboard-bypass total pressure was calibrated to obtain overboard-bypass mass-flow ratio.

Forward-slanted-slot pressure instrumentation is presented in figure 13. Total-pressure rakes were located just forward and aft of the upstream corner of the slot and in the slot passage. They were circumferentially indexed to avoid flow interference. Static pressures were also measured axially along the slot and are shown in figure 13.

Dynamic pressures throughout the inlet and stability-bypass ducts were measured by subminiature strain-gage transducers. Static pressures were measured by mounting the transducers flush with the local surface. Total-pressure probes were fashioned with a short coupling to the transducer such that the frequency response was flat to at least 1000 hertz. The static-pressure taps placed throughout the inlet throat are shown in figure 14(a). Four of these (D3 to D6) were available only on the distributed porous stability-bypass entrance configurations. Another main-duct static (D1) was located in the subsonic diffuser ahead of the overboard-bypass plenum (fig. 12). The location of the total-pressure dynamic probe (D8) at the valve face station in the stability-bypass plenum is shown in figure 14(a). In addition to this bypass plenum pressure, the forward-slanted-slot configuration also contained a static-pressure tap (D7) on the slot upper surface (fig. 14(b)). The response of the poppet valves was determined by instrumenting one of the 16 valves with an internal dynamic pressure transducer (fig. 14(a)) and two other valves with position potentiometers. A dynamic pressure tap (D10) was also located in the valve chamber (fig. 14(a)).

Test Procedure

An inlet operating point was selected. From this point, it was desired to determine the effect of the various stability-bypass exit controls on the maximum main-duct airflow reduction possible without causing unstart. The operating point was selected at an inlet recovery of 0.90, with 0.027-mass-flow-ratio centerbody bleed, and 0.02 mass-flow ratio through the stability-bypass system. The overboard bypass was closed for taking steady-state data but still passed 0.01 mass-flow ratio because of leakage. The centerbody bleed flow was set by the choked plugs. The stability-bypass choked plugs were fully open, and either the poppet valves were in place and closed or the vortex valves were in place and set at cutoff by varying the external supply pressure. With either valve the initial 0.02 mass-flow ratio through the stability-bypass system was provided by 64 holes that bypassed the valve control. Placement of these 1.032-centimeter holes for various configurations is shown in figure 15. Once these items were set, the steady-state stability limits were determined by simply closing the main-duct plug from the operating point until unstart occurred. In addition to the stability limits obtainable with the poppet and vortex valves, limits were also determined for a simple fixed exit on the small stability-bypass plenum. This exit was obtained by locking the poppet valves closed.

Stability limits were also obtained for transient internal airflow disturbances. The same initial operating point was set as previously described, except that about 60 percent of the main-duct flow was directed through the overboard bypass. The main duct was controlled by the plug or in some cases by the choke plate (fig. 3). The internal transients were generated by pulsing the overboard-bypass doors toward the closed position. A transient consisted of a single sine wave pulse, as shown in figure 16. Each transient command given to the bypass doors is described by the following equations:

$$b = \frac{-B}{2}\left[1 - \cos\frac{2\pi(\text{Time})}{\tau}\right] \quad \text{for } 0 \leq \text{Time} \leq \tau$$

$$b = 0 \quad \text{for Time} > \tau$$

where B is the amplitude of the commanded door transient, b is the instantaneous amplitude, and τ is the pulse width that was selected. The negative sign simply indicates that the doors were moved toward the closed position. The transient is then described by an equation of harmonic motion where the time span is limited to one period and the frequency is replaced by $1/\tau$. Because the pulse exists for only one period, $1/\tau$ is only a pseudofrequency. However, because people relate more easily to frequency, the results of the transient data are presented in terms of $1/\tau$, or psuedofrequency.

For each transient pulse width the pulse amplitude was increased until inlet unstart occurred. The amount of bypass-door travel that the inlet would tolerate without unstart was converted to a stability index by means of a bypass-door - mass-flow ratio calibration at 90 percent diffuser recovery. The width of the door pulse was varied to obtain the inlet unstart tolerance over a pseudofrequency range from 1 to 40 pseudohertz. At the higher pseudofrequencies the bypass doors were not capable of producing a pure sine wave at the large amplitudes required at the unstart limit. An example of the door response at 40 pseudohertz is shown in figure 16. The data obtained during the transient pulse tests (door commands, door responses, valve movements, and dynamic pressures) were recorded on analog tape for later analysis.

Transient stability data were obtained with the stability-bypass flow controlled by either the poppet valves, the vortex valves, or one of two variations of a fixed exit area. One variation was obtained as in the steady-state tests by locking the poppet valves closed. This created the small bypass plenum illustrated in figure 17(a). Plenum volume was 0.01 to 0.02 cubic meter, depending on the bypass configuration used. (See fig. 15(b) for an example of plenum size variation.) The other fixed-exit variation (fig. 17(b)) was obtained by locking the poppet valves open to create a large bypass-plenum volume of approximately 0.4 cubic meter from the throat bypass entrance region back to the bleed pipe plugs. A bypass mass-flow ratio of 0.02 was obtained by adjusting the choked-exit plugs. Whereas the small plenum volume was insignificant in relation to the inlet volume, the large plenum was almost equal to the inlet-coldpipe volume (table II).

The dynamic response of the shock position and several inlet pressures to internal and external sinusoidal disturbances was determined only for the inlet with the long coldpipe assembly. The internal disturbances were symmetrically created by in-phase sine wave oscillations of the six overboard-bypass doors. During the internal disturbance testing, the inlet was provided with normal performance bleed by using the fixed-exit, small-plenum configuration on the stability-bypass system. Shock position dynamics were obtained by using the inlet unstart method of reference 10. The terminal shock was set near the inlet throat for this procedure. Then the bypass doors were oscillated at a set frequency while the main plug was closed until unstart occurred. By using this mode of operation, the frequency range from 1 to 140 hertz was investigated. Shock position amplitude was assumed to be proportional to plug position. With this assumption, an equivalent normalized terminal shock oscillation amplitude ratio was obtained from the unstart plug position at each bypass-door frequency. Responses of the inlet pressures to the internal disturbances were obtained during the unstart method tests.

The response of the inlet to external disturbances was determined for various stability-bypass exit controls: the poppet valves, the fixed exit with small plenum, and the fixed exit with large plenum. The external disturbance was generated by a large trapezoidal gust plate mounted in the tunnel just upstream of the inlet, as shown in

figure 18. The gust plate presented a uniform two-dimensional flow to the inlet. Oscillations of the gust plate changed the local Mach number and angle of attack. With the inlet conditions set at the preselected operating point, the gust plate was sinusodially oscillated $\pm 1/2^{\circ}$ from 0° to -1° at frequencies to 15 hertz. All data obtained during the frequency response portion of the test were recorded on analog tape. Frequency responses of inlet pressures were obtained from a commercially available analog transfer function analyzer.

RESULTS AND DISCUSSION

Inlet Stability Data

The basic types of plots that are used in this report to present the steady-state inlet stability data are explained in this section by using figure 19. Various performance conditions have been labeled in the figure to aid in the discussion.

The stability-bypass performance is shown in figure 19(a), where the bypass total-pressure recovery is presented as a function of the bypass mass-flow ratio. The series of straight solid lines (AB, CD, etc.) represent the bypass performance obtainable with several different fixed exit areas. Corresponding inlet performance is presented in figure 19(b) by a series of standard diffuser total-pressure-recovery - mass-flow-ratio "canes." Each solid-line cane represents the performance obtainable with a fixed exit area and corresponds to the solid straight line of identical labeling in figure 19(a). Each of these solid-line curves is generated by reducing the inlet diffuser exit airflow from a supercritical value and causing the inlet terminal shock to move upstream until unstart occurs. By utilizing this mode of operation, locii (dashed curves) of supercritical bypass airflows (ACEG) and minimum stable bypass airflows (BDFH) are obtainable. The minimum bypass airflows correspond to supercritical operation, and the maximum bypass airflows are obtained at minimum stable conditions. The bypass and inlet performance maps obtained in the manner just described were initially generated in reference 4 for the inlet reported herein.

An airflow index, originally defined in reference 4, is presented in figure 19(c) for the inlet conditions of figures 19(a) and (b). Values of airflow index (AI) represent the percentage change in corrected airflow between any inlet operating condition and the minimum recorded corrected airflow at point H. Figure 19(c) thus illustrates the amount of stable margin available if the bypass exit area can be varied to guide the inlet operation from a preselected condition to an unstart at point H. If a fixed exit area were utilized to obtain the large stability-bypass airflow available at point H (fig. 19(a)), a prohibitively large amount of bypass airflow at supercritical conditions would be incurred, point G. If the fixed exit area is reduced to obtain an acceptably low level of

supercritical bypass airflow (point C), the amount of bypass airflow and consequently the stable margin at the minimum stable condition (point D) is also reduced. From the acceptable inlet operating condition of point C (i.e., a high-recovery level and small amount of bypass flow), it is apparent that a large stable margin can be had only if the bypass-exit area opens as the inlet proceeds from critical to minimum stable conditions. This type of bypass-exit-area control is provided by poppet valves at the bypass exit. Typical performance for two types of valves, the vortex valve and the poppet valve, is shown in figure 19. The vortex valves increase the stable margin by allowing the inlet to operate along line CV rather than line CD. A very large stable margin is provided by the poppet valves allowing the inlet to operate along line CM. This performance is very nearly that which would be provided by an ideal valve having a constant bypass pressure recovery characteristic.

Steady-State Inlet Stability Limits

The steady-state inlet stability data are presented in figures 20 to 33. A comparison of the inlet stability limits obtained with the four stability-bypass entrance configurations using various bypass exit controls is presented in figure 20. The data from which these stability limits were obtained are presented in figures 21 to 24. Of these figures, parts (a), (b), and (c) present for each bypass entrance configuration the basic data plots as described in figure 19. Parts (d), (e), and (f) of these figures contain the variation of inlet recovery with stability-bypass airflow, centerbody and forward-cowl bleed performance (where applicable), and compressor face distortion. These figures show the performance obtained with each tested stability-bypass exit control operating from supercritical to minimum stable. The performance envelope of each bypass entrance configuration as determined in reference 4 is also shown. In some cases, figures 21(a) and (b) for example, the minimum stable data obtained during the test were beyond the previously determined performance envelope. A slight bypass passage hardware difference between the two tests could account for some of the difference in the measured bypass total pressure. Also the fairing of the reference 4 data could account for some difference. However the dissimilar results appear to be real. There is a small but unaccountable difference in the minimum stable line.

The data figures (25 to 33) that follow the basic performance plots of figures 21 to 24 present for each bypass entrance configuration the pressure distributions and rake data obtained for each tested bypass exit control as it operated from supercritical inlet conditions to minimum stable. Cowl and centerbody pressure distributions through the inlet and total pressures at the throat exit, mid diffuser, and diffuser exit stations are presented in figures 25 to 33. In the case of the forward-slanted-slot configuration, figures 30 and 31 also present pressure distributions through the slot and total-pressure

profiles in the slot.

The inlet stability limits shown in figure 20 are presented in terms of stability index. Stability index (SI) is defined as the percentage change in corrected airflow from the preselected inlet operating point to the minium stable point. The preselected operating points recorded for each bypass entrance configuration and bypass exit control (approx. 0.9 inlet total-pressure recovery and approx. 0.02 stability-bypass mass-flow ratio) are shown by the tailed symbols in figures 21 to 24. By referring to the appendix, it can be seen that the definition of stability index (SI) is identical to that previously given for airflow index (AI). The difference between the two is as follows: the airflow index (AI) expresses the percentage change in corrected airflow from an operating point to an absolute minimum stable point (point H in fig. 19), and the stability index (SI) represents the percentage change in corrected airflow from an operating point to another minimum stable point reached by an actual bypass exit control (e.g., from point C to point M in fig. 19).

The best potential stability index for each of the tested bypass entrance configurations would be realized by using what is probably the ideal bypass exit control - one having a constant bypass recovery characteristic. Such a characteristic was imposed upon the experimental bypass performances, and the resulting ideal SI is shown in figure 20 for each bypass entrance configuration. It is evident that the porous configurations had the largest values of stability index. They obtained an ideal stability index of 27.5 to 31 percent, compared to only 18 percent for the forward-slanted-slot and educated configurations.

When an actual pressure-activated valve was used to control the bypass exit area, a large stable range was achieved with the inlet operating at the preselected high performance condition. Specifically, the poppet valves, used as the bypass exit control, provided stability indices of 26.5 and 28 percent for the distributed porous configurations I and II, respectively. This performance was very nearly equal to that obtainable with the ideal constant-recovery bypass exit control and was caused by the low-pressure-rise characteristic designed into the poppet valve. The low-pressure-rise characteristic that allowed the valve to pass large amounts of bypass flow can be seen in the performance curves of the poppet valve shown in figures 21(a) and 22(a). The very large "subcritical" stability that the use of the poppet valves gave to the inlet performance is illustrated in figures 21(b) and 22(b). These figures also show that the inlet total-pressure recovery increased 5 to 6 percent from the selected operating point to the minimum stable point when the poppet valves were used. Inasmuch as the stability index is a change in corrected airflow which reflects changes in inlet recovery as well as in mass flow, the increase in inlet total-pressure recovery obtained by the porous bypass configurations contributed about 20 percent of the stability index achieved by using the poppet valves.

When the poppet valves were used with the distributed porous configurations at steady-state conditions, they were observed to oscillate during some portion of their operating range. Figure 21 shows the region of valve instability to be between bypass mass-flow ratios of 0.04 and 0.09 for the porous configuration I. For porous configuration II the instability region is even smaller, being between bypass mass-flow ratios of 0.055 and 0.075. In either case, these oscillations produced only small pressure oscillations at the diffuser exit. The inlet did not unstart and no adverse operational effects were noted.

When the poppet valves were used with the forward-slanted-slot and distributed educated configurations they were observed to be unstable over the whole stability-bypass airflow range. Because these oscillations appeared to be rather severe, no steady-state valve operation data were taken with the forward-slanted-slot configuration except at the preselected inlet operating point (valves closed). Steady-state data were taken with the distributed educated configuration and the valves oscillating in order to document the performance during valve instability. These data are shown in figure 20 in terms of stability index and in figure 24 in terms of steady-state performance. Even though oscillating, the valves obtained a stability index of 12 percent out of a potential (or constant recovery) stability index of 18. As figure 20 shows, even this amount of SI is superior to that obtained with any other bypass exit control.

Details of the effects of poppet valve oscillations were obtained during operation with the distributed educated configuration. The instrumentation indicated that the 16 valves oscillated in unison at a frequency of about 44 hertz. The oscillation amplitude in terms of valve head travel was 1.85 centimeters out of a maximum possible stroke of 3.05 centimeters. Peak-to-peak pressure oscillations experienced inside the valves had an amplitude of 10 percent of free-stream total pressure, whereas pressure oscillations at the valve face had an amplitude of 27 percent of free-stream total pressure. These two pressures were 180° out of phase. It appeared that the valves were acting like second-order dynamic systems, operating well beyond their calculated natural frequency response of 12 hertz. (The natural frequency response was calculated by using the valve head mass and the effective spring constant of the trapped air in the valve.) The peak-to-peak pressure amplitudes recorded at the inlet throat were not too severe, being 7 percent of the total pressure. Static-pressure amplitudes at the compressor face were only 3 percent of the free-stream total pressure.

Bench tests of a poppet valve were performed after the wind tunnel tests. These tests, although not conclusive, indicated that a small amount of properly applied friction might eliminate the oscillations. Another approach to solving the oscillation problem is indicated by the valve performance shown in figures 21(a) and 22(a). These curves strongly suggest that during some part of the valve travel the pressure characteristic of the valve (as installed in the model) may have had a zero or slightly negative slope, and the valves may have been naturally unstable. In this case, a possible solution would be

to increase the slope of the valve characteristic (at a sacrifice of bleed capability) by redesigning the valve.

The vortex valves were investigated as a bypass exit control for two stability-bypass entrance configurations: the distributed porous configuration I (fig. 21) and the forward-slanted-slot configuration (fig. 23). As shown in figure 20, vortex valves used as a bypass exit control obtained inlet stability indices of 10 to 11 percent out of a possible (constant bypass total pressure) stability index of 18 percent for the forward-slanted slot and 27.5 percent for the porous configuration. These vortex valve stable ranges were also considerably less than the ranges achieved with the poppet valves. It was because of the rather steep slope of their performance curve that the vortex valves were unable to take advantage of the large airflow capability of either stability-bypass entrance configuration (figs. 21(a) and 23(a)). As was the case with the poppet valves, the rise in inlet total-pressure recovery contributed to the stability index. In the case of the porous configuration I (fig. 21(b)), 45 percent of the stability index resulted from inproved inlet recovery. For the slot configuration (fig. 23(b)), with a lower peak recovery, only 25 percent of the stability index resulted from increased recovery. Note in figure 23(a) that the initial stability-bypass airflow used for the vortex valves was 0.035 mass-flow ratio and was slightly higher than the nominal 0.02 mass-flow ratio used for other configurations. This was not by intent but the result of the location of the 64 holes that bypassed the flow around the vortex valves. Hole location in this instance (fig. 15(b-2)) increased the hole length-diameter ratio and also the flow coefficient. This higher flow could probably be reduced to at least the lower value without affecting stability index.

The vortex valves did not provide the large inlet stable airflow ranges achieved by using the poppet valves. However, figure 20 shows that they were capable of providing a significant improvement over the 4 to 5 percent stability available with a simple fixed exit as might be supplied with a typical throat performance bleed. One drawback of the vortex valve is that a tangential control flow must be supplied. During the test, this control flow, at a pressure level near that of a diffuser exit total probe, required a mass-flow ratio of only 0.007 to operate. An advantage of the vortex valve is that it contained no moving parts. In addition, no oscillations were recorded while using the vortex valves.

As previously noted, a fixed exit, when used as a stability-bypass exit control, obtained a stability index of only 4 to 5 percent with all bypass entrance configurations. The fixed-exit performance appears as a choked exit line in part (a) of figures 21 to 24. As can be seen by referring to part (b) of these same figures, most of the stability range obtained with the fixed exit was caused by the increase in inlet total-pressure recovery. Among the four bypass entrance configurations the average contribution of inlet recovery to stability index was 60 percent.

At the minimum stable conditions encountered with the various bypass entrance configurations and bypass exit controls, the flow conditions within the inlet were determined by examining the internal inlet pressure distributions. Pressure distributions for all inlet conditions are shown in parts (a) and (b) of figures 25 to 33. As the stability-bypass flow at minimum stable conditions was increased by changing the bypass exit control from a fixed exit to the vortex valves and then to the poppet valves, these figures show the expected increase in diffusion as an increase in static-pressure level through the inlet. This increase in stability-bypass flow at minimum stable conditions also thinned the cowl boundary layer. (Refer to the inlet rake pressures as presented in parts (c), (d), and (e) of figs. 25 to 33.) At minimum stable conditions the terminal shock location on the cowl side of the inlet also correlated with the change of bypass exit control. The shock moved upstream as the bypass flow was increased by changing bypass exit control (part (a) of figs. 25 to 33). When the fixed exit was used as the bypass exit control, the foot of the cowl-side shock pressure rise at minimum stable conditions occurred at an x/R_c of 3.32 to 3.34. The shock foot at minimum stable conditions moved forward to an x/R_c of 3.27 when the vortex valves were installed and to an x/R_c of 3.16 to 3.20 when the poppet valves were installed. Note that the variation of bypass entrance configuration had no significant effect on the shock location at minimum stable conditions.

Some of the other cowl-side flow conditions at minimum stable were not affected by changes in the bypass exit control nor by changes in the entrance configuration. There was an initial cowl pressure rise observed forward of the shock foot. Its position in the inlet at minimum stable conditions was invariant and occurred at an x/R_c of 2.91 ± 0.04. From the pressure distributions, this pressure rise appears similar to that produced by boundary layer separation. A cowl rake was in the vicinity of the pressure rise at an x/R_c of 3.069 during testing of the forward-slanted-slot configuration. The rake profiles, however, did not indicate that a boundary-layer separation had occurred (figs. 30(f) and 31(f)).

When the foot of the terminal shock was located over the bypass entrance at minimum stable conditions, the cowl pressures through the throat had a singular characteristic for all bypass entrance configurations and bypass exit controls. The initial cowl pressure rise was followed by a pressure plateau over the bypass entrance which ended in the terminal-shock foot. The single exception to this characteristic occurred for the distributed porous configuration I with the poppet valve. In this instance the terminal-shock foot fell forward of the bypass entrance (fig. 25(a)). For all other cases the plateau pressures were dependent only on the bypass entrance configuration - being 0.51 of the free-stream total pressure P_0 for the porous configuration I, approximately 0.47 P_0 for the porous configuration II, and 0.46 P_0 for the educated configuration. The 0.40 P_0 value recorded for the educated configuration with the poppet valve as a bypass exit control (fig. 32(a)) was deemed not representative because of the aforementioned

valve oscillation.

On the centerbody side of the inlet, the location of the initial pressure rise that is caused by the terminal shock at minimum stable conditions was found to be invariant. The pressure rise began at an x/R_c of 2.98±0.02 and appears to coincide with the reflection of the initial cowl pressure rise from an x/R_c of 2.91. This centerbody pressure rise location was also independent of changes in the bypass entrance configuration or the bypass exit control. It exactly coincided with the forward edge of the mid-centerbody bleed region. It was this pressure rise that led to a choking pressure ratio on the inlet centerbody. Choking on the centerbody occurred in all cases at an x/R_c of about 3.1. Thus, the forward position of the centerbody-side choking pressure ratio at minimum stable conditions seemed to be limited by the forward extent of the mid-centerbody bleed region. For the porous and educated bypass entrance configurations, this choking pressure ratio appears to be the factor setting the inlet minimum stable condition because the location of the cowl-side choking varied with the bypass exit control and occurred at a more aft location in the vicinity of the bypass entrance. (Refer to parts (a) and (b) of figs. 25 to 29, 32, and 33.) One inference that can be drawn from this condition is that a forward extension of the mid-centerbody bleed region would allow a more forward choke point at minimum stable conditions and perhaps increase those inlet stable ranges already achieved. With the forward-slanted-slot bypass entrance configuration, a forward-cowl bleed allowed the cowl-side choking pressure ratio to occur forward of the bypass entrance, at station 3.05 x/R_c. In this instance the cowl-side choke point could be the factor setting the minimum stable condition.

The flow conditions that occurred in the forward-slanted slot were recorded by the total-pressure profiles presented in figures 30(f), (g), and (h) for the vortex valve bypass exit control and in figures 31(f), (g), and (h) for the fixed bypass exit. Parts (f) of each figure show that the total-pressure profile just forward of the slot (slot rake A) did not indicate flow separation at the minimum stable point as previously noted, but did reflect the increased local pressure rise as minimum stable conditions were approached. The total-pressure profiles of slot rake B indicate that flow separation occurred near the slot leading edge on the upstream slot surface (figs. 30(g) and 31(g)). The depth of this separation at the rake station was a minimum of 0.4 of the slot height. The profiles of slot rake C indicate that the flow reattached prior to reaching the rake station (figs. 30(h) and 31(h)). At inlet flow conditions near critical, the slot static-pressure distributions (figs. 30(i) and 31(i)) indicated some expansion, or turning, of the supersonic flow at the slot leading edge. This initial expansion was followed by flow recompression a short way into the slot. At minimum stable conditions the main-duct flow was diffused to subsonic speeds before it entered the slot. Little diffusion occurred throughout the slot length.

Inlet Angle-of-Attack Tolerance

Data reported herein were obtained by pitching the inlet to angle of attack from the preselected inlet operating point. The maximum angle of attack obtained by the inlet prior to unstart was recorded for the various bypass entrance configurations and bypass exit controls. These data are summarized in figure 34.

Pressure distributions on the leeward side of the inlet cowl and centerbody at unstart angles of attack are presented in figure 35 for all bypass entrance configurations. For reference, the pressure distributions at zero-degree angle-of-attack initial inlet operating points are also shown for each configuration. These figures show that pitching the inlet to unstart angle of attack caused the airflow forward of the inlet throat to be compressed to higher pressures. This is in agreement with the results of reference 11. As the inlet angle of attack was increased, the cowl-lip shock angle on the leeward side also increased as a result of the increased local surface angle relative to the local airflow. The result was an upstream movement of the shock impingement location on the centerbody surface. As an example, the shock structure of porous configuration I is shown in the diagram of figure 36.

Because of the similarity of the current data to some of the data reported in reference 11, it is clear that the unstart angles of attack reported herein, like those of reference 11, were caused by flow changes upstream of the inlet throat and are therefore the same as unstart angles of attack at supercritical operation. Reference 11 states that the maximum inlet angle of attack is limited by inlet unstart and that the unstart in some cases was caused by local overcompression of the flow on the leeward side of the inlet to a subsonic condition forward of the inlet throat. With this type of unstart mechanism, it should be possible to increase the unstart angle of attack by bleeding flow from the inlet in the region of the overcompression. Further, removing flow from the inlet downstream of the overcompression should not affect the unstart angle of attack. However, data presented in reference 4 indicated that removing flow aft of the overcompression region can affect the unstart angle of attack. The local overcompression for configuration ND of reference 4 occurred just aft of the forward-cowl bleed region. Removing flow aft of this location through a stability-bypass entrance just forward of the inlet throat increased the unstart angle of attack from 4.96° to 7.6°. It is not clear why removing flow through the stability bypass (aft of the local choke point at the forward-cowl bleed) affected the unstart angle of attack. A probable answer is that there is boundary layer involvement. If a separated flow region was located over and forward of the stability-bypass entrance, added bypass flow would shrink the separation and increase the main-duct flow area at the local choke point.

Some results of the current test agree with those of reference 4, in that increasing airflow from the stability bypass increased the unstart angle of attack. This is illustrated by the forward-slanted-slot configuration shown in figure 34. For this configura-

tion an unstart angle of attack of 5.2°, obtained when a fixed exit controlled the bypass, was increased to 6.8° when either of the valve types controlled the bypass exit. Data obtained on the poppet valves during testing indicated that the valves reacted to higher pressures on the leeward side of the inlet and opened differentially to increase bypass flow as the angle of attack was increased to unstart. Pressure distribution on the leeward side of the inlet for the forward-slanted-slot configuration at unstart angle of attack are shown in figure 35(c). The cowl pressure distributions (fig. 35(c2)) show that the forward-cowl bleed has allowed higher than sonic values of pressure ratio to exist at the aft edge of the forward-cowl bleed in the converging portion of the inlet forward of the inlet throat.

Data for the distributed educated configuration (fig. 34) also show that the valves increased the angle-of-attack limit prior to unstart. An unstart angle of attack of 5.56° was obtained with the valves, whereas with a fixed exit on the stability bypass the unstart angle of attack was limited to 4.12°. The lower angle-of-attack tolerance of the distributed educated configuration as compared to the forward-slanted-slot configuration illustrated the effect of forward-cowl bleed. For the educated configuration there was no forward-cowl bleed and the maximum angle of attack was reduced to 5.56° from the 6.8° obtained with forward-cowl bleed. Figure 35(d2) illustrates that the lack of forward-cowl bleed prevented sonic pressure ratios from being reached in the converging portion of the duct, forward of the stability-bypass entrance. At the unstart angles of attack for this configuration, the pressures over the forward portion of the bypass entrance are too low to indicate a choked condition (i.e., a potential unstart condition). Because of the complicated surface on which the static-pressure taps were located, they may not indicate true static pressure but may, in fact, represent the maximum pressures allowable without causing unstart. In other words, a slight increase in angle of attack from the recorded limiting values may cause a sonic pressure ratio to appear forward of the bypass entrance in the converging portion of the inlet and result in unstart.

The distributed porous configuration I had the same general bleed and bypass arrangement as the distributed educated configuration, that is, forward centerbody bleed, mid-centerbody bleed, and a stability bypass entrance without forward-cowl bleed. Yet the maximum angle of attack obtained for porous configuration I, 4.45°, was less than the 5.56° obtained for the distributed educated configuration. This difference is probably caused by the fact that the stability-bypass entrance for the porous configuration I did not extend as far forward of the inlet throat as it did for the distributed educated configuration. (Compare the bypass entrance positions as indicated in figs. 35(a2) and (d2).) The pressure distributions for the porous configuration I (fig. 35(a)) show that a pressure ratio near the sonic value was located on the cowl forward of the stability bypass. This pressure ratio of 0.48 may represent the limiting pressure ratio in a region of no bleed.

As shown in figure 34, changing the bypass exit controls from fixed exit to valves did not affect the unstart angle of attack obtained with the distributed porous configura-

tion I. The pressures on the cowl (fig. 35(a2)) would indicate the formation of a near-sonic bubble embedded in supersonic flow forward of the stability bypass. This pressure distribution indicates acceleration of flow to supersonic speeds aft of the bubble. These pressures show no likelihood of a flow separation through which bypass airflow could affect the near-sonic region as was the case with the previously discussed configurations.

Distributed porous configuration II had the smallest unstart angle of attack of any configuration, 3.69°. This configuration had only the stability bypass and a mid-centerbody bleed for removing airflow. Although the stability-bypass entrance was more forward than that of porous configuration I, porous configuration II had no forward centerbody bleed. This lack probably resulted in the lowered angle-of-attack tolerance because, as the pressure distributions of figure 35 suggest, the lack of forward-cowl bleed switched the pressure rise leading to local overcompression from the cowl to the centerbody side of the inlet. The centerbody pressure rise beginning near station 2.97 x/R_c (fig. 35(b1)) shows the reflected shock at the forward edge of the mid-centerbody bleed region. Any increase in angle of attack from the limiting angle would require the shock to move forward of the bleed region and might trigger local flow overcompression.

The variation of bleed-region bypass entrance placement discussed in this section clearly suggests that inlet unstart angle-of-attack tolerance was increased as the bleed regions and bypass entrances were extended forward of the inlet throat.

Transient Inlet Stability Limits

This section of the report deals with the tolerance of the inlet to internally generated airflow transients. Generation of these transients was accomplished as explained in the section APPARATUS AND PROCEDURE. Transient inlet stability limits for each of the stability-bypass exit controls were determined at the selected inlet operating point (approx. 0.90 total-pressure recovery with approx. 0.02 stability-bypass mass-flow ratio). The effect on the transient stability limits of varying the inlet operation from the selected operating point is presented in figures 37 and 38, where the transient stability index for other operating points is presented as a function of transient pulse pseudofrequency $1/\tau$. These data were obtained with the forward-slanted-slot configuration and the inlet-coldpipe combination. Figure 37 presents data obtained with the large bypass plenum volume (0.391 m^3). Figure 38 presents data obtained with a medium bypass plenum volume of 0.213 cubic meter, which was generated by shortening the bypass pipe lengths shown in figure 1. The main-duct volume of the inlet-coldpipe combination was 0.42 cubic meter.

The stability-bypass and inlet performance data of figure 39 are presented to aid visualization of the operating-point changes referred to in figures 37 and 38. All three figures use a consistent set of symbols; a symbol in figures 37 and 38 is again used in

figure 39 to show the inlet operating point from which the data were obtained. The open symbols in figure 39 denote the variations of inlet total-pressure recovery used to obtain the data of figures 37(a) and 38(a). The solid symbols in figure 39 denote the variations of stability-bypass exit area used to obtain the data of figures 37(b) and 38(b).

Increasing the inlet total pressure from 0.85 to 0.915 by operating the inlet from supercritical conditions to minimum stable conditions reduced the transient stability index as expected. These data, shown in figures 37(a) and 38(a), were obtained with an initial stability-bypass mass-flow ratio of about 0.025. Crossplots of these data in figure 40, which present the transient stability index as a function of the inlet total-pressure recovery, show a steepening drop in stability index with increasing recovery. Near the selected operating-point recovery of 0.9, an increase in recovery of 0.01 (from 0.895 to 0.905) reduced the transient stability index 5 to 7 percent at a pulse pseudofrequency of 20 pseudohertz. The effect on the transient stability index of increased stability-bypass airflows was obtained with various openings of the stability-bypass choked plugs while the inlet recovery was maintained near 0.9 (figs. 37(b) and 38(b)). Significant reductions in transient stability index were obtained by increasing the stability-bypass airflow. At a pulse pseudofrequency of 20 pseudohertz for example, increasing the bypass flow from zero to a mass-flow ratio of 0.13 reduced the transient stability index by 10 to 17 percent. A rather nominal increase in stability-bypass flow at 20 pseudohertz from zero to 0.035 mass-flow ratio dropped the transient stability index by 4 to 8 percent.

The transient inlet stability limits obtained for the various bypass exit controls and bypass entrance configurations are presented in figure 41. These data were obtained with the inlet-coldpipe assembly operating at the preselected operating point. This point is shown for each bypass entrance configuration and exit control by the tailed symbols in figures 21 to 24. The precise inlet total-pressure recovery that was recorded prior to obtaining each transient data set is shown in figure 41. Bypass plenum volumes for each configuration are also shown in the figure.

When the fixed exit with the small bypass plenum volume was installed in the stability-bypass systems of the inlet-coldpipe combination, the resulting transient stability index was smaller than with any other bypass exit control. For all bypass entrance configurations tested, the inlet transient stability index ranged from 3 to 7 percent at a pulse pseudofrequency of 1 pseudohertz and varied from 20 to 33 percent at a pulse pseudofrequency of 40 pseudohertz. Each of the fixed-exit-with-small-plenum-volume performance curves in figure 41 represents the capabilities of a normal inlet bleed system. The increase in the inlet transient stability index with pseudofrequency reflects the transient absorption ability of the inlet-coldpipe system volume. The considerable variation in inlet transient stability index among the bypass entrance configurations using the fixed bypass exit with the small plenum volume (fig. 41) was probably a result of the configuration-to-configuration variation in the inlet total-pressure recovery. As pre-

viously noted, figure 40 shows that increased recovery reduced the transient stability index. Figure 41 shows that the fixed-exit-with-small-volume configurations having the higher operating-point recoveries recorded the lower inlet transient stability indices. These trends were also evident with the fixed-exit-with-large-volume configurations. With the more sophisticated bypass exit controls (the pressure-activated valves), these trends are not always clear and are probably overshadowed by interaction effects between the valves and the conditions presented by the various bypass entrances.

As previously mentioned in the discussion of steady-state performance, the vortex valves were used as the bypass exit control on just two bypass entrance configurations: the distributed porous configuration I and the forward-slanted-slot configuration. The use of the vortex valves, rather than the fixed exit with small volume, as a stability-bypass exit control improved the inlet transient stability index 5 to 12 percent over the tested pseudofrequency range for the porous configuration I (fig. 41(a)), but only 1 to 4 percent for the forward-slanted-slot configuration (fig. 41(c)). The stability index obtained by the vortex valves varied from 9 to 14 percent at a pulse pseudofrequency of 1 pseudohertz and varied from 37 to 44 percent at a pseudofrequency of 40 pseudohertz. The smaller indices were obtained by the vortex valves with the slot configuration and were the result of this particular vortex valve installation, which increased the stability-bypass airflow at cutoff and thereby reduced the inherent stability index. The tailed symbols of figures 21(a) and 23(a) illustrate that all these configuration combinations passed a stability-bypass mass-flow ratio of 0.02 prior to the transient except the vortex valves with the slot configuration, which passed 0.035 mass-flow ratio.

When a large-volume bypass plenum was used ahead of the stability-bypass fixed exit, the inlet transient stability index obtained at the low pulse pseudofrequency of 1 pseudohertz was nearly the same (within 3 percent) as the index recorded for the fixed exit with the small volume (fig. 41). However, with the large plenum volume, the stability index increased rapidly with increasing pulse pseudofrequency. In fact, at the highest tested pseudofrequencies, the transient stability indices were so large that they exceeded the transient pulse amplitude limits of the overboard-bypass doors. The best performance using the fixed exit with large volume was recorded by the distributed porous configuration I. This configuration increased the transient stability index most rapidly with pseudofrequency and reached the overboard bypass door limit at a pseudofrequency of 27 pseudohertz with a transient stability index of 54 percent. This is a gain in stability index of 33 percent over the performance obtained when the small bypass plenum was used. Other bypass entrance configurations using the fixed exit with large volume increased the stability index with pseudofrequency less rapidly than did the porous configuration I. These configurations when using the fixed exit with large volume obtained a stability index in excess of 40 percent at a pulse pseudofrequency of 30 pseudohertz. Their performance was somewhat similar in that the stability index curves of all three fell within a stability index band of 6 percent (fig. 41).

The ability of the inlet-coldpipe combination with the large stability-bypass plenum to absorb the large transient pulse amplitudes at the higher internal pulse pseudofrequencies results from the long fill time of the large volume. Recall that the volume of the large plenum, about 0.4 cubic meter, when added to the inlet coldpipe volume of 0.42 cubic meter nearly doubled the total system volume. Such a large bypass plenum might be obtained in an actual aircraft by using empty fuel tanks or an internal nacelle volume.

When the poppet valves were installed as a stability-bypass exit control, the transient stability index obtained by the inlet-coldpipe assembly at low pulse pseudofrequencies was larger than that obtained with any other bypass exit control (fig. 41). At 1 pseudohertz for example, the transient stability index obtained with the poppet valves varied from 20 to 35 percent among the four bypass entrance configurations. These numbers represent a transient stability index increase of 11 to 31 percent over the index obtained with other bypass exit controls. The smallest increase in transient stability index at 1 pseudohertz was recorded for the bypass entrance configurations that experienced the most severe steady-state valve oscillations: the forward-slanted-slot and educated configurations. At higher pulse pseudofrequencies, 30 pseudohertz for example, the use of poppet valves increased the inlet transient stability index 15 to 30 percent above the index obtained with the small-volume fixed exit or the vortex valves. As shown by the curves in figure 41, the configurations using the poppet valves as a bypass exit control produced stability index curves that fell below those produced by the fixed exit with large plenum as the pulse pseudofrequency increased through the range of 15 to 25 pseudohertz. The forward-slanted-slot and educated configurations with poppet valves (figs. 41(c) and (d)) experienced a transient stability index increase with pseudofrequency comparable to that obtained with the small-volume fixed exit. The porous configurations with poppet valves, which produced the largest low-pseudofrequency transient stability index, experienced the smallest stability index increase with pseudofrequency, as shown by their relatively flat slopes in figures 41(a) and (b). The porous configurations recorded transient stability indices of over 33 percent for the tested pulse pseudofrequency range. The worst-performing bypass entrance configuration with poppet-valve bypass exit control provided a stability index of over 19 percent at all tested pseudofrequencies. In addition, the poppet valves were the only bypass exit control system that yielded large improvements in transient stability index over the small-volume fixed-exit values for the complete pulse pseudofrequency range. Among the four bypass entrance configurations, the minimum stability index improvement of between 13 and 17 percent was provided by the slot configuration over the pseudofrequency range from 1 to 30 pseudohertz. The maximum improvement in transient stability index was recorded by the educated configuration and porous configuration I. For these configurations, the transient stability index obtained by the small-volume fixed exit was improved with poppet-valve installation by between 19 and 30 percent over the pulse pseudofrequency range from 1 to 40 pseudohertz.

Placement of a choke plate at the inlet diffuser exit, to more closely simulate inlet-engine volume, reduced the inlet system volume from 0.42 to 0.16 cubic meter. The transient inlet stability limits obtained with this reduced inlet volume were determined for the distributed porous configuration I and are presented in figure 42. A comparison of this transient stability range with the stability limits obtained using the inlet-coldpipe combination (fig. 41(a)) reveal the expected result: the reduction in system volume reduced the stability range at the higher transient pulse pseudofrequencies. The size of the reduction increased as the pseudofrequency increased. With the fixed stability-bypass exit, the inlet transient stability index at a pseudofrequency of 1 pseudohertz was reduced by only 1 percent by the inlet volume change. But at a pulse pseudofrequency of 40 pseudohertz, the transient stability index obtained with the small-volume fixed exit was reduced from 32 to 17 percent. Similar results were observed when the large-volume fixed exit bypass control was used. The inlet volume reduction reduced the transient stability index from 51 to 39 percent at a pseudofrequency of 25 pseudohertz. With the poppet valves used as a bypass exit control, the inlet transient stability index was rather insensitive to the inlet volume change at transient pulse pseudofrequencies below 12 pseudohertz. Above this pseudofrequency the trends with volume changes are similar to those observed with the fixed exits. At a pulse pseudofrequency of 35 pseudohertz, the inlet volume reduction reduced the transient stability index obtained with the poppet valves from 51 to 31 percent. In spite of such reductions, the inlet with the choke plate and the poppet valves as a stability-bypass exit control provided a transient stability index of 30 percent or greater over the pulse pseudofrequency range of 1 to 40 pseudohertz.

The stable airflow operating range provided by the stability-bypass systems reported herein may possibly be improved by combining the performance of these systems with the performance of other inlet control hardware. For example, the better-performing configuration with the vortex valves at the stability-bypass exit would provide a large stable airflow range over the complete pseudofrequency spectrum if combined with a closed-loop controlled-high-response overboard-bypass system such as reported in reference 12. If a large stability-bypass plenum volume with a fixed exit were combined with an overboard bypass, only a moderate overboard-bypass pseudofrequency response to improve the lower pseudofrequency capability would be required to obtain a large capacity over the entire pseudofrequency range. Since the poppet valves provide a large transient stability capability at all pseudofrequencies, an inlet using the valves would need only a relatively slow overboard-bypass system such as normally used to match inlet-engine airflow requirements. If necessary, the transient stability provided by using the poppet valves could be increased at the higher pseudofrequencies by placing the valves at the exit of a large bypass plenum to utilize the very large high-pseudofrequency stability afforded by the large volume.

Internal Transient Response

Figure 43 presents selected time history plots that reflect the inlet and stability-bypass system reaction to internal transient pulses. The analysis of the internal transients was accomplished by examining time history plots for every transient data point presented in figures 41 and 42. But only representative combinations of bypass entrance configurations, bypass exit control, and pulse pseudofrequency were chosen for presentation. These are shown by the tailed symbols in figures 41 and 42, which indicate the amplitude of each pulse in terms of stability index. The plot at the top of each part of figure 43 shows the transient pulse in terms of overboard-bypass-door movement. The remaining plots of each part are ordered from top to bottom and present first the main-duct pressures from the diffuser exit forward through the inlet. Below these plots, the pressure at the valve face station is presented. When data for the large stability-bypass plenum volume are presented, the static pressure in the valve mounting chamber is also presented. When the poppet valves are used, the lower two plots show the valve opening and the internal valve pressure.

Configurations having dynamic pressure taps through the inlet throat revealed that the transient induced pressure pulse that propagated forward through the inlet reached a maximum amplitude in the inlet throat at the location of pressure tap D3. Because the inlet terminal shock was normally positioned at approximately the location of D3, it is clear that this maximum pressure amplitude reflected the pressure rise across the forward-moving terminal shock. For configurations allowing a large overboard-bypass-door pulse amplitude (e.g., figs. 43(e) and (f)), a maximum forward movement of the normal shock produced a peak pressure rise in the throat (D3) of 0.5 P_0. This pressure rise magnitude is the same as the maximum rise obtained from supercritical to minimum stable during steady-state inlet operation. (Refer to fig. 25(a) at an x/R_c of 3.38.) Peak transient pressures produced by the smallest stability indices had a magnitude of 0.2 and 0.3 P_0.

As illustrated in figure 43(a1), the pulse-generated throat pressure rise exhibited a rise time more rapid than that of the overboard-bypass-door pulse as a result of the normal shock response to the door-generated pulse. Thus, an effective stability-bypass exit control such as a poppet valve would be required to react with a frequency response greater than that of the original disturbance. The time delay from initiation of the overboard-bypass-door movement to the beginning of the throat pressure rise was observed to vary with pulse pseudofrequency in a manner commensurate with a constant phase relationship. Forward of tap D2, the transient induced pressure pulses were modified by the effects of the stability-bypass entrance configuration and the relieving effects of the particular bypass exit control. The transient cowl pressure rise between D4 and D5 was the pulse magnitude communicated into the stability-bypass plenum at probe D8.

Figures 43(a) to (c) present some of the transient response pulses obtained with the small-volume fixed exit installed on the inlet stability-bypass system. In general, the pressure response pulses obtained with the small-volume fixed exit roughly follow the imposed sine wave transient. As will be discussed later, this was not the case with other bypass exit controls. With the small-volume fixed exit on the bypass system, the inlet response pulses in the 5-pseudohertz range were very similar for the distributed porous configuration I and the educated configuration. An example of this response is shown in figure 43(a1). When the distributed porous configuration II and the slot configuration were used, these responses were modified by high-frequency oscillations that appeared on the decay side of the pressure pulses in the inlet throat and stability-bypass plenum. (These oscillations were measured by using high-speed strip charts (not shown).) For the porous configuration II a frequency of about 1700 hertz was measured in the inlet throat by taps D2, D3, D4, and D6 (fig. 43(b1)). With the slot configuration, the taps D2, D7, and D8 recorded a primary frequency of 340 hertz (fig. 43(c)). A smaller amplitude oscillation was also observed at 1700 hertz. These high-frequency oscillations also occurred during the transients imposed at the higher tested pulse pseudofrequencies, as shown, for example, by figure 43(b2). The maximum peak-to-peak amplitude of these oscillations was about 0.1 P_0.

At the higher pulse pseudofrequencies of 40 pseudohertz, the transient induced pressure pulses that were recorded for the inlet with the small-volume fixed exit as the stability-bypass exit control were observed to follow very closely to the imposed transient sine wave form only when the choke plate was placed at the diffuser exit (fig. 43(a2)). With the inlet-coldpipe assembly, the 40-pseudohertz response pulses were double peaked, as shown, for example, by figure 43(b2). The second peak was probably a reflection of the primary wave from the end of the long coldpipe.

As previously shown by figure 41, the transient stability curve of the inlet with a vortex-valve bypass exit control was similar in shape to that obtained with the small-volume fixed-exit bypass control. The internal transient pressure pulses obtained with the vortex-valve bypass exit control were so similar to those obtained with the small-volume fixed exit that they are not presented. There is one difference in the pressure pulse data between the two bypass exit controls, and this occurred with the forward-slanted slot configuration. The use of the vortex valves produced a single high-frequency oscillation of 1100 hertz rather than the two frequencies observed with the small-volume fixed exit.

Figures 43(d) and (e) present some of the transient response data that were obtained with the inlet using the large-volume fixed exit as a stability-bypass exit control. With this bypass exit control, the transient pressure pulses in the inlet throat and bypass system tended to follow the initial transient pulse only to the peak. Beyond the peak, the pressure response pulses did not follow the initial pulse but decayed slowly over a period of about 0.2 second. The slow pressure decay is, of course, an effect of the

very large volume of the bypass plenum. Transient pressure response pulses typical of those at a pseudofrequency of 5 pseudohertz are presented in figure 43(d1). At a pulse pseudofrequency of 20 pseudohertz and above, pressure in the throat and bypass ducts of some of the bypass entrance configurations exhibited a 47-hertz oscillation superimposed on top of the pressure decay curve. A very good example of this is shown in figure 43(d2) at a pulse pseudofrequency of 30 pseudohertz. These pressure transients were obtained for the inlet with choke plate using the distributed porous configuration I. The magnitude of the 47-hertz oscillation in this case with 0.1 P_0 - the largest obtained. The distributed porous configuration I with the inlet-coldpipe combination did not generate any 47-hertz pressure oscillations (fig. 43(e)). However, all the other stability-bypass entrance configurations experienced the pressure oscillation, but at a lesser amplitude than obtained for the inlet with choke plate.

Figures 43(f) and (g) present typical examples of the inlet transient response pulses that were obtained when the stability-bypass flow was controlled by the poppet valves. The large amplitude of the throat pressure pulses that occurred as shown in figure 43(f) reflects the large shock movement and large inlet transient stability index that was obtained with the poppet valves as a bypass exit control. The effects of shock response at the lower pulse pseudofrequency of 5 pseudohertz (fig. 43(f1)) allowed the throat pressure (D3) to rise to peak in 0.04 second for the initial overboard-bypass-door pulse that peaked in 0.1 second. The poppet valves followed the throat pressure rise quite well in allowing the large shock movement and opened in 0.05 second. Just as importantly, the valves were able to closely follow the decay side of the transient pulse and returned the inlet to normal operation without undue lag time. In fact, the valves were essentially closed by the time the transient door pulse ended. The forms of the valve pulse curve and the valve internal pressure curve shown in figure 43(f1) appear to consist of the throat pressure pulse form superimposed with a slight amount of valve self-oscillation. (The unsteady trace of D2 in figure 43(f1) that occurred before and after the 5-pseudohertz transient indicates some shock instability at the steady-state operating condition.)

Response pulses that were typical of those obtained with the poppet valve in the 20- to 40-pseudohertz range are shown in figure 43(f2). As the figure shows, the poppet valves were able to respond satisfactorily at the higher pulse pseudofrequencies. With an imposed overboard-bypass-door pulse reaching a peak in 0.017 second, the throat pressure rise occurred in 0.010 second, and the valves opened in 0.015 second. The valves closed in 0.02 second for a total valve pulse time of approximately 0.035 second compared to the initial door pulse width of 0.033 second. The inlet was not returned to normal operation in this time span, however. The valves were observed to bounce or chatter several times after the initial pulse. And pressure tap D2 in figure 43(f2) shows that the terminal shock was pulled downstream for approximately 0.1 second at the end of the transient. This phenomenon was apparently caused by overreaction of the poppet valves because it did not occur with other stability-bypass exit controls. It occurred

with all the distributed porous configurations when the imposed pulse pseudofrequency was above 10 pseudohertz.

The transient response pulses that were obtained using the forward-slanted-slot configuration with the poppet valves as a bypass exit control are presented in figure 43(g). With this bypass exit control at the lower pseudofrequencies, 5 pseudohertz for example, the pressure response pulses obtained with the slot were similar to those previously shown for the porous configuration, although lower in amplitude. The poppet-valve response was also similar in that the valves again opened in about 0.05 second and still showed a slight amount of self-oscillation.

The reactions to internal transients of the inlet using the forward-slanted-slot configuration and poppet valves become unique above a transient pulse pseudofrequency of about 10 pseudohertz. At the end of each transient pulse a large-amplitude pressure oscillation having a frequency of 160 hertz occurred in the stability-bypass plenum and inlet throat. Without external action these oscillations would continue indefinitely and prevent a return to normal inlet operation. During the testing, the oscillations were stopped by forced closure of the poppet valves. The largest magnitude of these oscillations (0.25 P_0) was recorded in the bypass plenum, as shown in figure 43(g2) by probe D8. Another bypass duct probe that was located 90° from probe D8 indicated the same large oscillation amplitude. Although not shown in figure 43(g2), this probe indicated that asymmetrical conditions occurred at 0.2 second from the transient start. Whereas D8, located at a circumferential position of 124°, continued to read a pressure oscillation amplitude of 0.25 P_0, the probe at a position of 34° recorded a drop in the pressure oscillation amplitude to 0.10 P_0 at 0.2 second. The oscillations recorded by the two probes remained in phase. The amplitude of the pressure oscillations that reached near the diffuser exit (D1) was only about 0.05 P_0. During the initial part of the 160-hertz oscillations, the poppet valves (not having the frequency response to follow the imposed oscillations) floated open, as shown in figure 43(g2). The valves closed momentarily at the 0.2-second mark. Beyond this mark the valves responded to the asymmetrical conditions, with the valves nearest the higher pressure oscillation amplitudes floating open, as shown in figure 43(g2), and the valves nearest the lower oscillation amplitudes remaining closed (not shown).

Inlet Dynamic Response

This section of the report presents the dynamic response of the inlet-coldpipe combination to oscillating internal and external disturbances. The internal disturbances were symmetrically created by oscillating the overboard-bypass doors. As explained earlier in the section APPARATUS AND PROCEDURE, the shock position dynamic response to internal disturbances was obtained by using the inlet unstart method of

reference 10. Normally, the determination of shock position dynamics is made by noting the shock crossing times of each throat transducer as the terminal shock moves through the inlet throat in a sinusoidal manner. The times of shock crossing for each transducer are combined with transducer location to obtain a sinusoidal curve fit, which then provides the amplitude and phase shift of the shock position. In the present case, this method could not be used because the shock did not cross a sufficient number of throat transducers. (The transducers were placed in the throat to investigate the inlet transients and were not in optimum locations for determining shock position dynamics.) The unstart method does not require throat transducers.

A limitation of the unstart method is that it provides dynamics of the terminal shock only at the limit of the inlet's stable range. At this condition (minimum stable) the relationship of the terminal shock to the inlet bleed regions or bypass entrance is quite different than at the normal operating point. In addition, the terminal shock is compressed into a plane wave just prior to unstart, whereas at normal operating conditions the shock may be more complex. Further, with the unstart method the terminal shock does not oscillate about the same mean position when the amplitude is determined at different bypass-door frequencies and no phase information is obtained.

The dynamic response of the inlet to an internal disturbance is presented in figure 44 for the inlet-coldpipe combination using the distributed porous configuration I and the small-plenum fixed exit as the bypass exit control. This stability-bypass combination was selected for the inlet to simulate a normal performance bleed system. The data of figure 44 show an initial reduction in the amplitude ratio of the dynamic responses as the disturbance frequency was increased to 30 hertz. According to reference 5, this type of response represents the first-order lag resulting from the large internal volume. For the shock position dynamics (fig. 44(a)) a resonance was observed at a frequency of about 58 hertz, with a second resonance observed at about 110 hertz. This response was similar to that of the inlet of reference 5, which recorded resonances of 60 and 120 hertz, as well as an amplitude valley near 30 hertz, while using the inlet unstart method. Such similarities in response between the two inlets was expected because the inlets are nearly identical in size. The amplitude ratio of the shock position at the first resonance was 1.0 for the inlet of reference 5 but only 0.27 for the inlet of this test.

Figure 44(b) presents the response of a transducer located in the inlet diffuser just forward of the bypass cavity. These data were obtained at the varying conditions dictated by the use of the inlet unstart method. The first resonance of this transducer's response also occurred at 58 hertz with an amplitude ratio of 0.43. These results compare favorably with results reported in reference 5 and obtained from an identically located transducer which measured internal disturbances with the inlet at the normal operating condition. The reference 5 data show an amplitude valley at 30 hertz followed by a first resonance at 50 hertz with an amplitude ratio of 0.58. The curves of phase shift were very similar: for both inlets the curve minima occurred at the identical

frequencies of 20 and 80 hertz. The curve maximum occurred at a frequency of 40 hertz for both inlets. These data comparisons suggest that dynamic response data obtained at varying conditions near the inlet unstart limit are only moderately different from data obtained near normal inlet operating conditions such as "critical."

The dynamic response of the inlet to an external disturbance was determined by sinusoidally oscillating the gust plate, which was positioned so as to disturb the inlet Mach number and angle of attack. Disturbances in the free stream through which the inlet must fly are of special interest since they may cause the inlet to unstart. For example, a perturbation which causes a reduction in the free-stream Mach number or an increase in the angle of attack beyond those tolerated by the inlet will cause unstart. Positive gust-plate angles, which would cause a Mach number decrease along with a pitch change, were not used for this test because the particular stability-bypass configuration (distributed porous I) allowed inlet unstart to occur at very small Mach number reductions: (The Mach number tolerance of this inlet with the distributed porous configuration I is given in reference 11.) The plate was therefore oscillated only from 0° to -1°. This mode of oscillation can only increase the free-stream Mach number. Increased Mach number is also of interest because an increase may cause the inlet terminal shock to move downstream sufficiently to increase distortion beyond that tolerated by the engine.

The inlet dynamic response to the gust-plate oscillations is presented in figure 45. Data are shown for the pressure transducer located in the diffuser just forward of the overboard-bypass cavity. Figures 45(a) to (c) present data that were obtained by using different stability-bypass exit controls, specifically, the poppet valves and the fixed exit with the large and small plenum volumes. The data show that changing the stability-bypass exit controls had absolutely no effect on the measured diffuser pressure response. For all these bypass exit controls, the amplitude ratio of the pressure response decreased to 0.4 as the disturbance frequency was increased to 15 hertz. Also, there was a gradual increase in the phase lag of the pressure response, which reached 110° as the frequency was increased to 15 hertz. These data were similar to the inlet-coldpipe data of reference 5, which were obtained under identical circumstances and were recorded by a transducer located in the overboard-bypass cavity. The transducer of reference 5 measured a gradual reduction in amplitude ratio, which reached 0.3 as the frequency was increased to 15 hertz. The phase lag was 150° at a frequency of 15 hertz.

The 0° to -1° oscillations of the gust plate that were used as the external disturbance produced a small inlet terminal-shock movement that affected only two throat pressure transducers. The method of using the shock crossing times of the throat transducers was therefore unusable and shock-position dynamic plots were not obtained. The responses of the throat pressure transducers were identical for all three stability-bypass exit controls. A typical response is presented in figure 46, where the gust-plate angle and the pressures recorded by transducers D2 and D3 are plotted against time. Prior to

the oscillations the terminal shock was located between these transducers. As the figure shows, the terminal shock did not cross either transducer location at a frequency of 1 hertz. At a frequency of 6 hertz the shock travel had increased and the shock began to affect D2 and D3. At 15 hertz the shock movement had further increased and was strongly affecting the pressures recorded by transducers D2 and D3. The trend of these data is clear: a lead effect is indicated by the amplitude ratio of the shock position as it increased with frequency.

Figure 47 presents for comparison the shock dynamics obtained for the inlet-coldpipe system of reference 5 with gust-plate oscillations from 0° to -1°. The figure shows that the shock-position amplitude ratio of the reference 5 inlet also increased with frequency. The shock-position phase lag of the reference 5 inlet is also presented in figure 47. Included in the figure are shock-position phase lag data obtained during the present test and determined from the pressure plots of figure 46 at frequencies of 6 and 15 hertz. The figure shows that the shock-position phase lag was nearly identical for both inlets.

SUMMARY OF RESULTS

A stability-bypass system was installed on the cowl side of a Mach 2.5 mixed-compression inlet having 40 percent internal contraction. Airflow entered the bypass system through either a distributed porous surface, distributed educated slots, or a forward-slanted slot. The bypass airflow exit was controlled by either poppet valves, vortex valves, or fixed exits. Steady-state and transient stability limits of the inlet with coldpipe were determined for alternate combinations of bypass entrance configurations and bypass exit controls. Additional transient stability limits were obtained for the inlet with a choke point at the diffuser exit. Transient stability limits were also measured for various bypass plenum volumes, bypass exit areas, and inlet pressure recoveries. Inlet unstart angle of attack was determined for alternate combinations of stability-bypass entrance configurations and bypass exit controls.

The inlet with coldpipe was dynamically tested with internal sinusoidally oscillating disturbances to 140 hertz and external sinusoidally oscillating disturbances to 15 hertz. A limited amount of dynamic response data was obtained. The test was conducted in the Lewis 10- by 10-Foot Supersonic Wind Tunnel at a Mach number of 2.5 with the following results:

1. With the inlet operating at a total-pressure recovery of 0.9 the stability-bypass systems with valve-controlled exits provided a large stable airflow operating range.

2. During steady-state operation, the stability-bypass flow controlled by poppet valves allowed the inlet airflow to be reduced by as much as 28 percent without causing unstart. Using vortex valves resulted in a smaller stable operating range of 11 percent,

and using a small comparable fixed exit area in only 5 percent.

3. The ability of the inlet-coldpipe combination using a small stability-bypass plenum with a fixed exit area to absorb internal transients increased with pseudofrequency (1 divided by the pulse period) for all bleed configurations. A stable airflow operating range of 3 to 7 percent of engine airflow for a 1-pseudohertz transient increased to a range of 20 to 33 percent for a 40-pseudohertz transient. This increase in tolerance with pseudofrequency represents the ability of the inlet-coldpipe volume to absorb a transient.

4. Replacing the fixed exit on the small stability-bypass plenum with vortex valves increased the transient inlet stable airflow operating range over the tested pseudofrequency range by 5 to 12 percent of engine airflow for a porous stability-bypass entrance configuration, but only by 1 to 4 percent for the forward-slanted-slot configuration.

5. Replacing the fixed exit on the small stability-bypass plenum with poppet valves provided a large transient stable airflow range (above 33 percent of engine airflow for the porous configurations) over the pseudofrequency range investigated. With some configurations (notably the forward-slanted-slot and distributed educated configurations), the poppet valves were unstable and oscillated at a frequency of 44 hertz.

6. A large bypass plenum with a fixed exit area provided the inlet-coldpipe combination with the largest transient stable airflow operating range at the higher pseudofrequencies (a transient stability of 54 percent of engine airflow at 27 pseudohertz for a porous configuration and over 40 percent at 30 pseudohertz for all other stability-bypass entrance configurations). The same configuration obtained no improvement in the inlet transient stability achieved at a pseudofrequency of 1 pseudohertz with the small-plenum fixed exit area.

7. With the inlet terminated by a choke point at the diffuser exit, the transient stable margin obtained at the higher pseudofrequencies was smaller than that obtained with the larger volume inlet-coldpipe combination. Despite these reductions, a porous bypass entrance configuration with the poppet valves controlling the bypass exit obtained a transient stable margin above 30 percent over the 1- to 40-pseudohertz range.

8. Large-amplitude pressure oscillations (0.25 P_0) were induced in the small bypass plenum of the forward-slanted-slot configuration when poppet valves controlled the bypass exit and transients with a pseudofrequency of 20 pseudohertz or greater were imposed. The resulting 160-hertz resonance was self-sustaining and prevented the inlet from returning to normal operation.

9. Pressure oscillations with amplitudes to 0.1 P_0 and a frequency of 47 hertz occurred in the inlet throat and bypass plenum when the large bypass plenum was used with fixed exit area and transients with a pseudofrequency of 20 pseudohertz or greater were imposed. These oscillations decayed in 0.2 second.

10. Because the pressure wave from a transient disturbance was modified by the response of the terminal shock, a bypass exit control such as the poppet valves was

required to react to a faster pressure rise than that of the originating pulse.

11. Maximum inlet angle of attack was limited by inlet unstart. All angle-of-attack data were obtained from an initial inlet pressure recovery of 0.9. The largest angle of attack (6.85°) was obtained when the forward-cowl bleed was employed and valves controlled the exit of the stability-bypass system. The poppet valves reacted to the higher pressures on the leeward side of the inlet and opened differentially at angle of attack.

12. The attainable angle achieved prior to unstart increased as the bleed regions and bypass entrances were extended forward of the inlet throat.

13. When subjected to an oscillating internal disturbance the inlet dynamic response was characterized by a gradual reduction in response amplitude to 30 hertz and by a primary resonance at 58 hertz.

14. When subjected to an oscillating external disturbance the inlet dynamic response exhibited a lead characteristic in the amplitude ratio of the shock position near 15 hertz.

Lewis Research Center,
National Aeronautics and Space Administration,
Cleveland, Ohio, August 27, 1973,
501-24.

APPENDIX - SYMBOLS

A	flow area, m^2
AI	airflow index in percent, $AI = 100\left\{1-\left[(W_{corr})_{min\ s}/(W_{corr})_{op}\right]_5\right\}$
A_c	cowl-lip capture area, 0.1757 m^2
CO	converging vortex generator pair
DI	diverging vortex generator pair
d	distance from local surface, cm
h	annulus height, cm
L	axial distance from leading edge of slot throat bypass entrance, cm
M	Mach number
m	mass flow, kg/sec
P	total pressure, N/m^2
p	static pressure, N/m^2
R_c	inlet-cowl-lip radius, 23.66 cm
r	radius, cm
SI	stability index in percent, $SI = 100\left\{1-\left[(W_{corr})_{min\ s}/(W_{corr})_{op}\right]_5\right\}$
W_{corr}	corrected airflow, kg/sec
x	axial distance from cone tip, cm
α	angle of attack, deg
θ_l	cowl-lip position parameter, $\tan^{-1}\left[1/(x/R_c)\right]$
τ	transient pulse width, sec
ϕ	circumferential position, deg

Subscripts:

av	average
b	bleed
e	exhaust
l	local
max	maximum
min	minimum

min s	minimum stable inlet operating point
op	inlet operating point
pv	poppet valve
pvi	poppet valve, internal
ref	reference
sb	stability bypass
t	tangential
un	unstart limit
vve	vortex valve exit
x	value at distance x
0	free stream
5	diffuser exit

REFERENCES

1. Sanders, Bobby W.; and Cubbison, Robert W.: Effect of Bleed-System Back Pressure and Porous Area on the Performance of an Axisymmetric, Mixed-Compression Inlet at Mach 2.50. NASA TM X-1710, 1968.
2. Bowditch, David N.; Coltrin, Robert E.; Sanders, Bobby W.; Sorensen, Norman E.; and Wasserbauer, Joseph F.: Supersonic Cruise Inlets. Aircraft Propulsion. NASA SP-259, 1971, pp. 282-312.
3. Sanders, Bobby W.; and Mitchell, Glenn A.: Increasing the Stable Operating Range of a Mach 2.5 Inlet. Paper 70-686, AIAA, June 1970.
4. Sanders, Bobby W.; and Mitchell, Glenn A.: Throat-Bypass Bleed Systems for Increasing the Stable Airflow Range of a Mach 2.50 Axisymmetric Inlet with 40-Percent Internal Contraction. NASA TM X-2779, 1973.
5. Wasserbauer, Joseph F.: Dynamic Response of a Mach 2.5 Axisymmetric Inlet with Engine or Cold Pipe and Utilizing 60 Percent Supersonic Internal Area Contraction. NASA TN D-5338, 1969.
6. Cubbison, Robert W.; Meleason, Edward T.; and Johnson, David F.: Effect of Porous Bleed in a High-Performance Axisymmetric, Mixed-Compression Inlet at Mach 2.50. NASA TM X-1692, 1968.
7. Wasserbauer, Joseph F.; and Choby, David A.: Performance of a Bicone Inlet Designed for Mach 2.5 with Internal Distributed Compression and 40-Percent Internal Contraction. NASA TM X-2416, 1971.
8. Coltrin, Robert E.; and Calogeras, James E.: Supersonic Wind Tunnel Investigation of Inlet-Engine Compatibility. Paper 69-487, AIAA, June 1969.
9. Gebben, Vernon D.: High-Capacity, Compact Vortex Valves for Increasing Stability of Supersonic Mixed-Compression Inlets. NASA TN D-6662, 1973.
10. Wasserbauer, Joseph F.; and Whipple, Daniel L.: Experimental Investigation of the Dynamic Response of a Supersonic Inlet to External and Internal Disturbances. NASA TM X-1648, 1968.
11. Choby, David A.: Tolerance of Mach 2.50 Axisymmetric Mixed-Compression Inlets to Upstream Flow Variations. NASA TM X-2433, 1972.
12. Crosby, Michael J.; Neiner, George H.; and Cole, Gary L.: Restart and High Response Terminal Shock Control for an Axisymmetric Mixed-Compression Inlet with 60-Percent Internal Contraction. NASA TM X-1792, 1969.

TABLE I. - INLET INTERNAL SURFACE COORDINATES

(a) Centerbody

Axial distance from cone tip, x/R_c	Inlet cowl-lip radius ratio, r/R_c	Axial distance from cone tip, x/R_c	Inlet cowl-lip radius ratio, r/R_c
0	0	4.900	0.5448
10^o Conical section		4.950	.5320
1.0323	.1820	5.000	.5195
18.5^o Conical section		5.050	.5075
2.7620	.7608	5.100	.4983
2.800	.7696	5.150	.4895
2.850	.7794	5.200	.4805
2.900	.7874	5.250	.4715
2.950	.7937	5.300	.4622
3.000	.7986	5.350	.4534
3.050	.8025	5.400	.4444
3.100	.8045	5.450	.4352
3.150	.8043	5.500	.4264
3.200	.8030	5.550	.4175
3.250	.8015	5.600	.4085
3.300	.8000	5.650	.3995
3.350	.7982	5.700	.3900
3.400	.7964	5.750	.3815
3.450	.7944	5.800	.3732
3.500	.7925	5.850	.3650
3.550	.7906	5.900	.3566
3.600	.7886	5.950	.3488
3.650	.7862	6.000	.3412
3.700	.7834	6.050	.3339
3.750	.7798	6.100	.3266
3.800	.7757	6.150	.3196
3.850	.7711	6.200	.3130
3.900	.7655	6.250	.3068
3.950	.7590	6.300	.2985
4.000	.7513	6.350	.2910
4.050	.7426	6.400	.2845
4.100	.7330	6.450	.2780
4.150	.7230	6.500	.2716
4.200	.7133	6.550	.2655
4.250	.7036	6.600	.2597
4.300	.6924	6.650	.2545
4.350	.6810	6.700	.2501
4.400	.6692	6.750	.2464
4.450	.6577	6.800	.2430
4.500	.6455	6.850	.2410
4.550	.6330	6.900	.2400
4.600	.6205	6.950	.2396
4.650	.6085	7.000	.2394
4.700	.5960	Cylinder	
4.750	.5825	7.8858	.2394
4.800	.5700		
4.850	.5573		

(b) Cowl

Axial distance from cone tip, x/R_c	Inlet cowl-lip radius ratio, r/R_c	Axial distance from cone tip, x/R_c	Inlet cowl-lip radius ratio, r/R_c
2.1167	1.0000	4.450	0.9538
2.150	1.0028	4.500	.9481
2.200	1.0070	4.550	.9426
2.250	1.0111	4.600	.9374
2.300	1.0154	4.650	.9324
2.350	1.0193	4.700	.9276
2.400	1.0228	4.750	.9232
2.450	1.0261	4.800	.9191
2.500	1.0290	4.850	.9153
2.550	1.0317	4.900	.9120
2.600	1.0340	4.950	.9087
2.650	1.0360	5.000	.9050
2.700	1.0373	5.050	.9044
2.750	1.0382	5.100	.9049
2.800	1.0386	5.150	.9058
2.850	1.0386	5.200	.9071
2.900	1.0381	5.250	.9086
2.950	1.0370	5.300	.9102
3.000	1.0356	5.350	.9118
3.050	1.0337	5.400	.9132
3.100	1.0320	5.450	.9145
3.150	1.0304	5.500	.9157
3.200	1.0290	5.550	.9166
3.250	1.0275	5.600	.9173
3.300	1.0262	5.650	.9177
3.350	1.0251	5.700	.9179
3.400	1.0239	Cylinder	
3.450	1.0227	6.1747	.9179
3.500	1.0215	Bypass gap	
3.550	1.0204	6.7847	.8868
3.600	1.0192	6.800	.8865
3.650	1.0176	6.850	.8855
3.700	1.0160	6.900	.8846
3.750	1.0144	6.950	.8837
3.800	1.0124	7.000	.8823
3.850	1.0100	7.050	.8805
3.900	1.0071	7.100	.8785
3.950	1.0037	7.150	.8760
4.000	1.0000	7.200	.8734
4.050	.9955	7.250	.8707
4.100	.9908	7.300	.8677
4.150	.9858	7.350	.8654
4.200	.9808	7.400	.8639
4.250	.9756	7.450	.8631
4.300	.9702	7.500	.8627
4.350	.9659		
4.400	.9595	7.550	.8623
		7.600	.8621
		Cylinder	
		7.8858	.8621

TABLE II. - INLET VOLUMES

Configuration	Main-duct volume, m^3	Stability-bypass plenum volume, m^3
Inlet-coldpipe combination with small stability-bypass plenum	0.42	~0.01 to 0.02
Inlet-coldpipe combination with large stability-bypass plenum	.42	~0.4
Inlet with choke plate and small stability-bypass plenum	.16	~0.01 to 0.02
Inlet with choke plate and large stability-bypass plenum	.16	~0.4

TABLE III. - COWL STATIC-PRESSURE-TAP LOCATIONS

[Top centerline.]

(a) Distributed porous configuration

Axial distance from cone tip, x/R_c
2.684
2.807
2.859
2.894
2.930
2.964
2.999
3.038
3.066
3.101
3.136
3.170
3.205
3.240
3.275
3.310
3.345
3.380
3.434
3.489
3.639
3.677
3.779
3.950
4.192
4.519
4.847
5.202
5.529
6.119
6.742
7.311

(b) Forward-slanted-slot configuration

Axial distance from cone tip, x/R_c
2.684
2.807
2.859
2.894
2.930
2.964
2.999
3.038
3.069
3.311
3.343
3.390
3.434
3.489
3.639
3.677
3.779
3.950
4.192
4.519
4.847
5.202
5.529
6.119
6.742
7.311

(c) Educated configuration

Axial distance from cone tip, x/R_c
2.684
2.807
2.838
2.892
2.945
2.999
3.053
3.106
3.160
3.213
3.267
3.321
3.375
3.434
3.489
3.639
3.677
3.779
3.950
4.192
4.519
4.847
5.202
5.529
6.119
6.742
7.311

TABLE IV. - CENTERBODY STATIC-PRESSURE-TAP LOCATIONS

Axial distance from cone tip, x/R_c
2.308
2.603
2.670
2.716
2.751
2.775
2.802
2.834
2.858
2.893
2.963
3.030
3.102
3.140
3.173
3.210
3.247
3.285
3.317
3.353
3.389
3.441
3.489
3.543
3.586
3.629
3.671
3.714
3.795
3.875
3.951
4.192
4.519
4.847
5.202
7.311

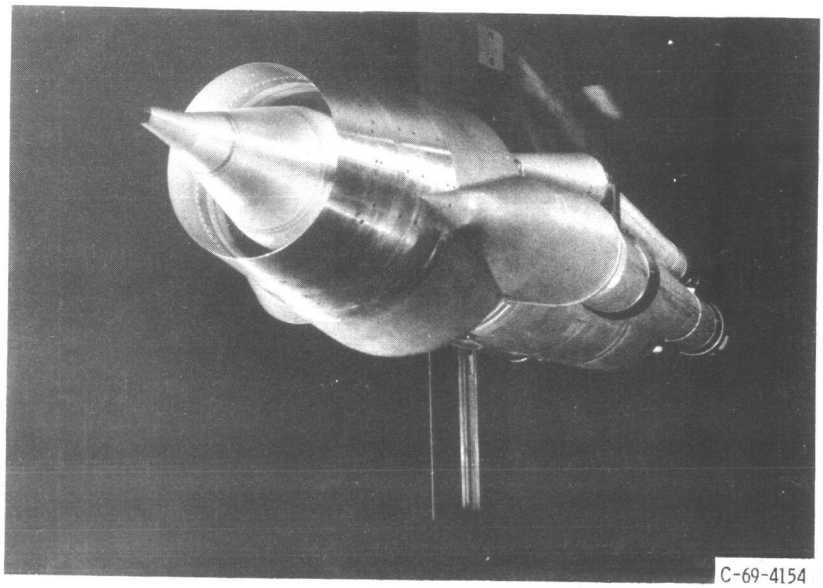

(a) Front view.

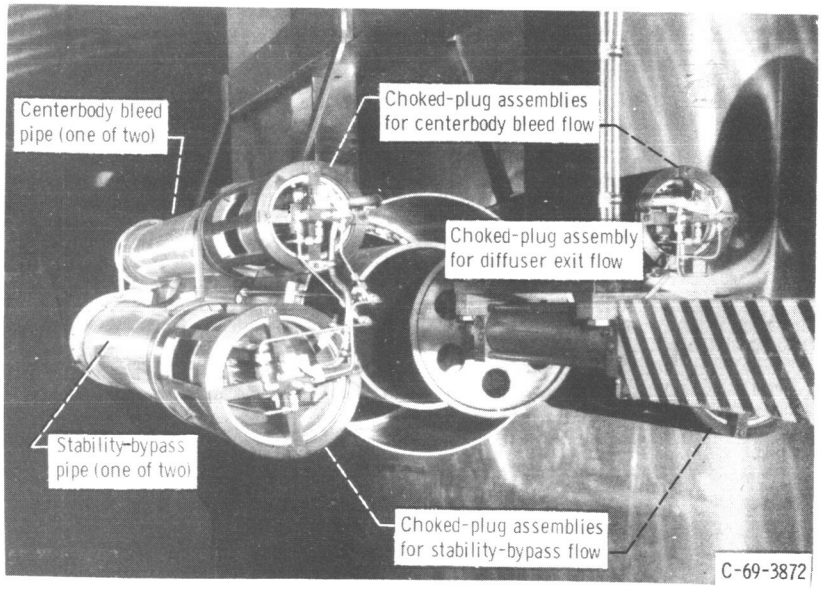

(b) Model installation showing choked-exit mass-flow throttling controls.

Figure 1. - Model installed in 10- by 10-Foot Supersonic Wind Tunnel.

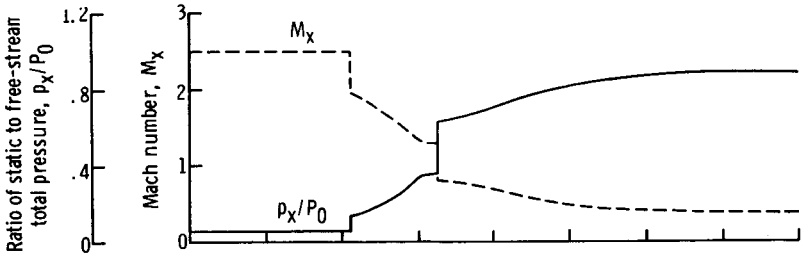

(a1) Cowl surface conditions.

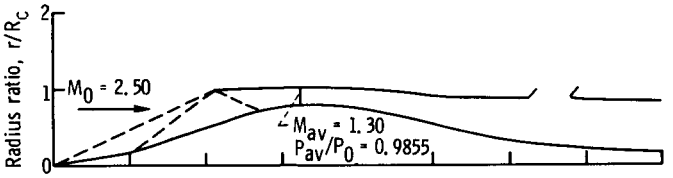

(a2) Inlet contours.

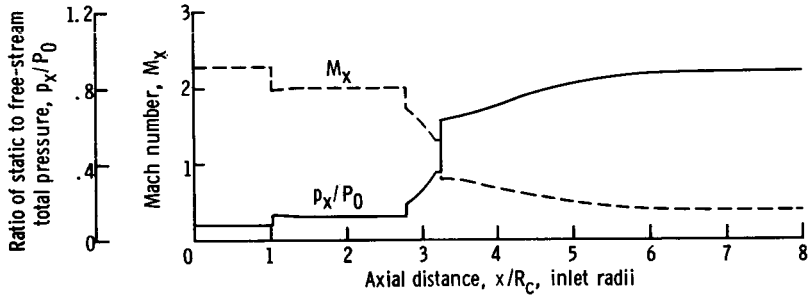

(a3) Centerbody surface conditions.

(a) Inlet dimensions and airflow conditions. Free-stream Mach number, $M_0 = 2.50$.

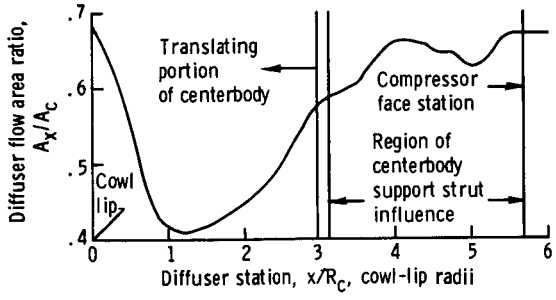

(b) Diffuser area variation.

Figure 2. - Aerodynamic details. Cowl-lip position parameter, $\theta_l = 25.27^o$.

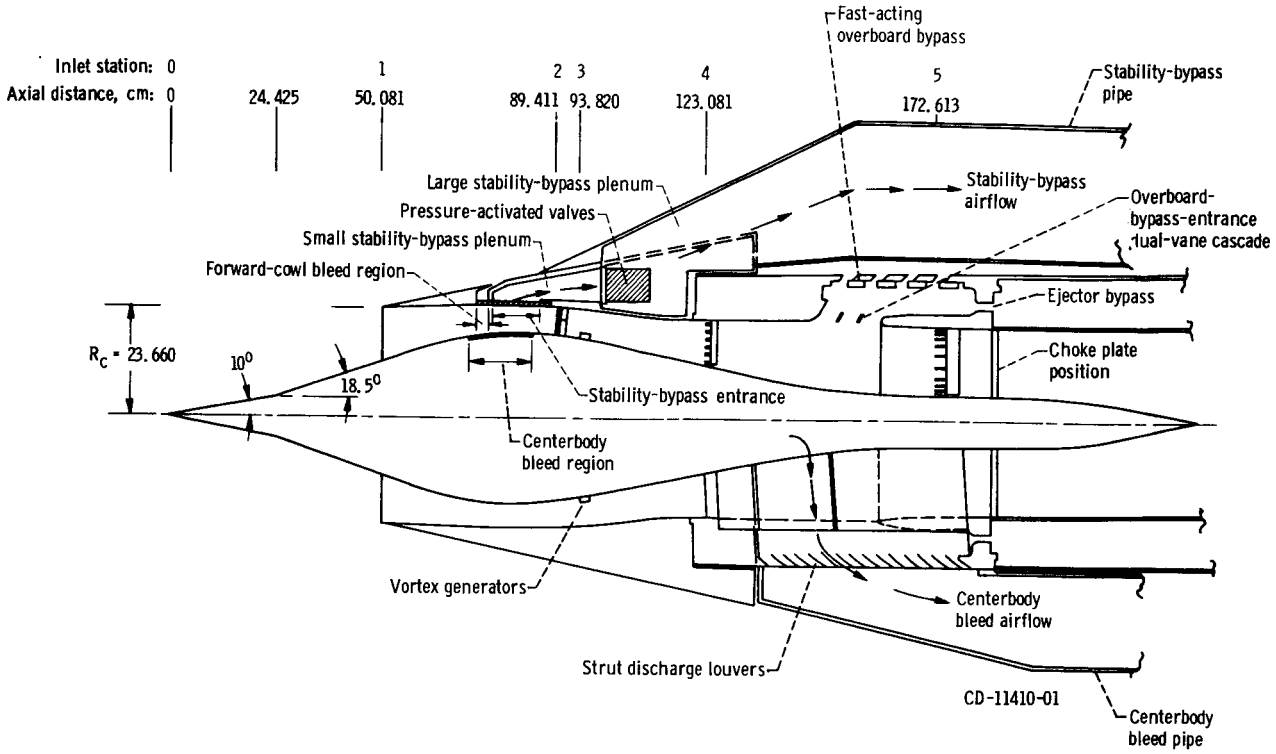

Figure 3. · Inlet details. Dimensions are in centimeters.

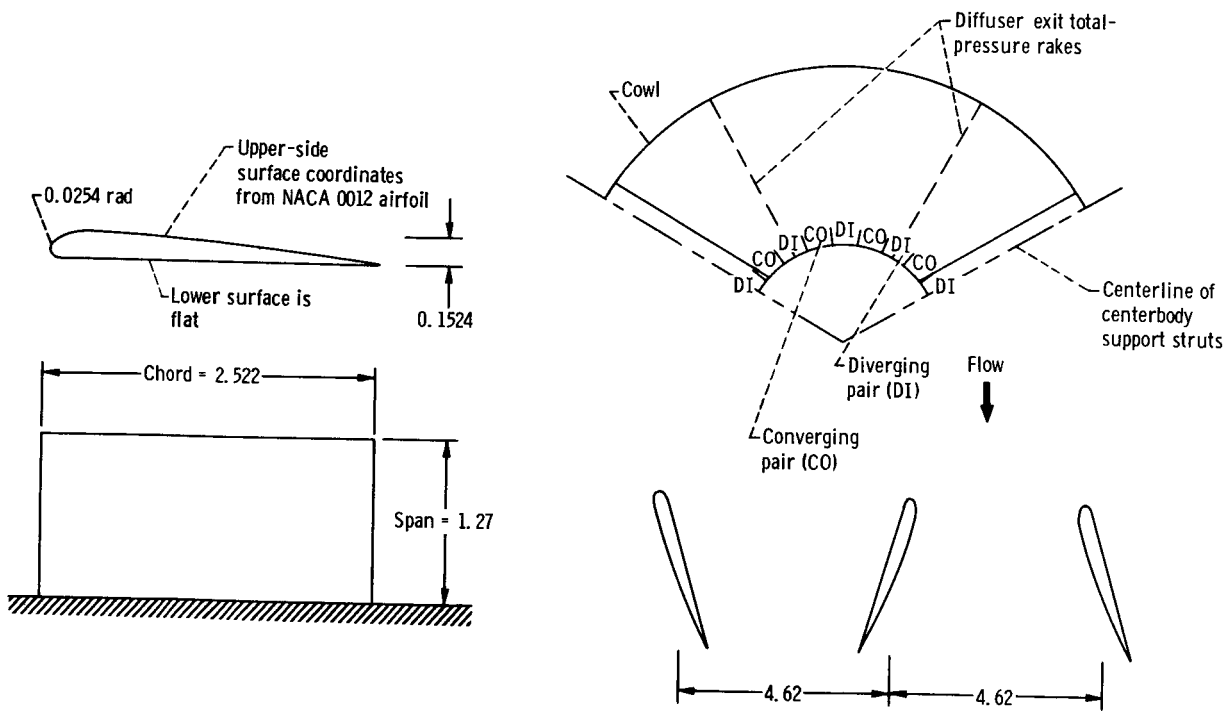

Figure 4. - Vortex generator design. Dimensions are in centimeters.

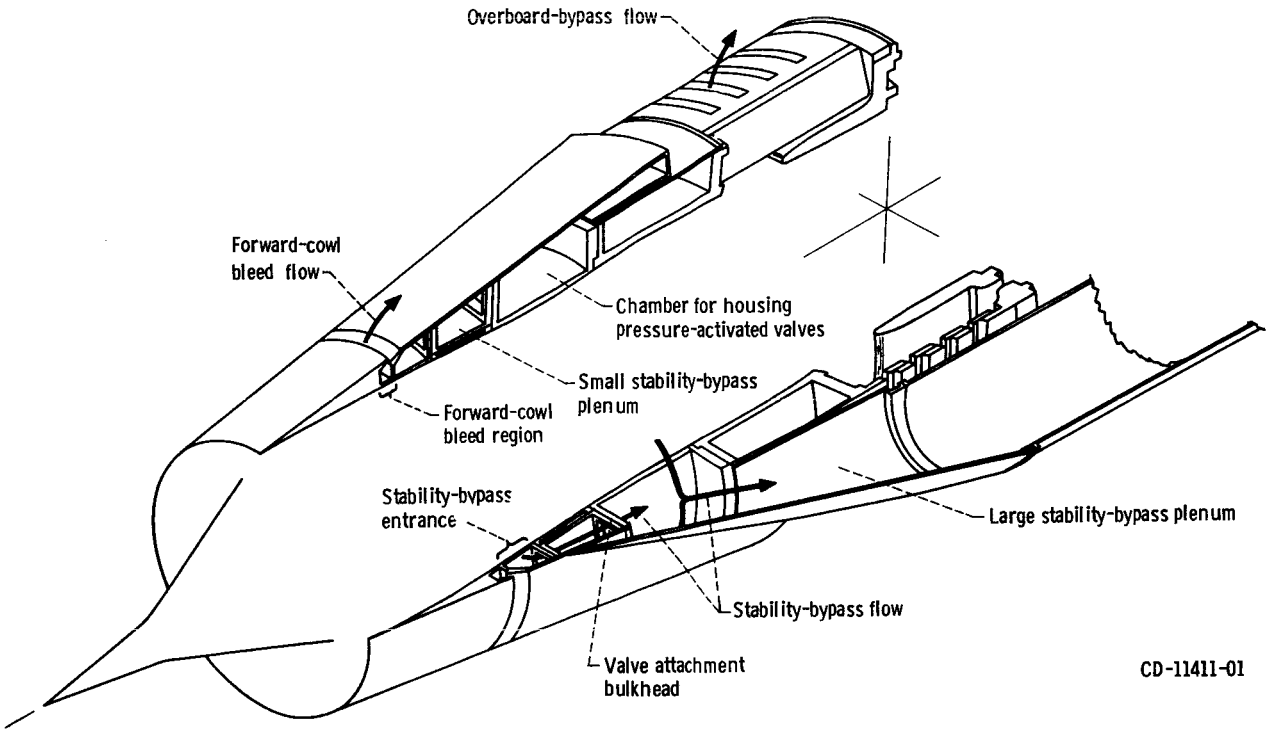

Figure 5. - Sketch of inlet cowl showing cowl bleed and bypass ducting.

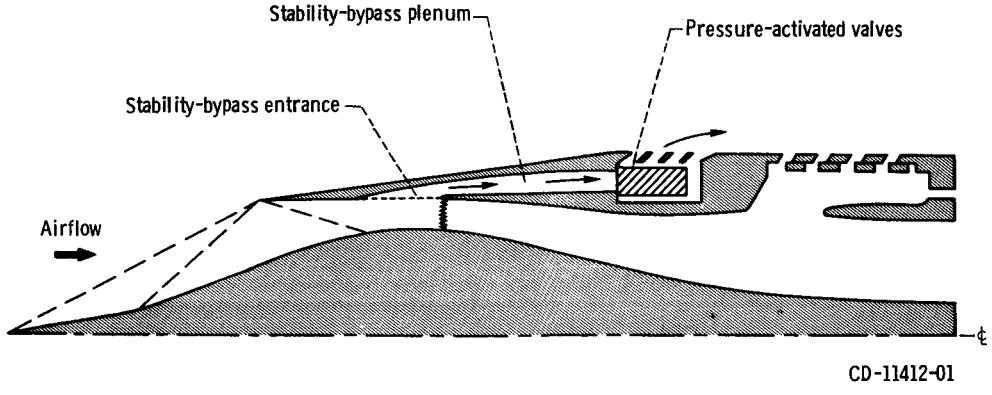

Figure 6. - Possible arrangement of a stability-bypass system for a flight inlet.

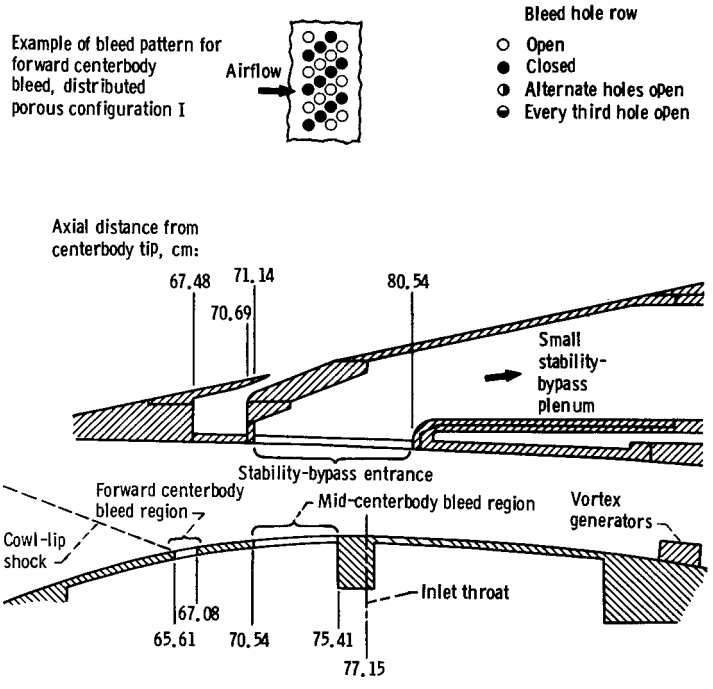

Hole pattern schematic

Distributed porous configuration	Forward centerbody bleed region	Mid-centerbody bleed region	Stability-bypass entrance
I	◑◑◑◑	○○○○○○○○○○○○	●●●●●●●○○○○○○○○○○○○○
II	●●●●	○○○○○○○○○○○○	○○○○○○○○○○○○○○○○○○○○

Inlet throat

(a) Schematic of distributed porous stability-bypass entrance configurations and associated centerbody performance bleed regions.

Figure 7. - Inlet stability-bypass entrance and bleed region configurations. Dimensions are in centimeters.

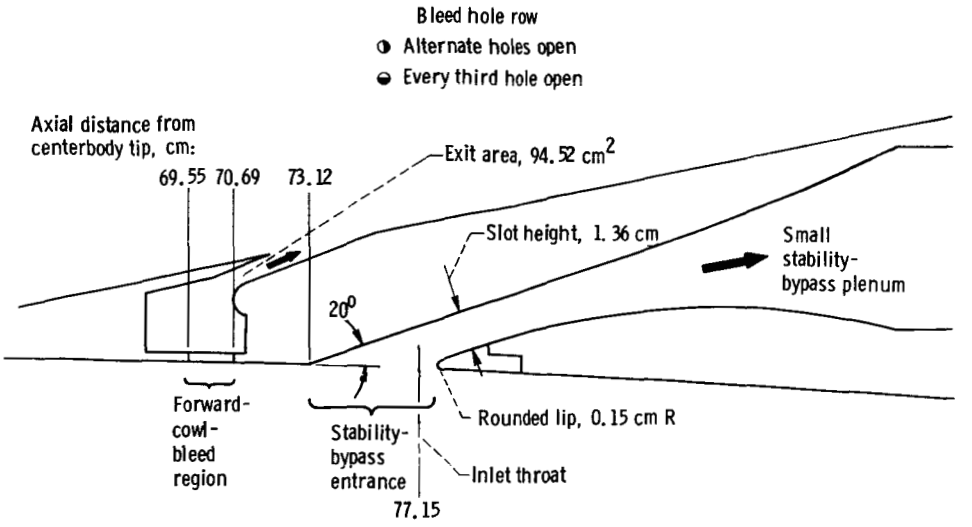

Hole pattern schematic

Forward-cowl bleed region	Forward centerbody bleed region	Mid-centerbody bleed region
◑◑◑	◑◑◑◑	◒◒◒◒◒◒◒◒◒◒◒

(b) Schematic of forward-slanted-slot stability-bypass entrance configuration and associated forward-cowl and centerbody bleed hole patterns.

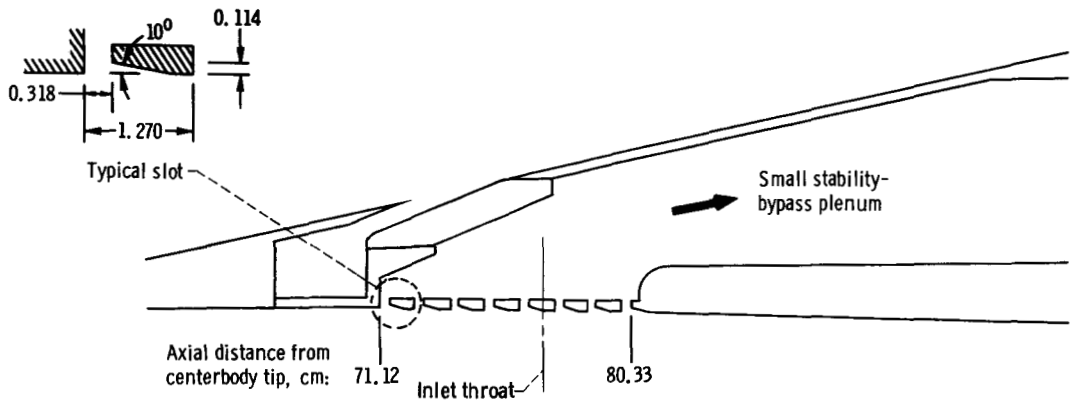

Hole pattern schematic

Forward centerbody bleed region	Mid-centerbody bleed region
◑◑◑◑	◒◒◒◒◒◒◒◒◒◒◒

(c) Schematic of distributed educated stability-bypass entrance configuration and associated centerbody bleed hole patterns.

Figure 7. - Concluded.

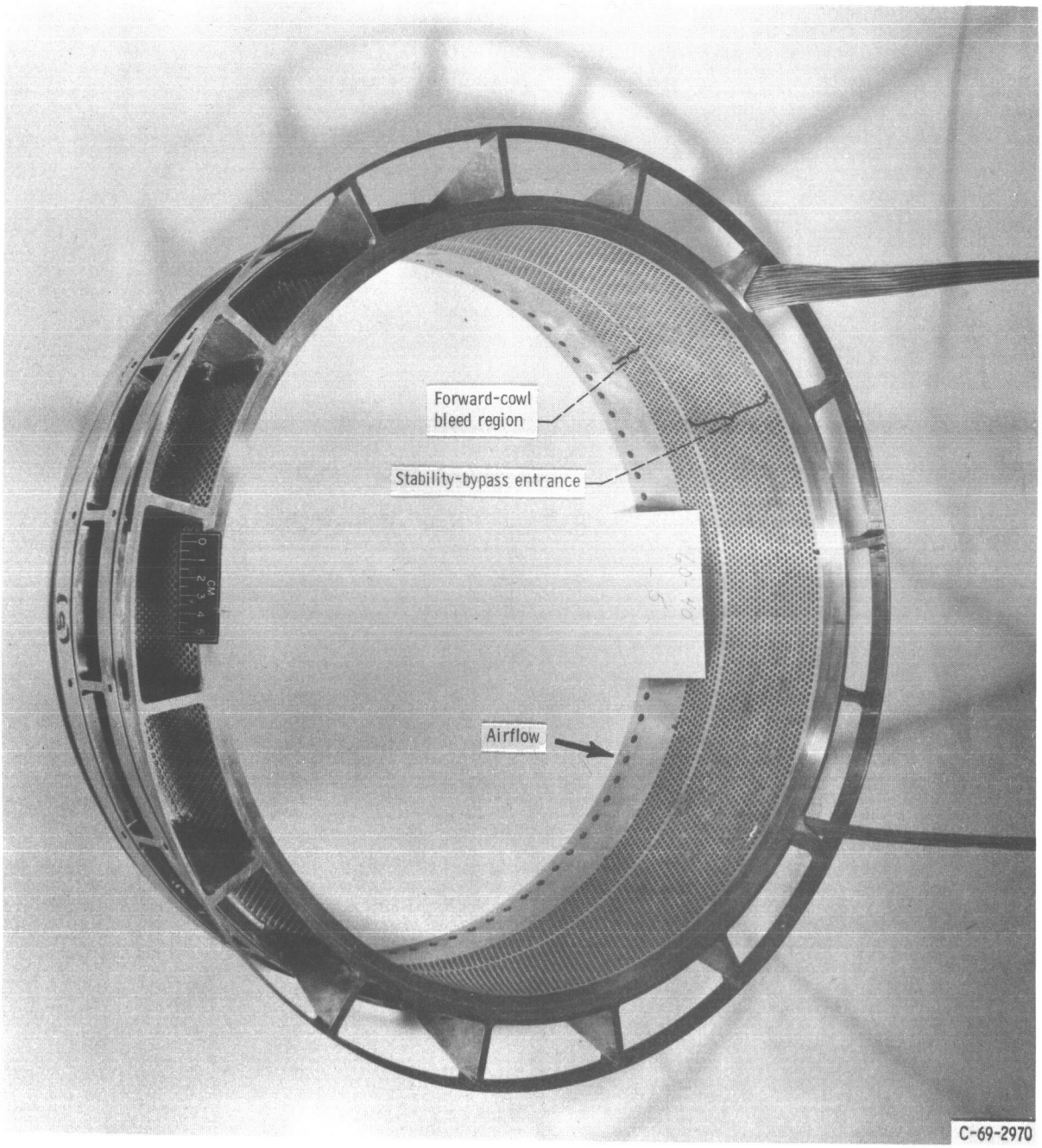

(a) Hole patterns of forward-cowl bleed region and stability-bypass entrance for distributed porous configurations.

Figure 8. - Cowl pieces illustrating some bleed regions and stability-bypass entrances.

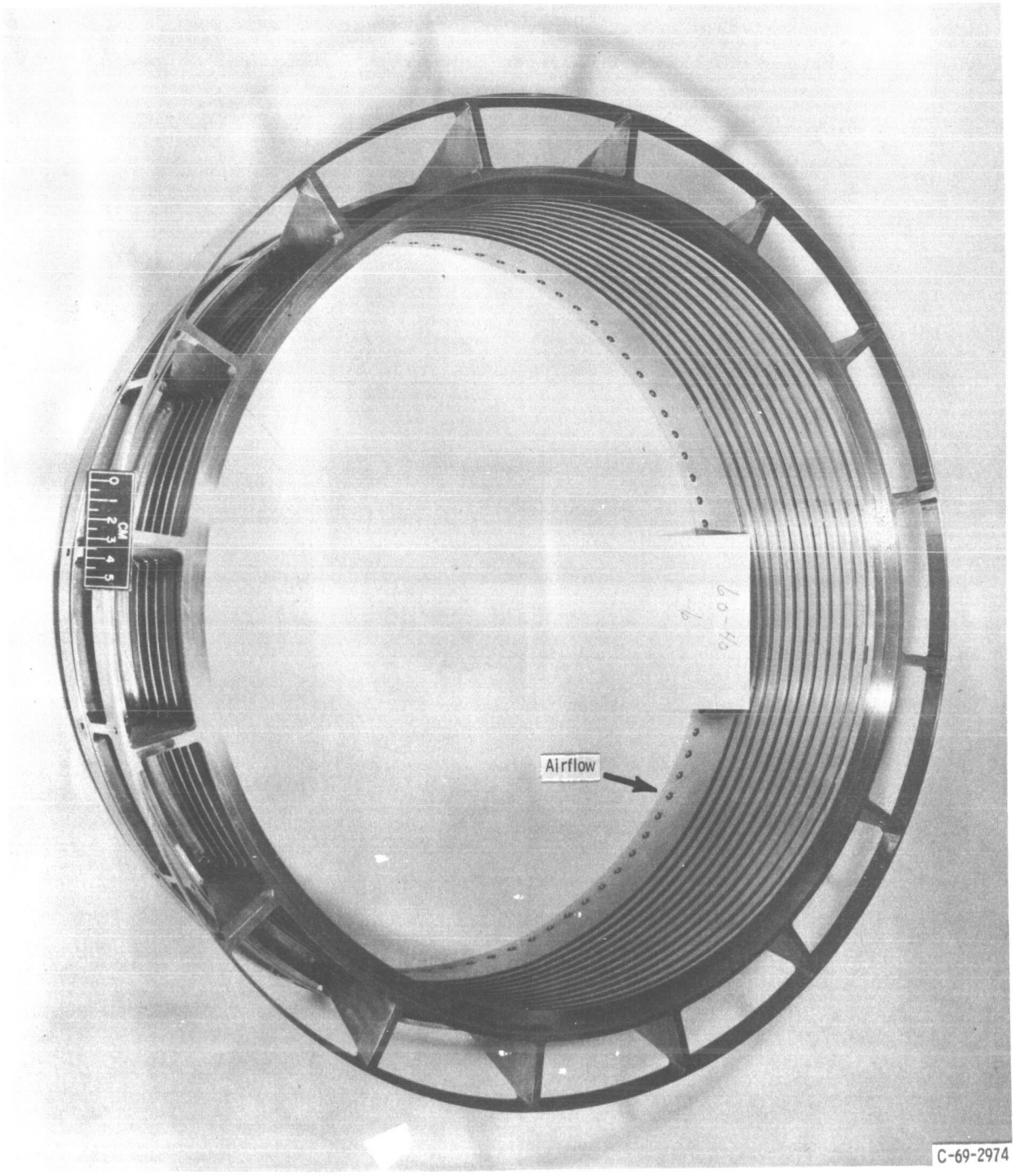

(b) Slots used for distributed educated configuration.

Figure 8. - Concluded.

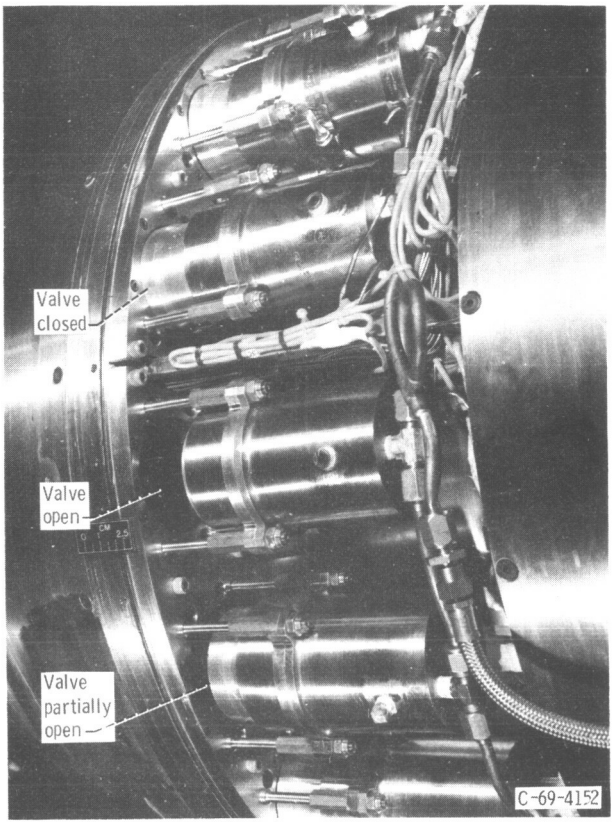

(a) Poppet-valve installation, several valve positions shown.

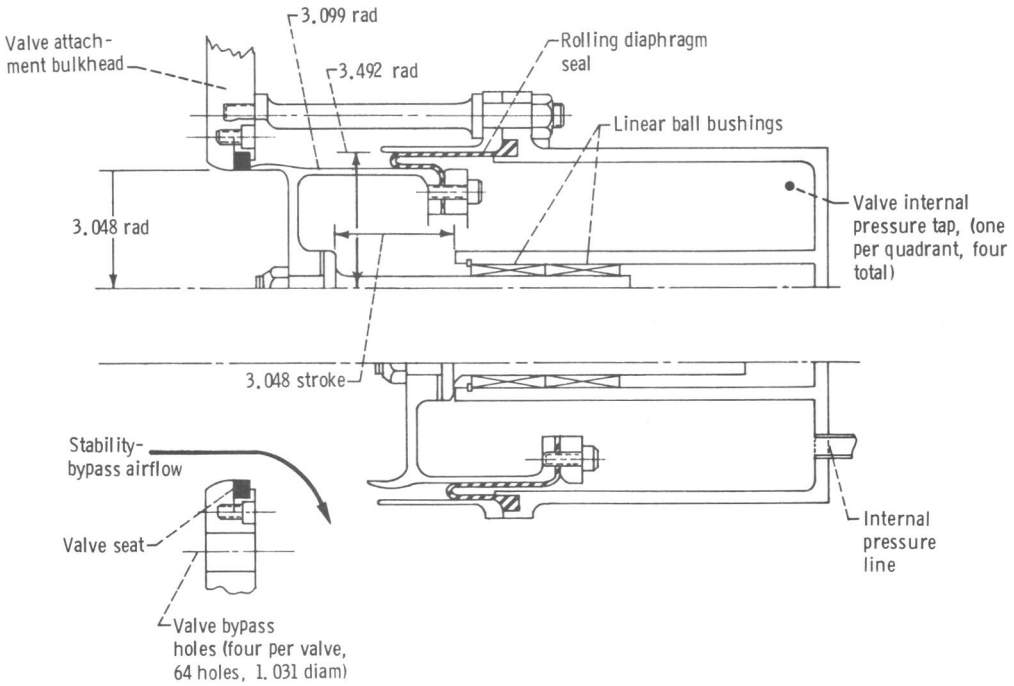

(b) Poppet-valve details. Dimensions are in centimeters.

Figure 9. - Poppet valve.

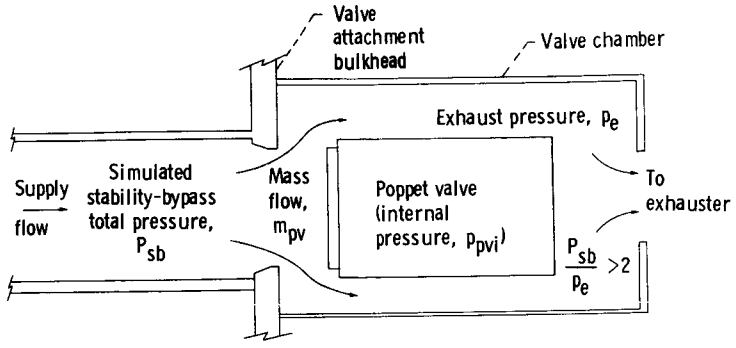

Schematic of bench test

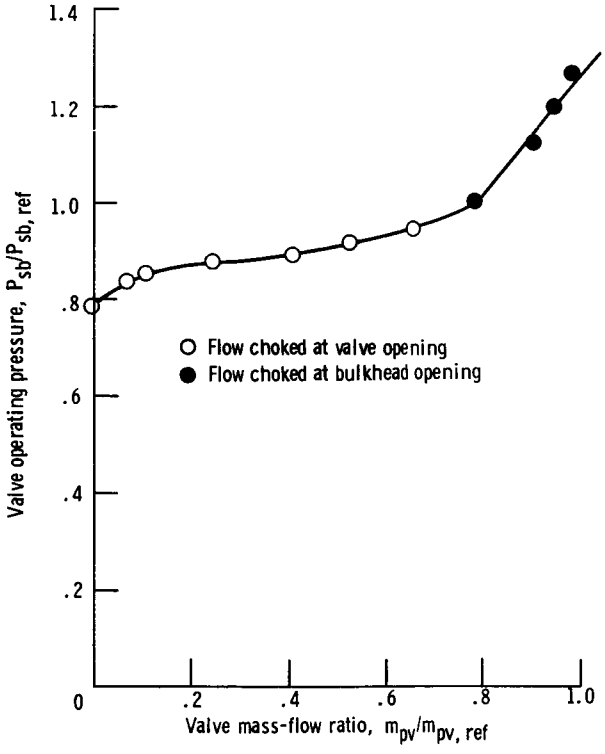

(c) Poppet-valve performance. Initial stability-bypass total pressure, P_{sb} = 3.1 N/cm^2; reference pressure, $P_{sb,ref}$ = 3.9 N/cm^2; exhaust pressure, p_e = 0.77 to 1.01 N/cm^2.

Figure 9. - Concluded.

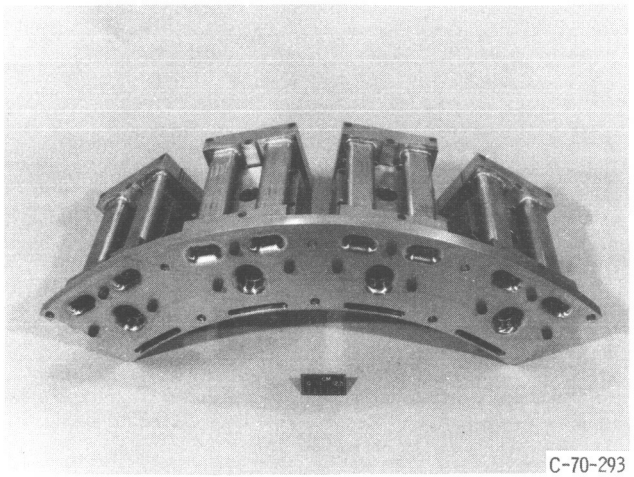

(a) Vortex valves and mounting plate.

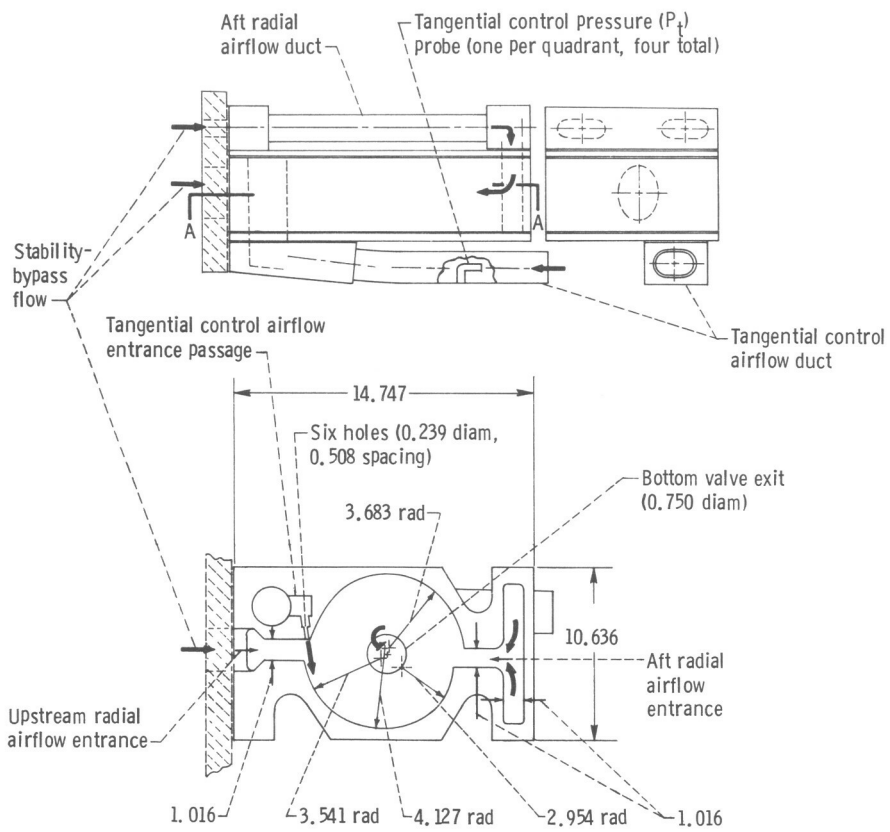

Section A-A

(b) Vortex valve details. Dimensions are in centimeters.

Figure 10. - Vortex valve.

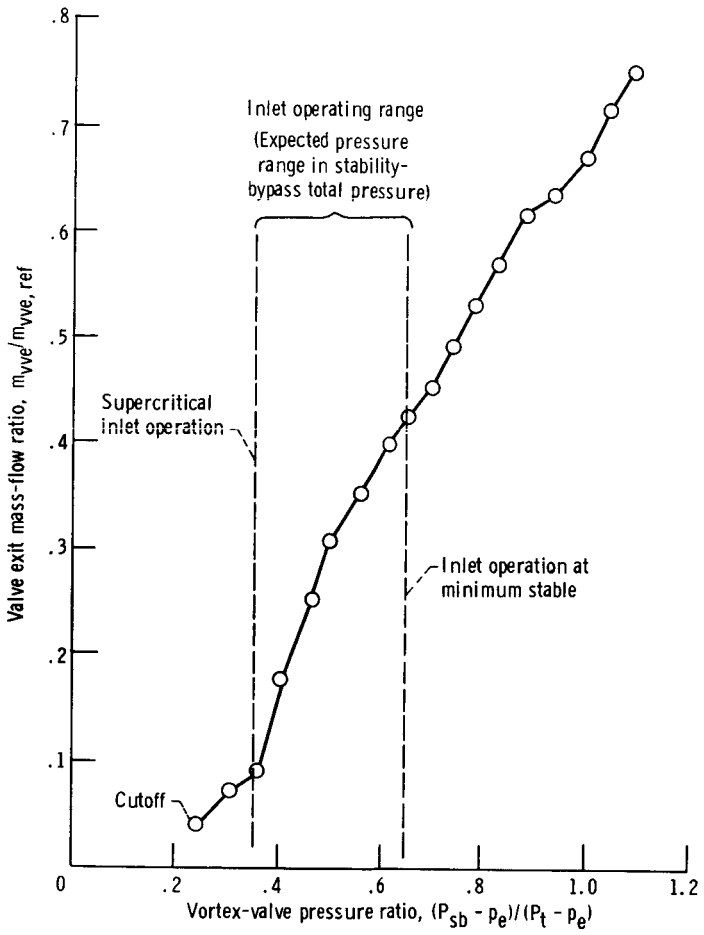

(c) Vortex-valve performance. Tangential nozzle supply pressure, P_t = 8.1 N/cm^2; exhaust pressure, p_e = 0.77 to 1.01 N/cm^2; radial supply pressure (stability-bypass total pressure), P_{sb} = 2.6 to 8.7 N/cm^2.

Figure 10. - Concluded.

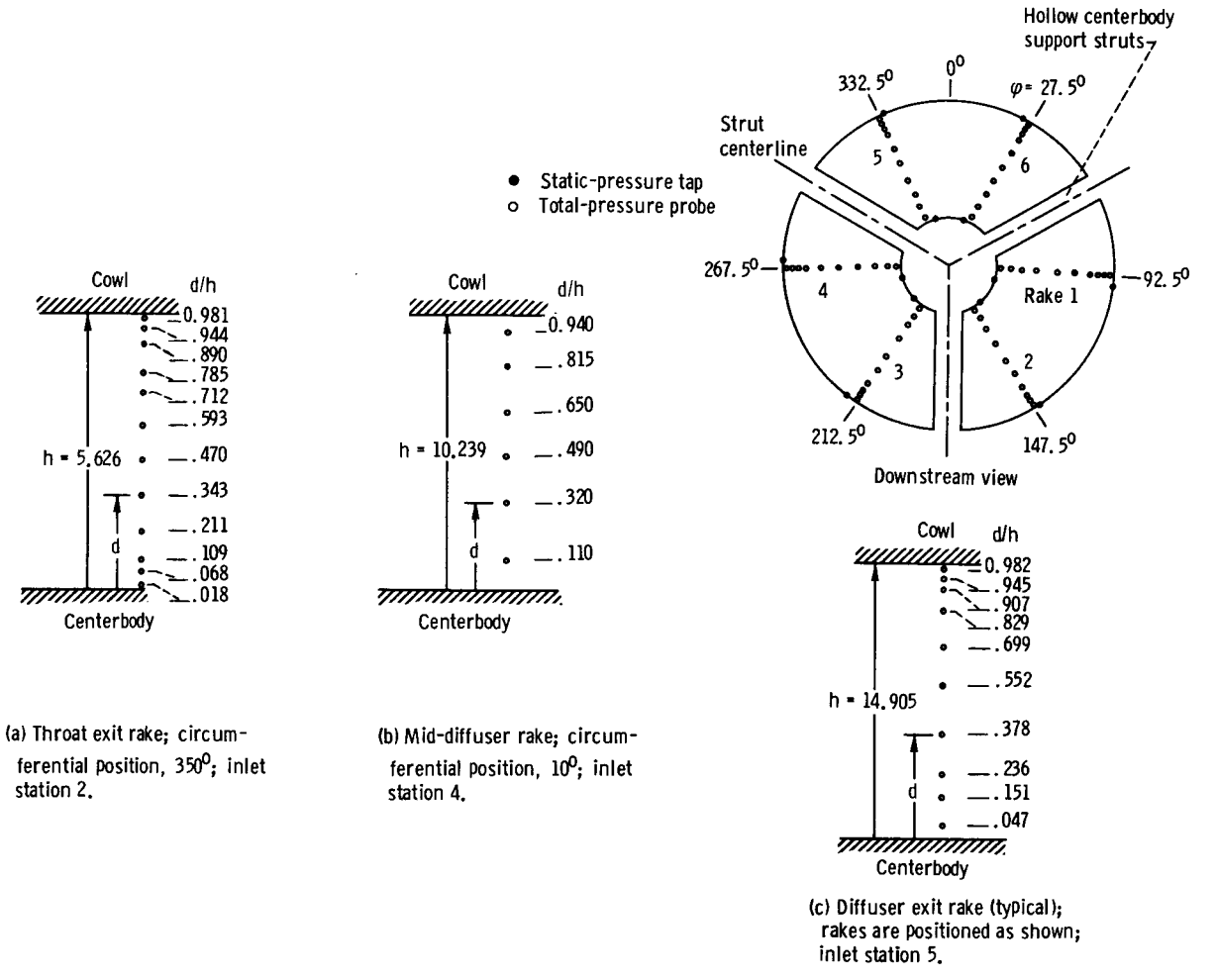

(a) Throat exit rake; circumferential position, 350°; inlet station 2.

(b) Mid-diffuser rake; circumferential position, 10°; inlet station 4.

(c) Diffuser exit rake (typical); rakes are positioned as shown; inlet station 5.

Figure 11. - Subsonic diffuser total-pressure rakes.

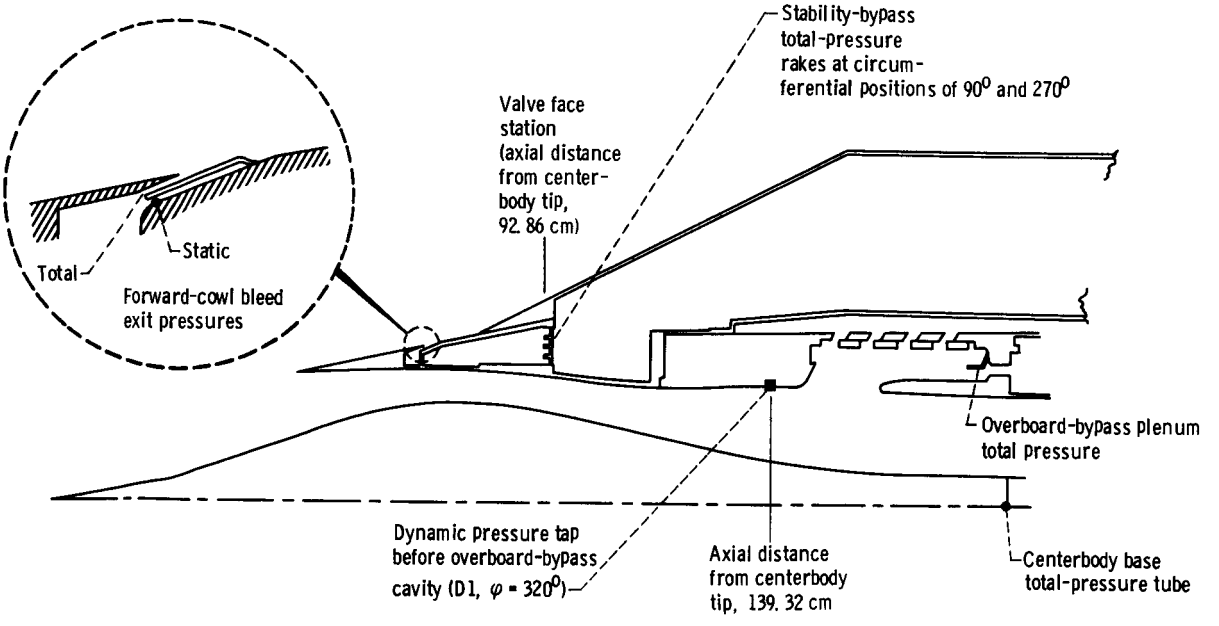

Figure 12. - Bleed and bypass pressure instrumentation.

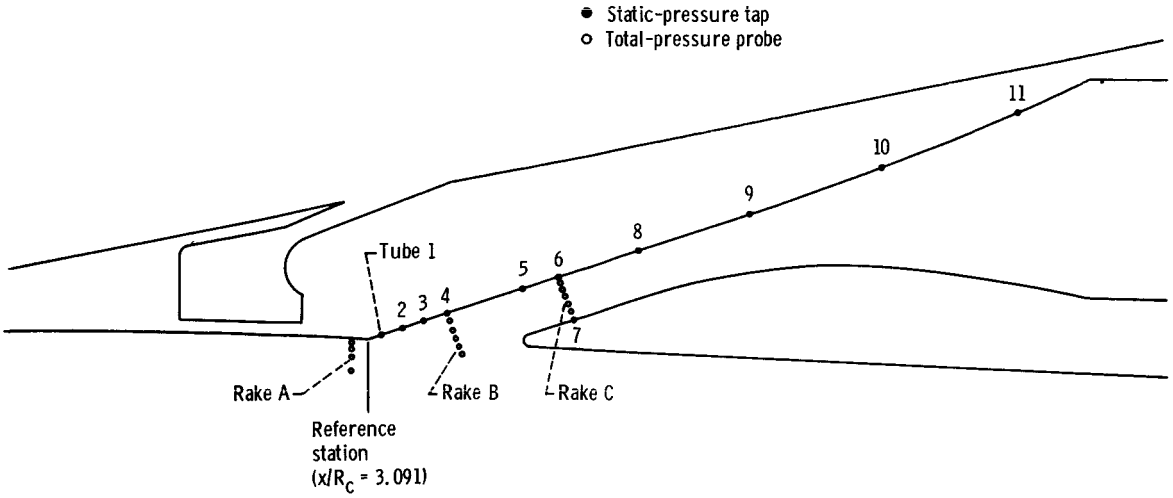

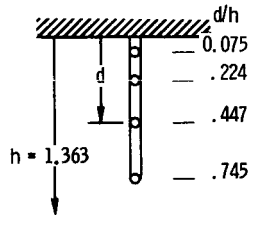

(a) Rake A; axial distance ratio, x/R_c = 3.069; circumferential position, 5°.

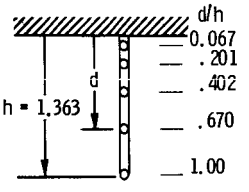

(b) Rake B; axial distance ratio, x/R_c = 3.215; circumferential position, 20°.

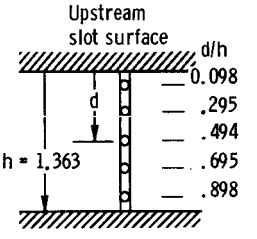

(c) Rake C; axial distance ratio, x/R_c = 3.335; circumferential position, 350°.

Slot static-pressure taps, top centerline	
Tube	Axial distance from reference station, L/R_c
1	0.015
2	.052
3	.088
4	.124
5	.200
6	.244
7	.264
8	.347
9	.470
10	.613
11	.760

Figure 13. - Forward-slanted-slot pressure instrumentation.

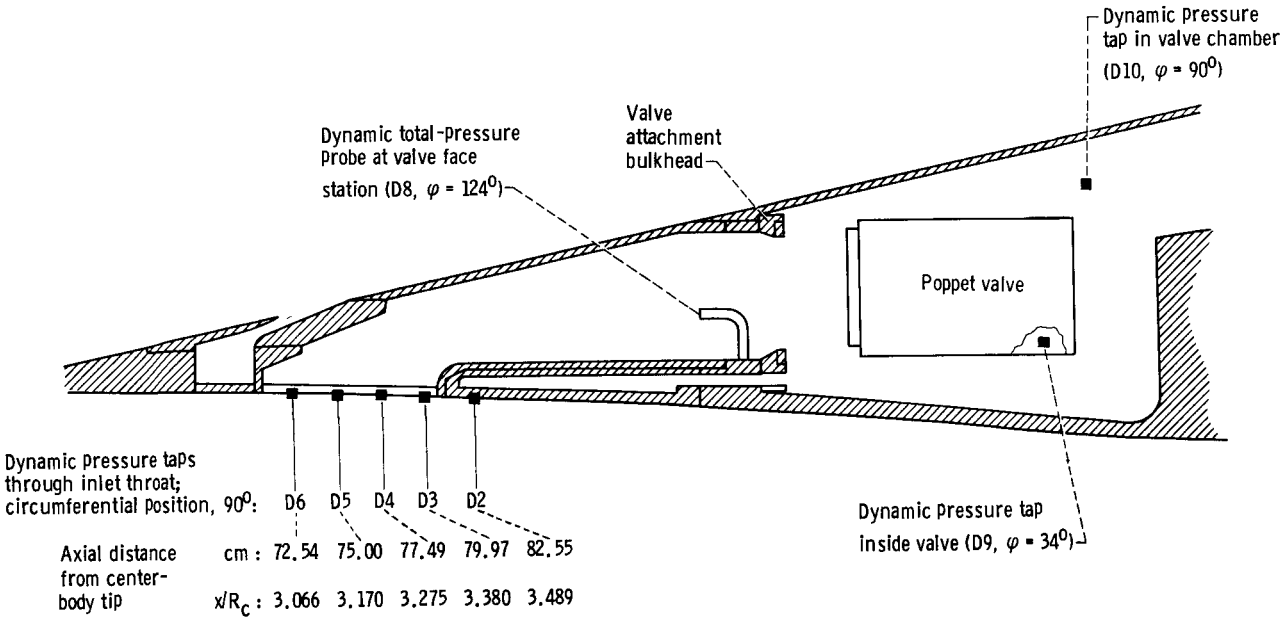

(a) Distributed porous configurations.

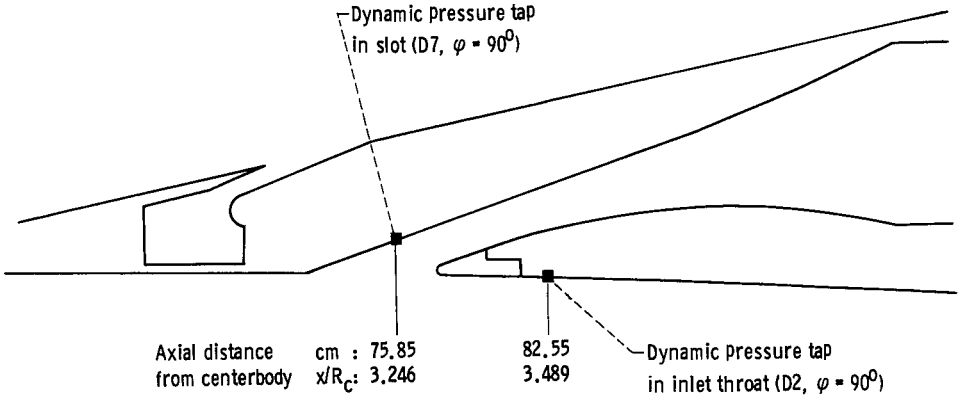

(b) Forward-slanted-slot configuration.

Figure 14. - Dynamic pressure instrumentation.

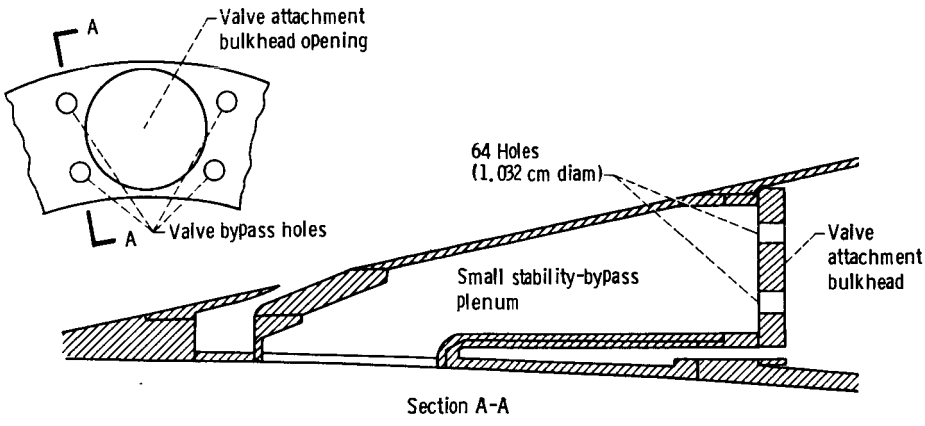

Section A-A

(a) Valve bypass hole locations for bypassing approximately 0.02 stability-bypass-to-free-stream mass-flow ratio with poppet valves closed.

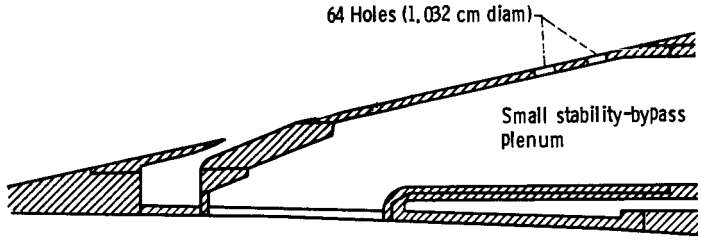

(b1) Distributed porous or distributed educated configurations.

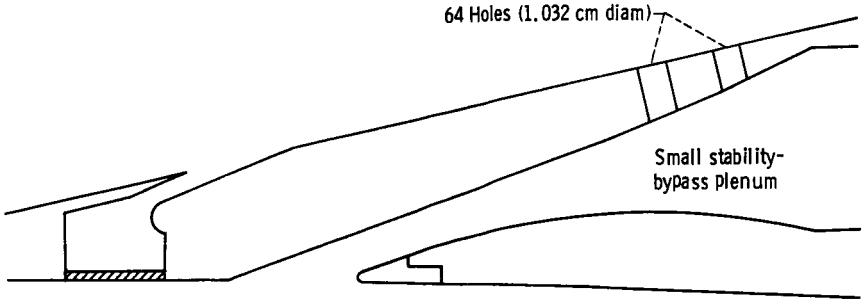

(b2) Forward-slanted-slot configuration.

(b) Valve bypass hole locations for bypassing approximately 0.02 stability-bypass-to-free-stream mass-flow ratio with vortex valves at cutoff.

Figure 15. - Placement of valve bypass holes.

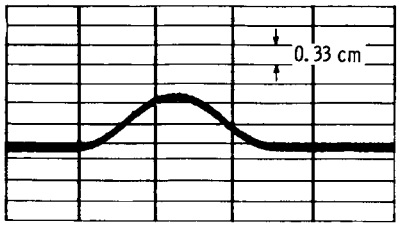

(a) Commanded overboard-bypass-door movement.

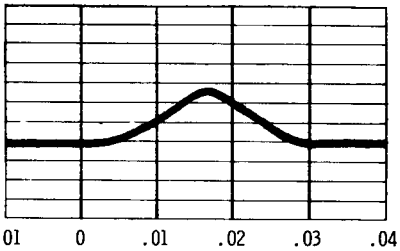

(b) Overboard-bypass-door response.

Figure 16. - Overboard-bypass-door response at a transient pulse frequency of 40 pseudohertz.

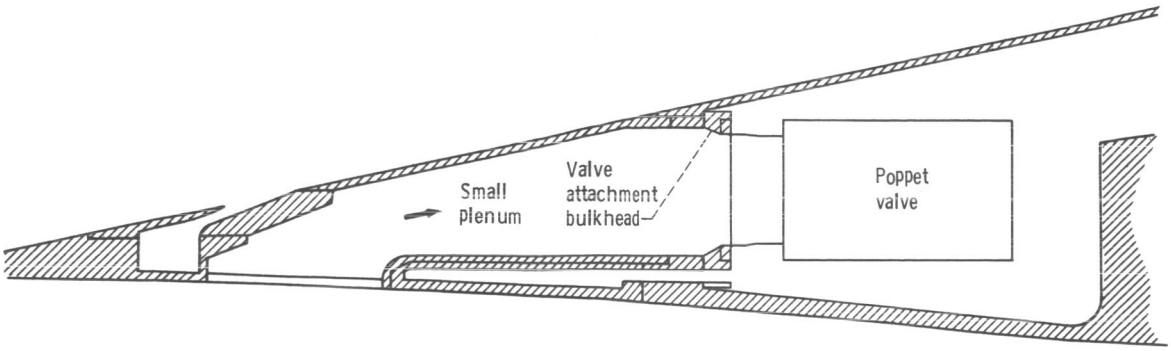

(a) Poppet valve closed; small stability-bypass plenum volume.

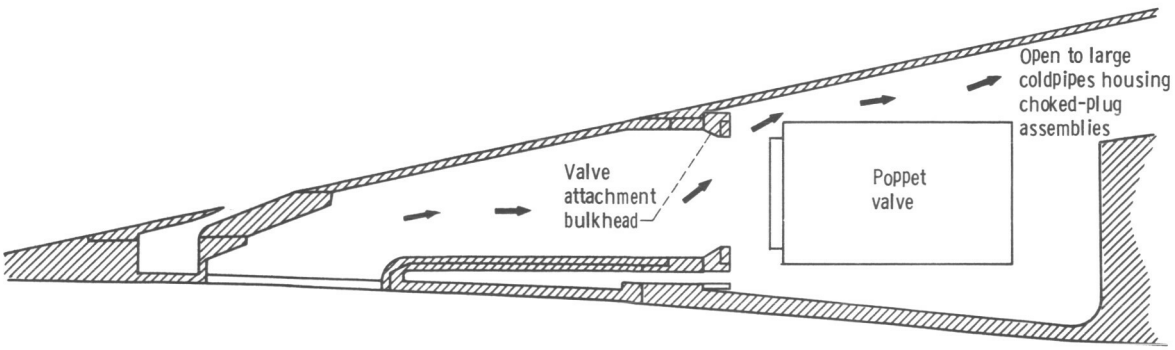

(b) Poppet valve open; large stability-bypass plenum volume.

Figure 17. - Small and large stability-bypass plenum volumes.

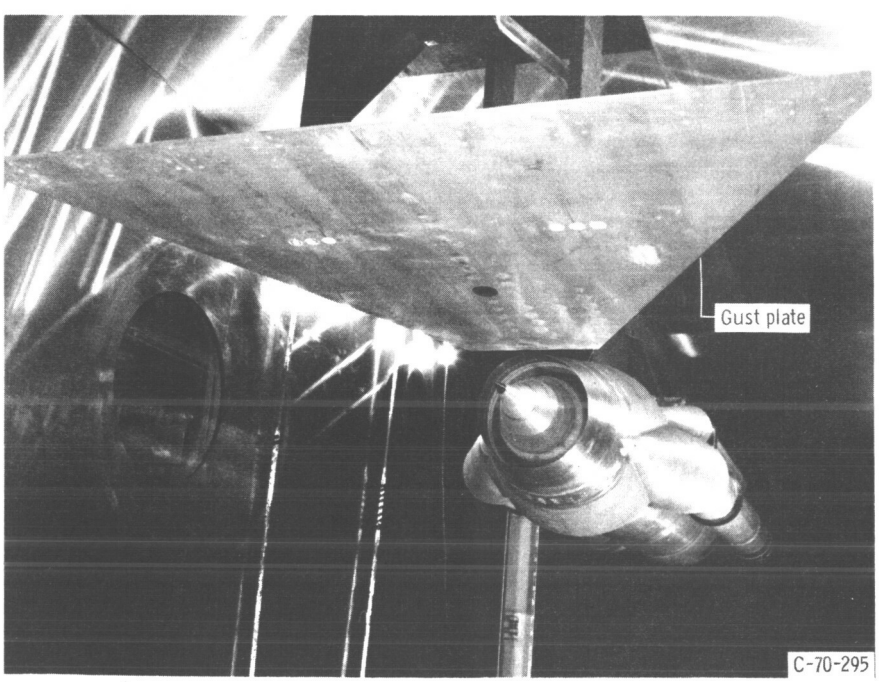

Figure 18. - External disturbance generator and inlet model installed in 10- by 10-Foot Supersonic Wind Tunnel.

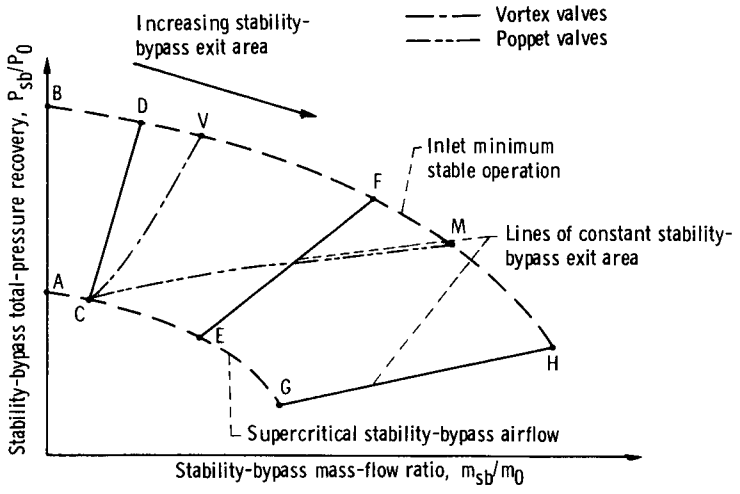

(a) Stability bypass performance.

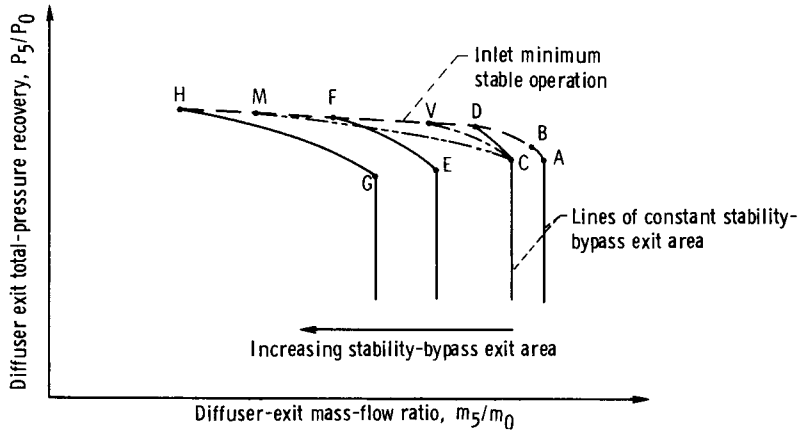

(b) Inlet performance.

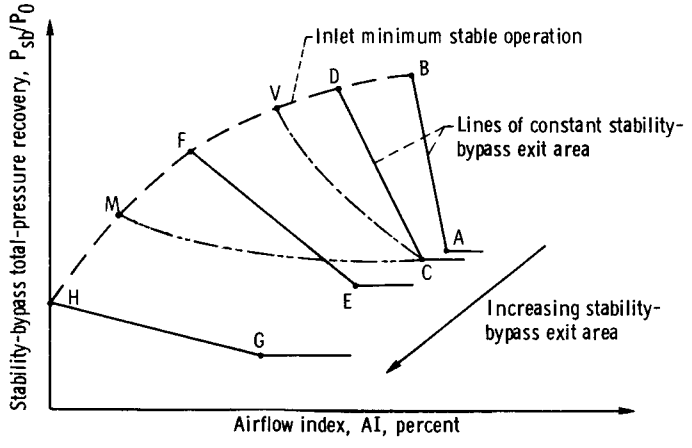

(c) Airflow index.

Figure 19. - Inlet stability data.

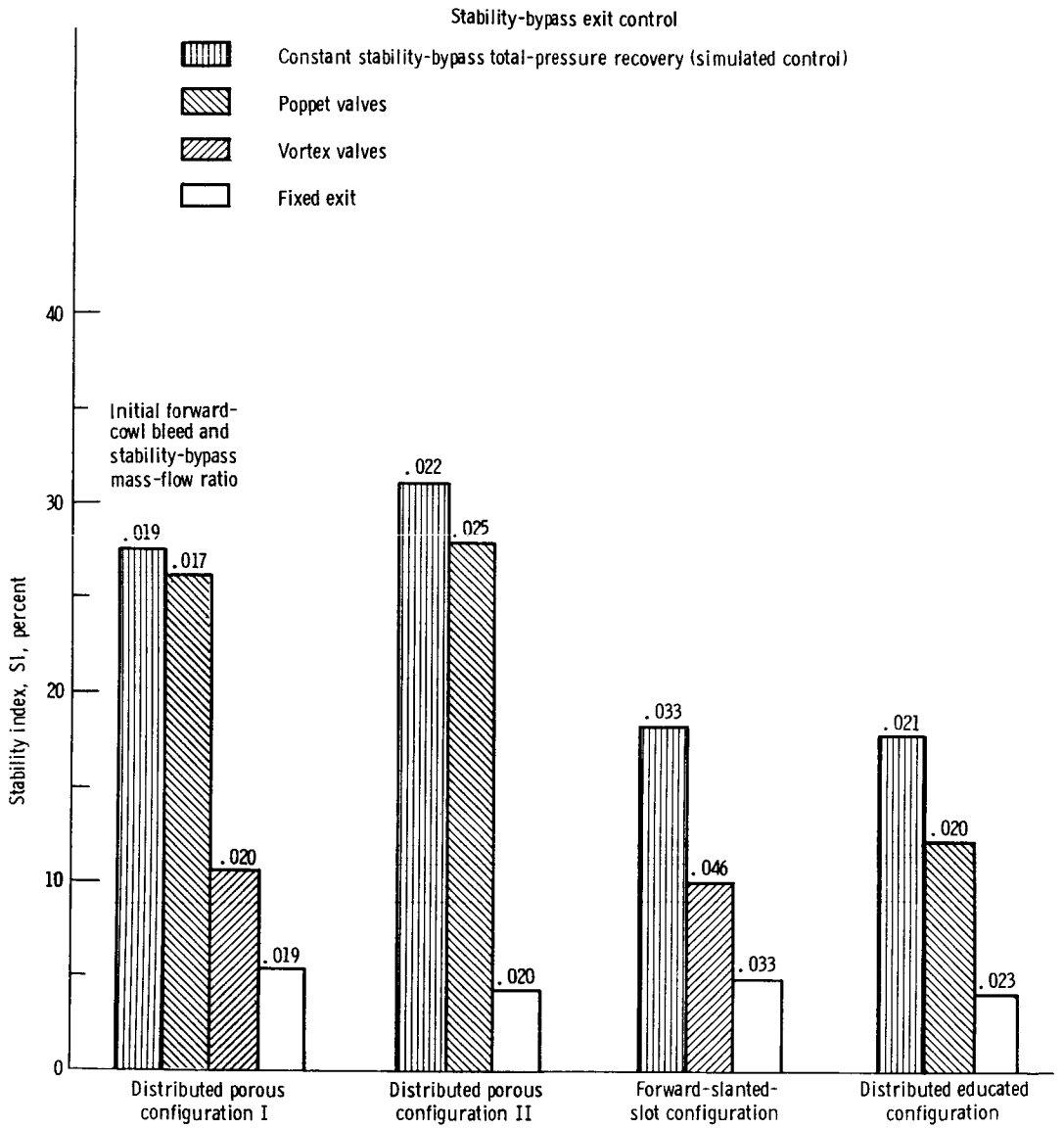

Figure 20. - Stability index obtained with various stability-bypass exit controls and stability-bypass entrance configurations. Initial inlet total-pressure recovery, $P_5/P_0 \approx 0.90$.

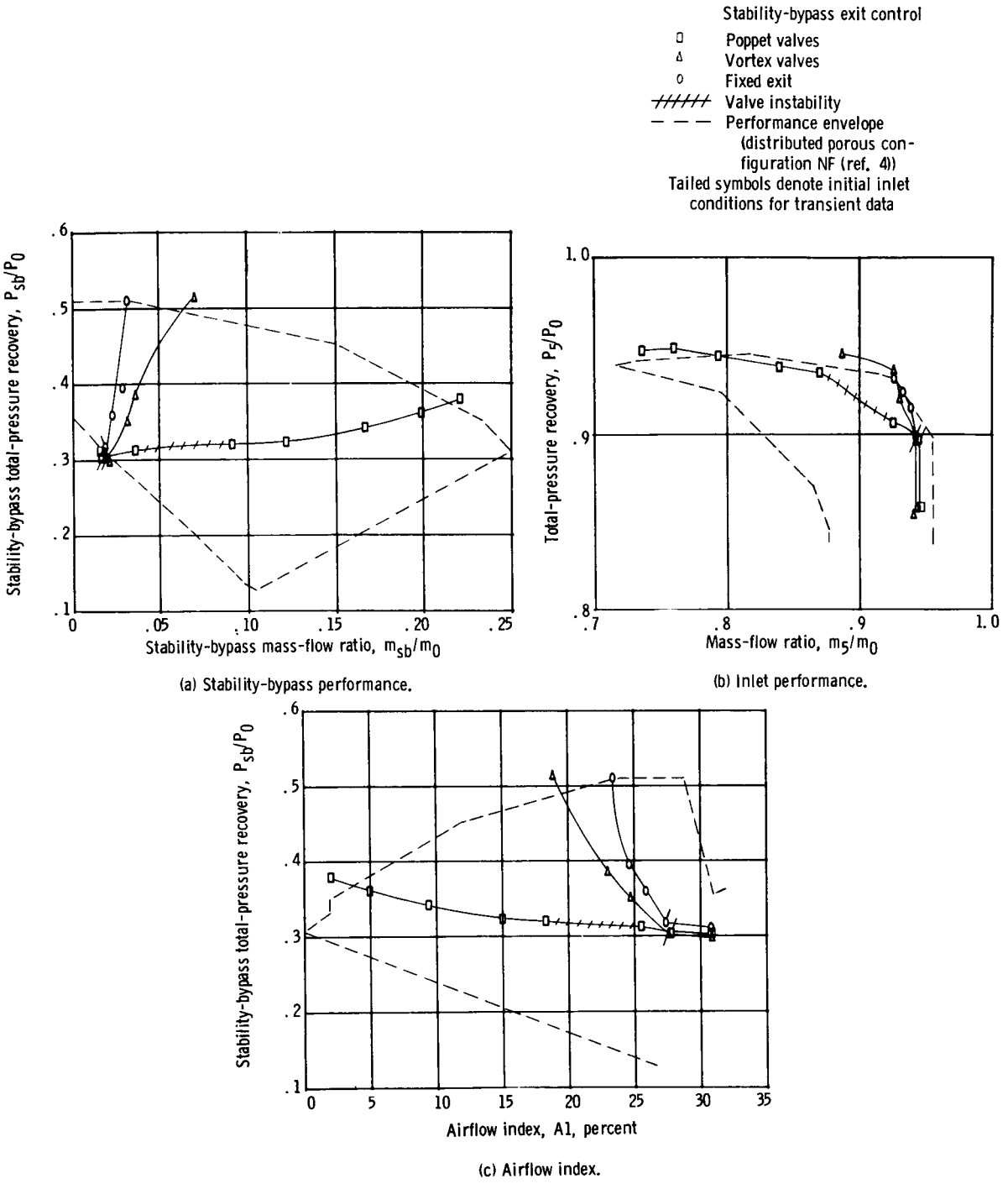

(a) Stability-bypass performance.

(b) Inlet performance.

(c) Airflow index.

Figure 21. - Performance of stability-bypass exit controls with distributed porous configuration I as the stability-bypass entrance configuration.

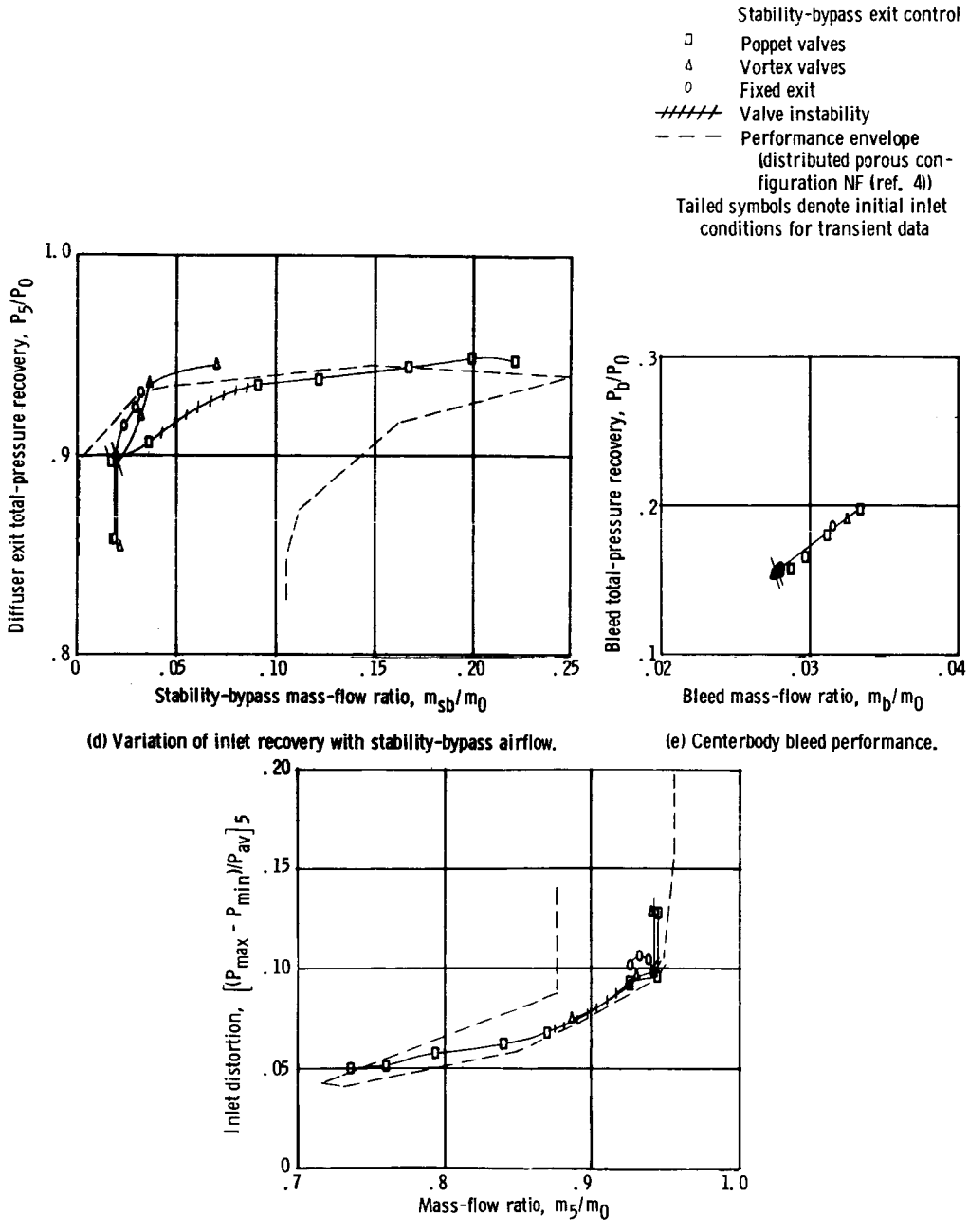

(d) Variation of inlet recovery with stability-bypass airflow.

(e) Centerbody bleed performance.

(f) Distortion.

Figure 21. - Concluded.

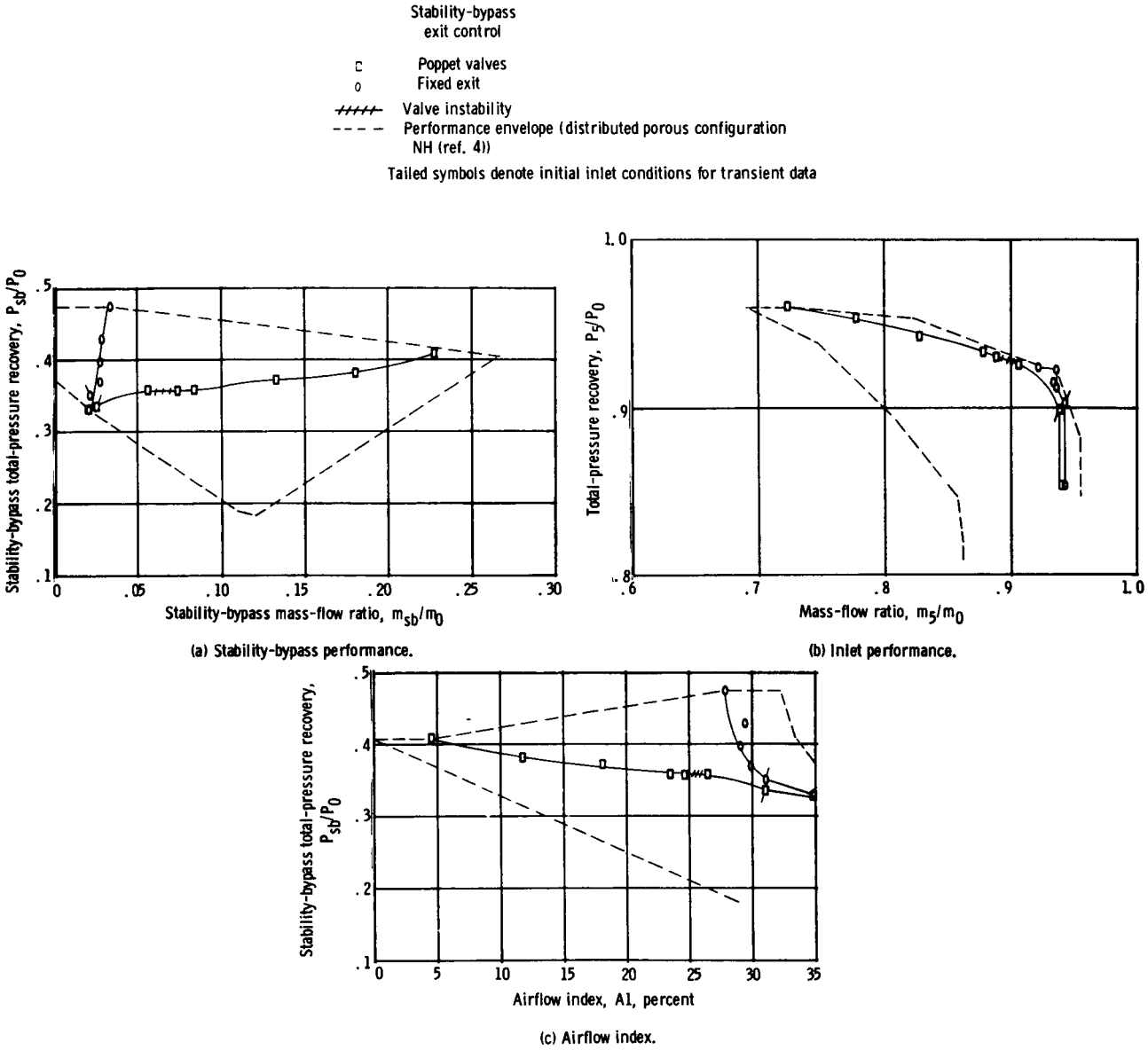

Figure 22. - Performance of stability-bypass exit controls with distributed porous configuration II as the stability-bypass entrance configuration.

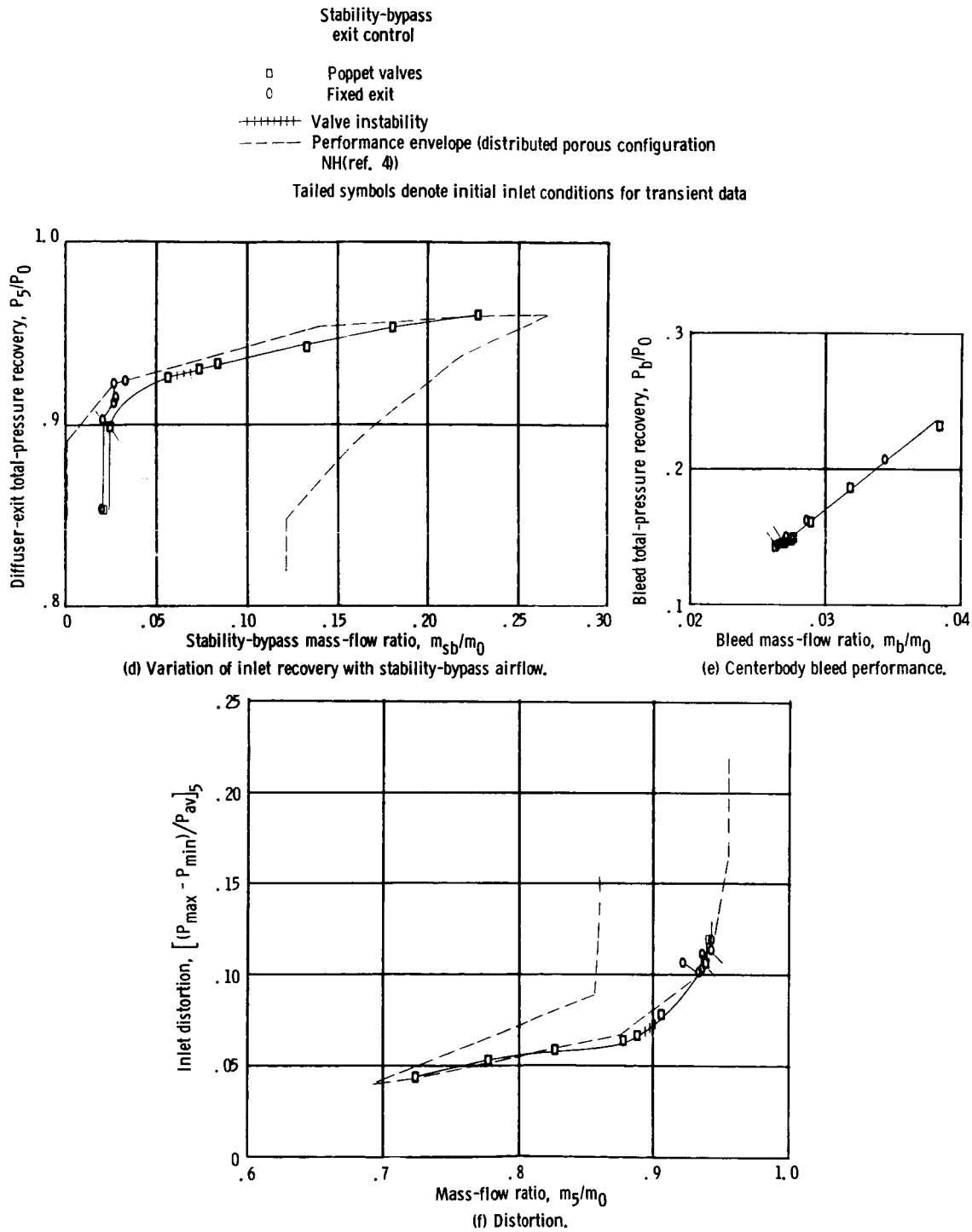

(d) Variation of inlet recovery with stability-bypass airflow.

(e) Centerbody bleed performance.

(f) Distortion.

Figure 22. - Concluded.

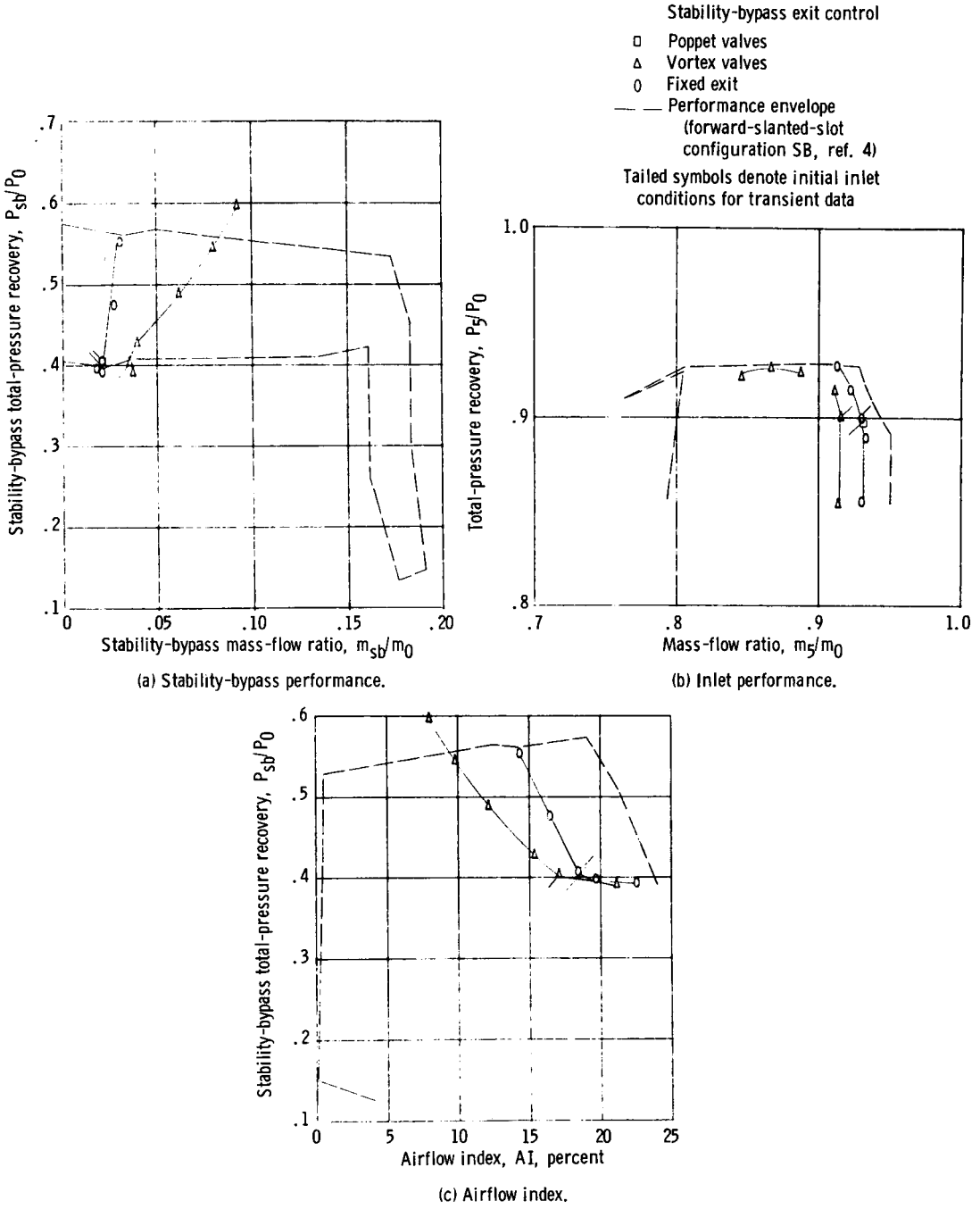

(a) Stability-bypass performance.

(b) Inlet performance.

(c) Airflow index.

Figure 23. - Performance of stability-bypass exit controls with forward-slanted-slot stability-bypass entrance configuration.

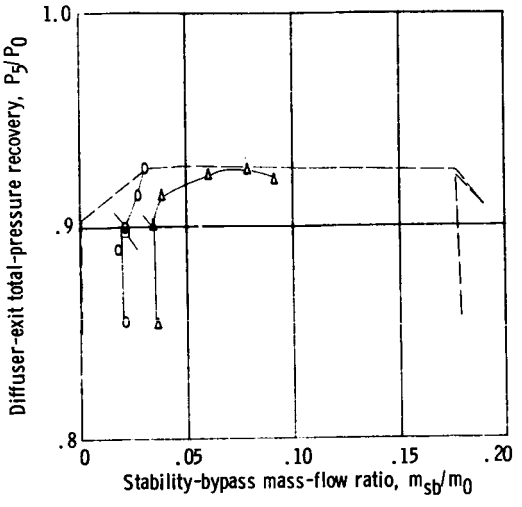

(d) Variation of inlet recovery with stability-bypass airflow.

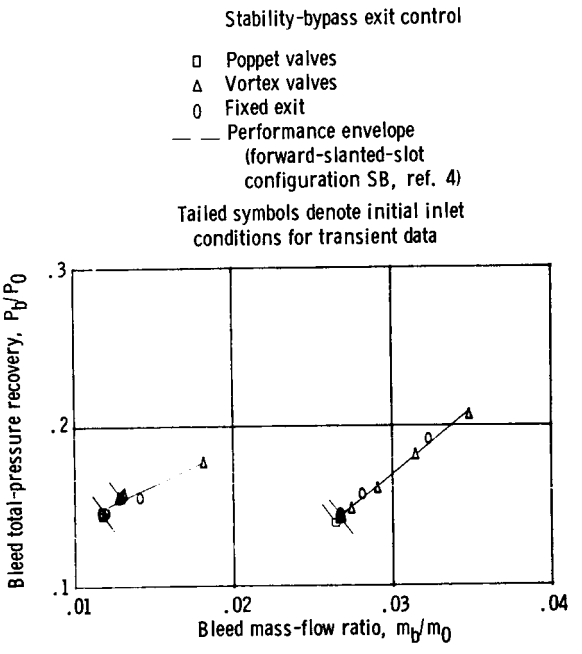

(e) Forward-cowl and centerbody bleed performance.

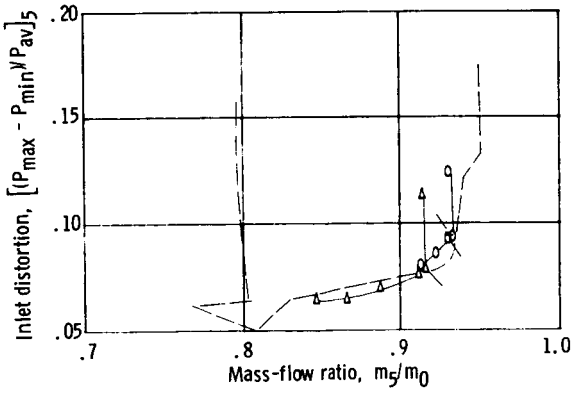

(f) Distortion.

Figure 23. - Concluded.

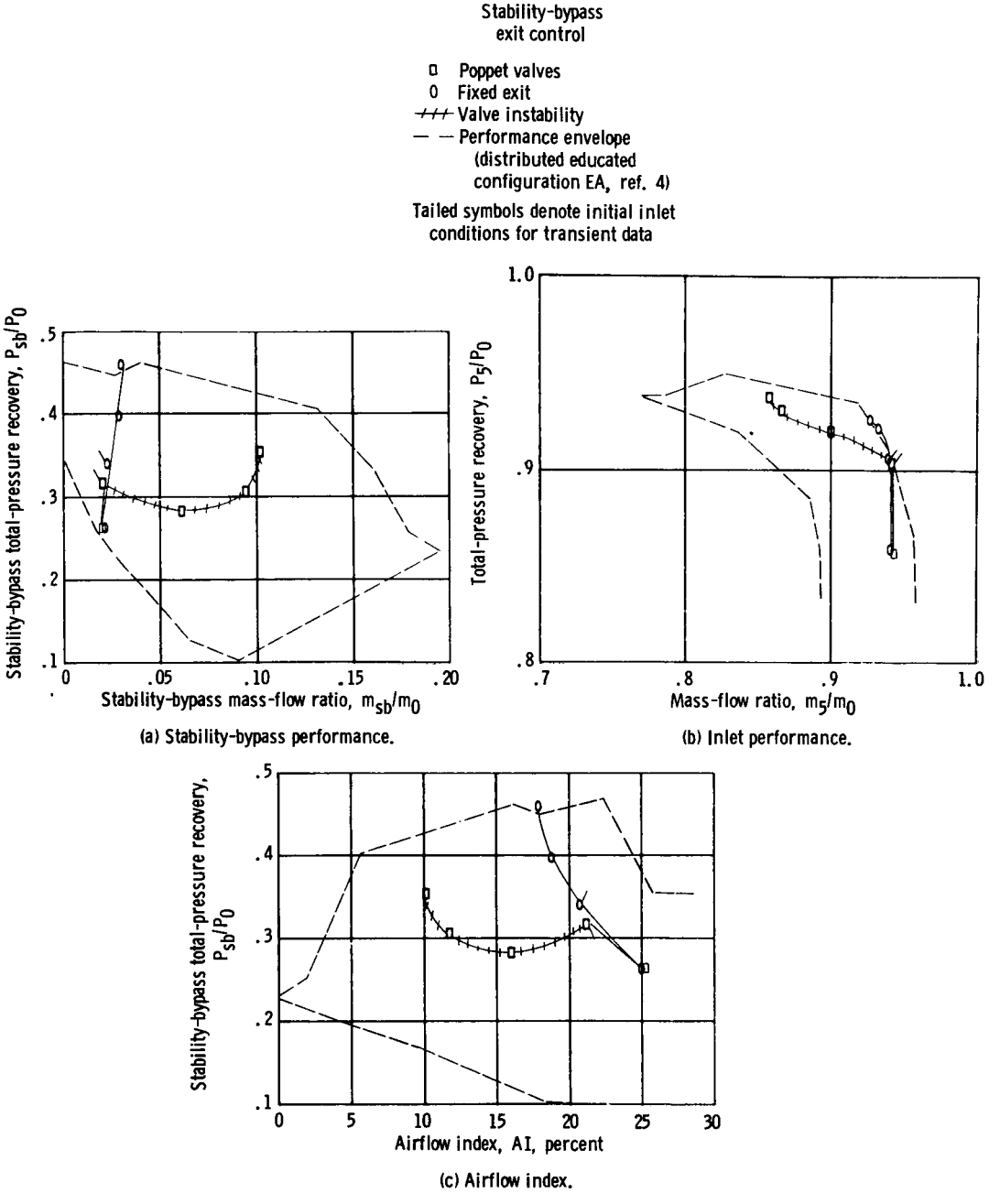

(a) Stability-bypass performance.

(b) Inlet performance.

(c) Airflow index.

Figure 24. - Performance of stability-bypass exit controls with distributed educated stability-bypass entrance configuration.

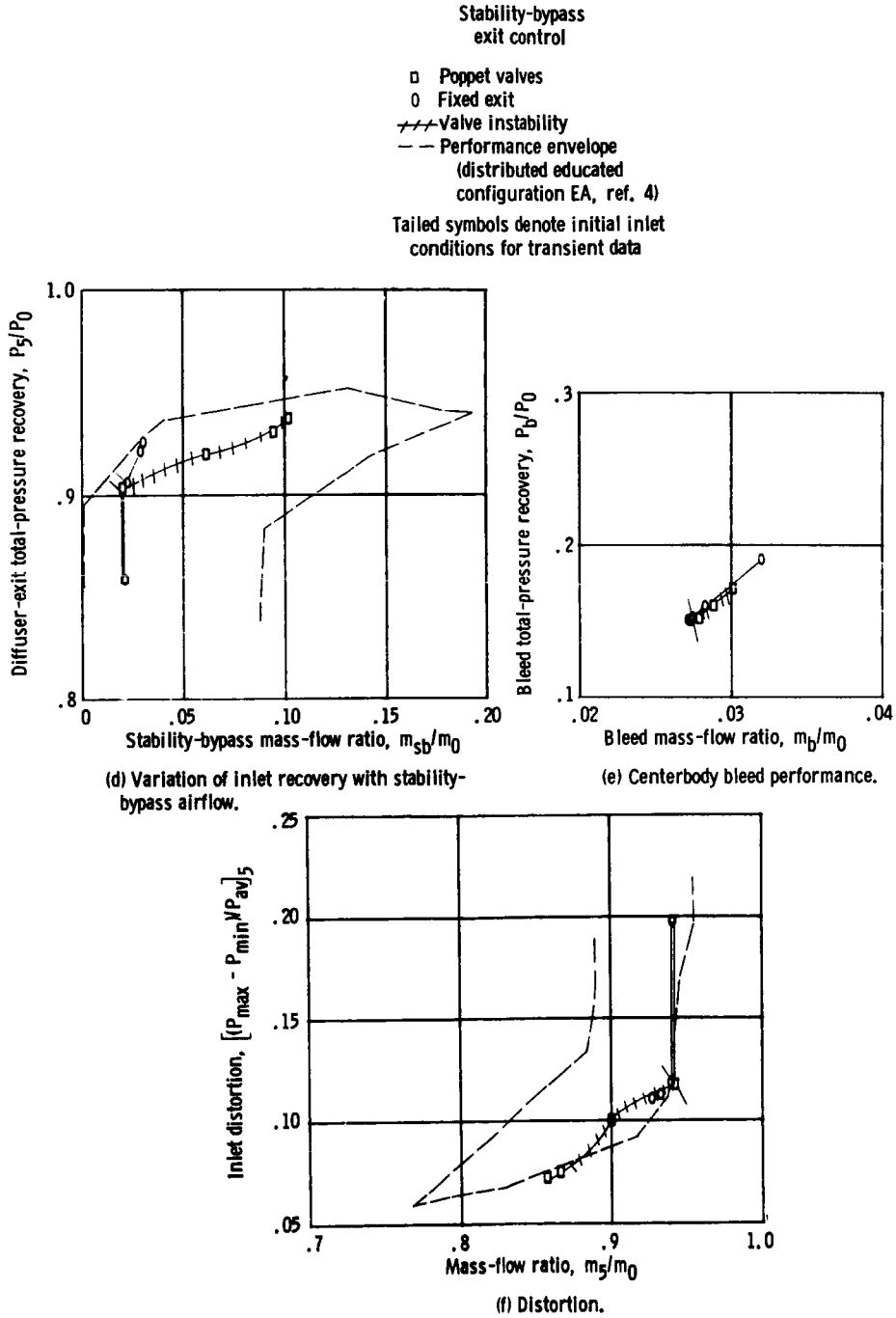

(d) Variation of inlet recovery with stability-bypass airflow.

(e) Centerbody bleed performance.

(f) Distortion.

Figure 24. - Concluded.

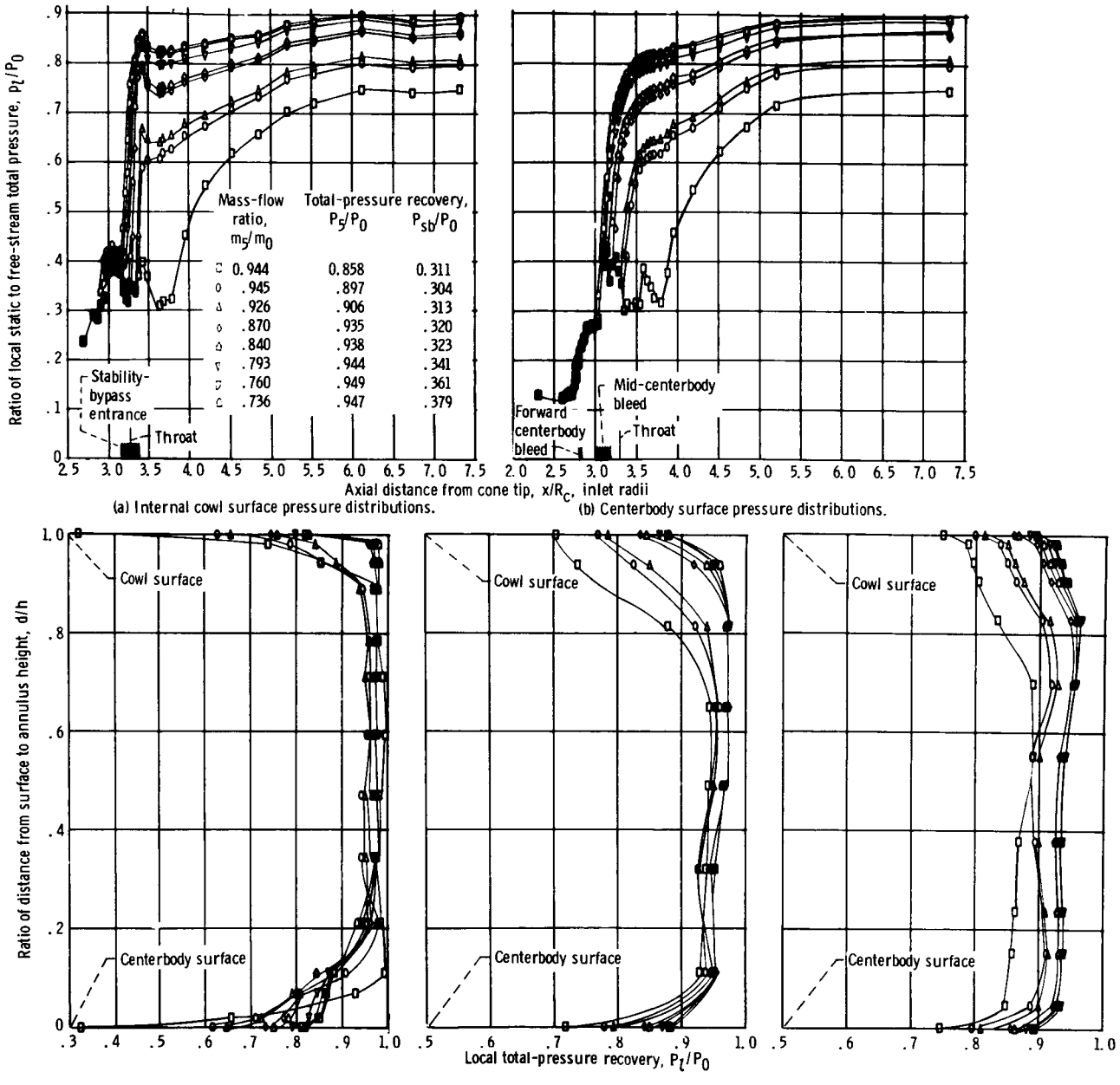

(a) Internal cowl surface pressure distributions.

(b) Centerbody surface pressure distributions.

(c) Throat exit, station 2. (Symbols at 0 and 1.0 d/h denote static pressures.)

(d) Mid diffuser, station 4. (Symbols at 0 and 1.0 d/h denote static pressures.)

(e) Diffuser exit, station 5, rake 6. (Symbols at 0 and 1.0 d/h denote static pressures.)

Figure 25. - Diffuser static- and total-pressure distributions obtained with poppet valves and distributed porous configuration I.

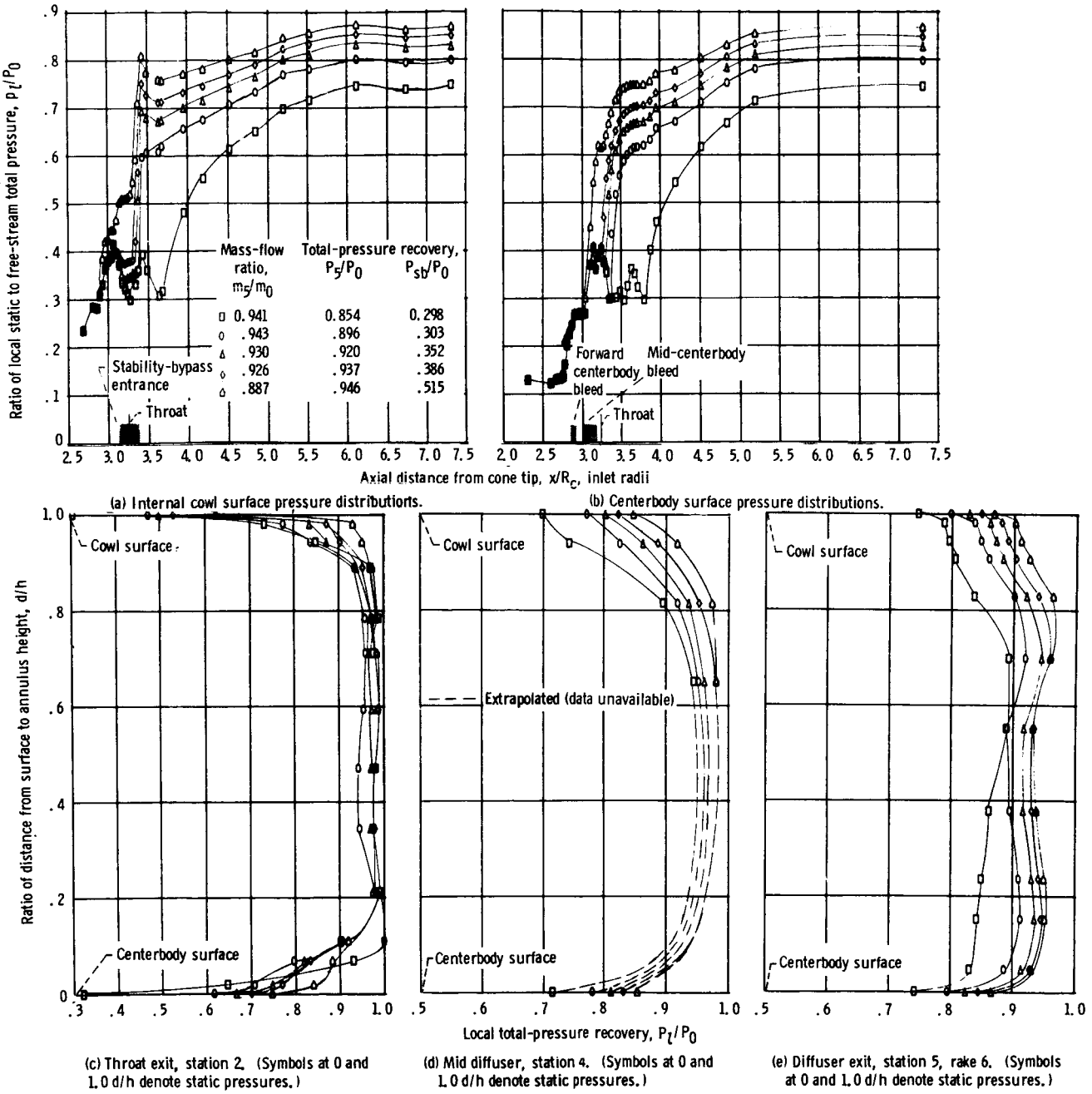

(c) Throat exit, station 2. (Symbols at 0 and 1.0 d/h denote static pressures.)

(d) Mid diffuser, station 4. (Symbols at 0 and 1.0 d/h denote static pressures.)

(e) Diffuser exit, station 5, rake 6. (Symbols at 0 and 1.0 d/h denote static pressures.)

Figure 26. - Diffuser static- and total-pressure distributions obtained from vortex valves and distributed porous configuration I.

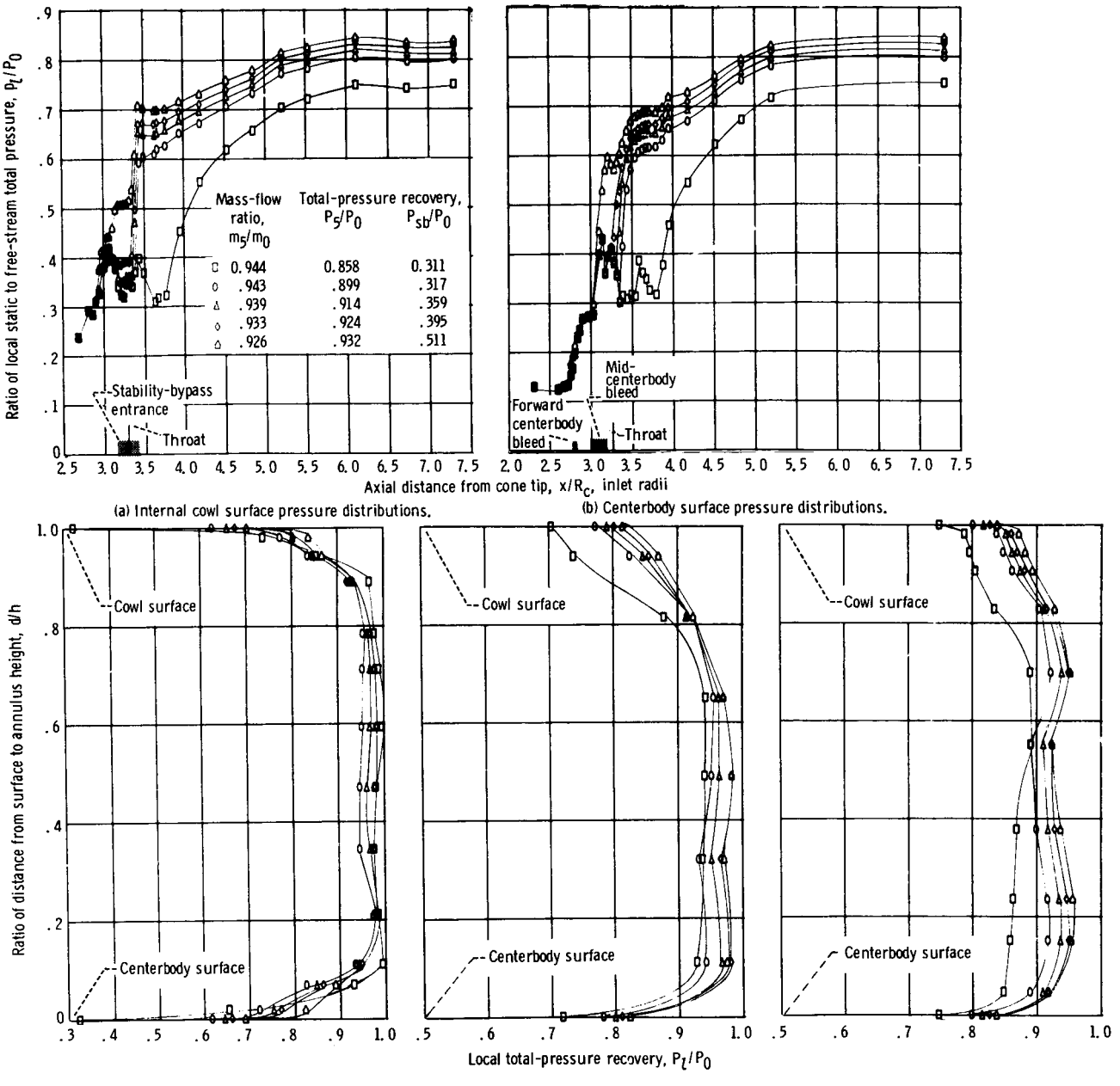

Figure 27. - Diffuser static- and total-pressure distributions obtained with fixed exit and distributed porous configuration I.

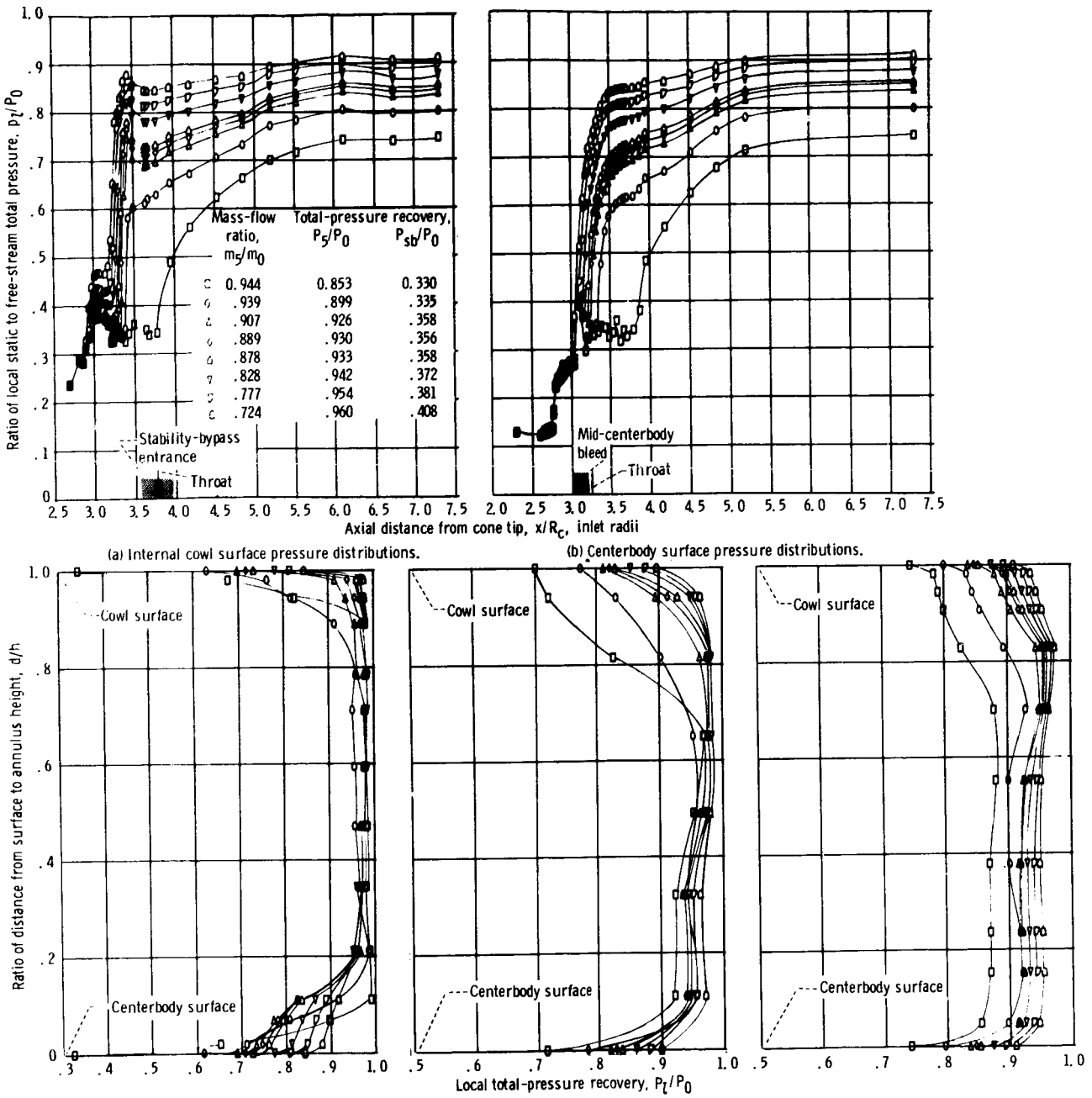

(c) Throat exit, station 2. (Symbols at 0 and 1.0 d/h denote static pressures.)

(d) Mid diffuser, station 4. (Symbols at 0 and 1.0 d/h denote static pressures.)

(e) Diffuser exit, station 5, rake 6. (Symbols at 0 and 1.0 d/h denote static pressures.)

Figure 28. - Diffuser static- and total-pressure distributions obtained with poppet valves and distributed porous configuration II.

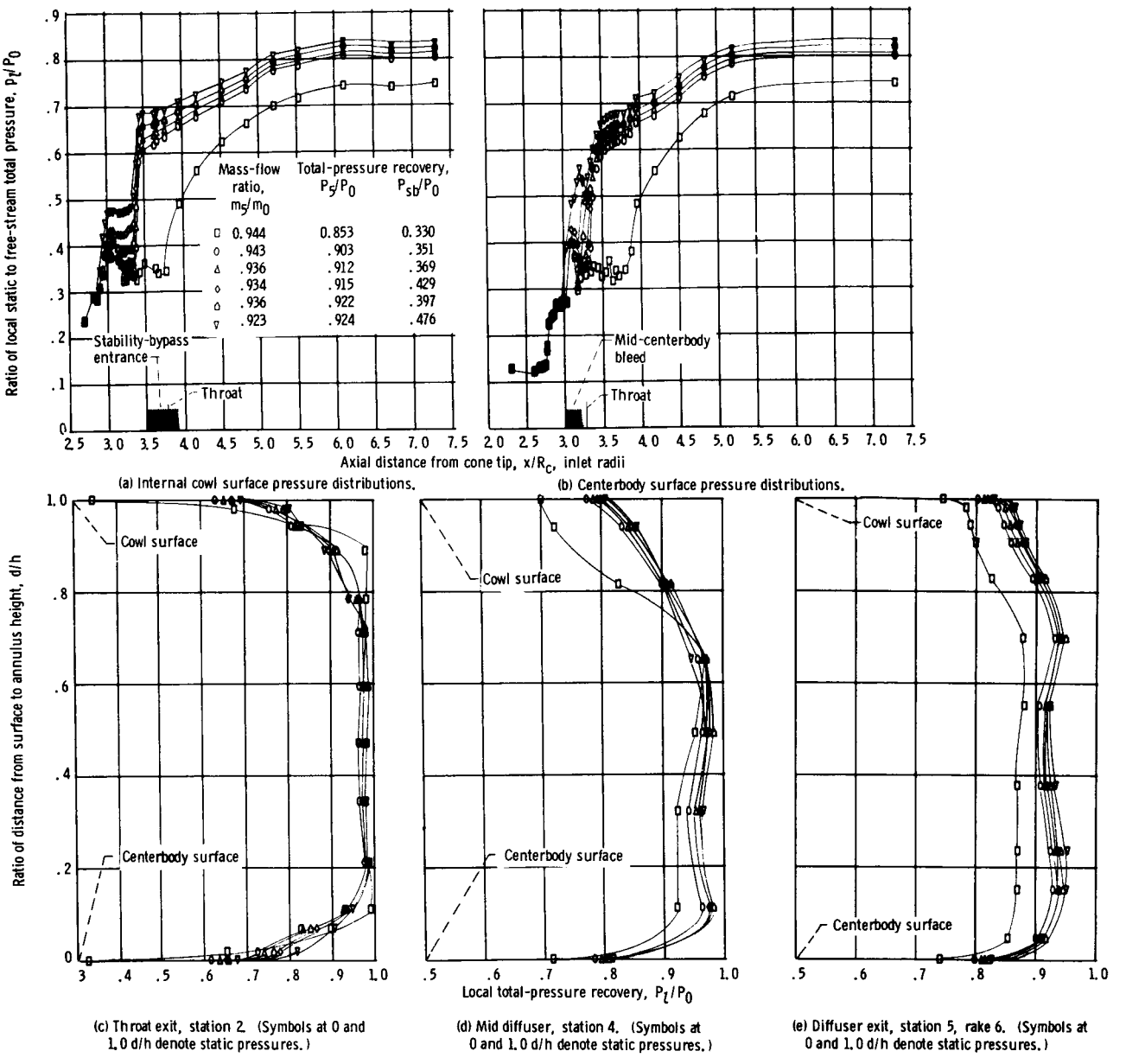

Figure 29. - Diffuser static- and total-pressure distributions obtained with fixed exit and distributed porous configuration II.

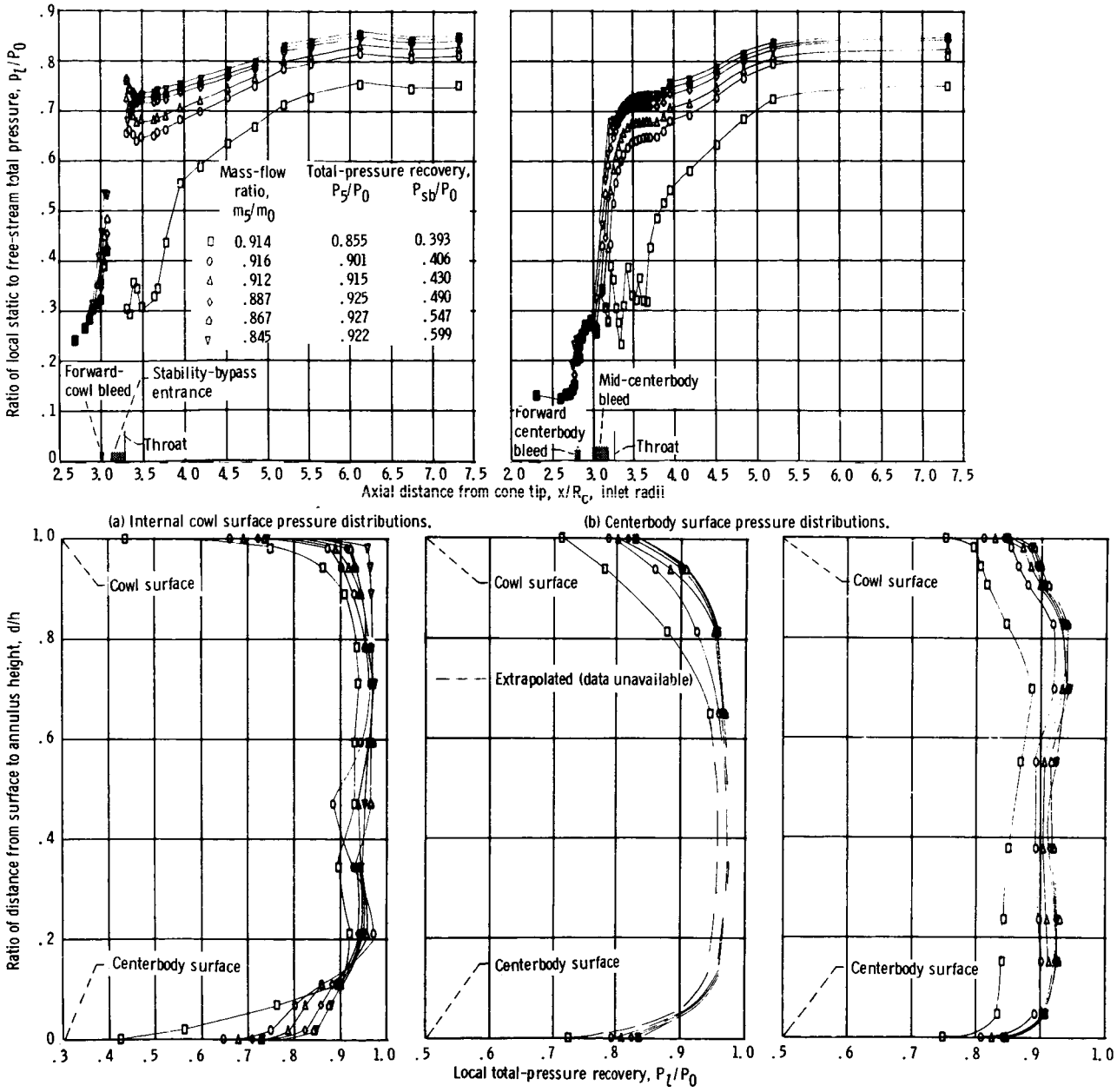

(c) Throat exit, station 2. (Symbols at 0 and 1.0 d/h denote static pressures.)

(d) Mid diffuser, station 4. (Symbols at 0 and 1.0 d/h denote static pressures.)

(e) Diffuser exit, station 5, rake 6. (Symbols at 0 and 1.0 d/h denote static pressures.)

Figure 30. - Inlet diffuser and stability-bypass slot static- and total-pressure distributions obtained with vortex valves and forward-slanted-slot configuration.

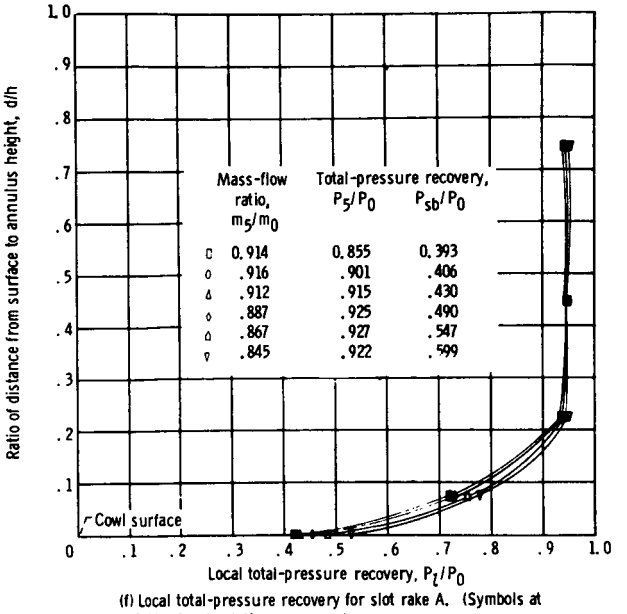

(f) Local total-pressure recovery for slot rake A. (Symbols at 0 d/h denote static pressures.)

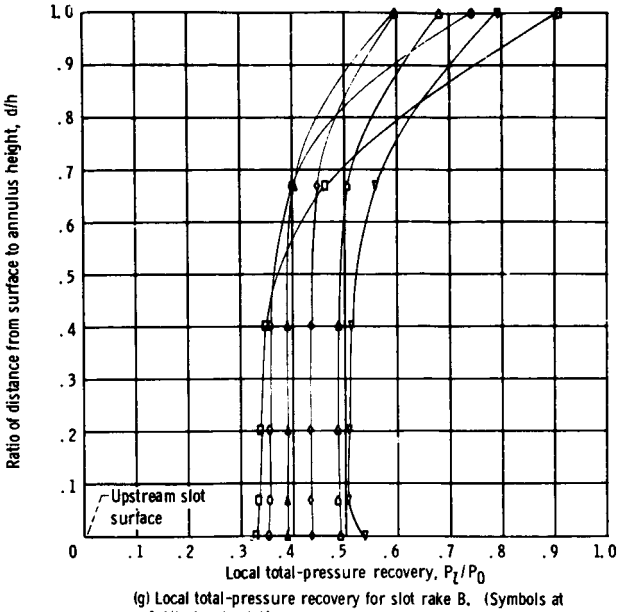

(g) Local total-pressure recovery for slot rake B. (Symbols at 0 d/h denote static pressures.)

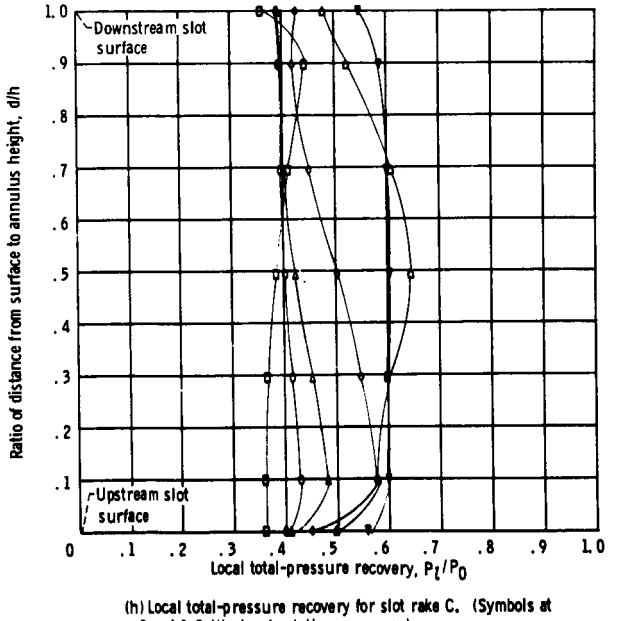

(h) Local total-pressure recovery for slot rake C. (Symbols at 0 and 1.0 d/h denote static pressures.)

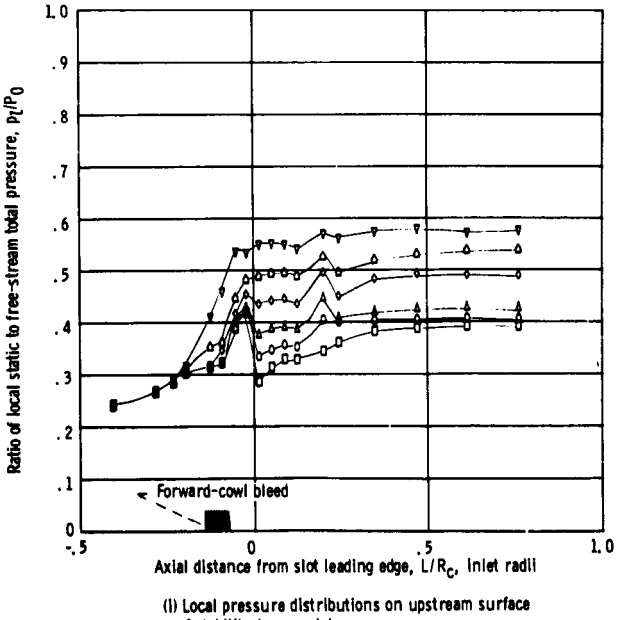

(i) Local pressure distributions on upstream surface of stability-bypass slot.

Figure 30. - Concluded.

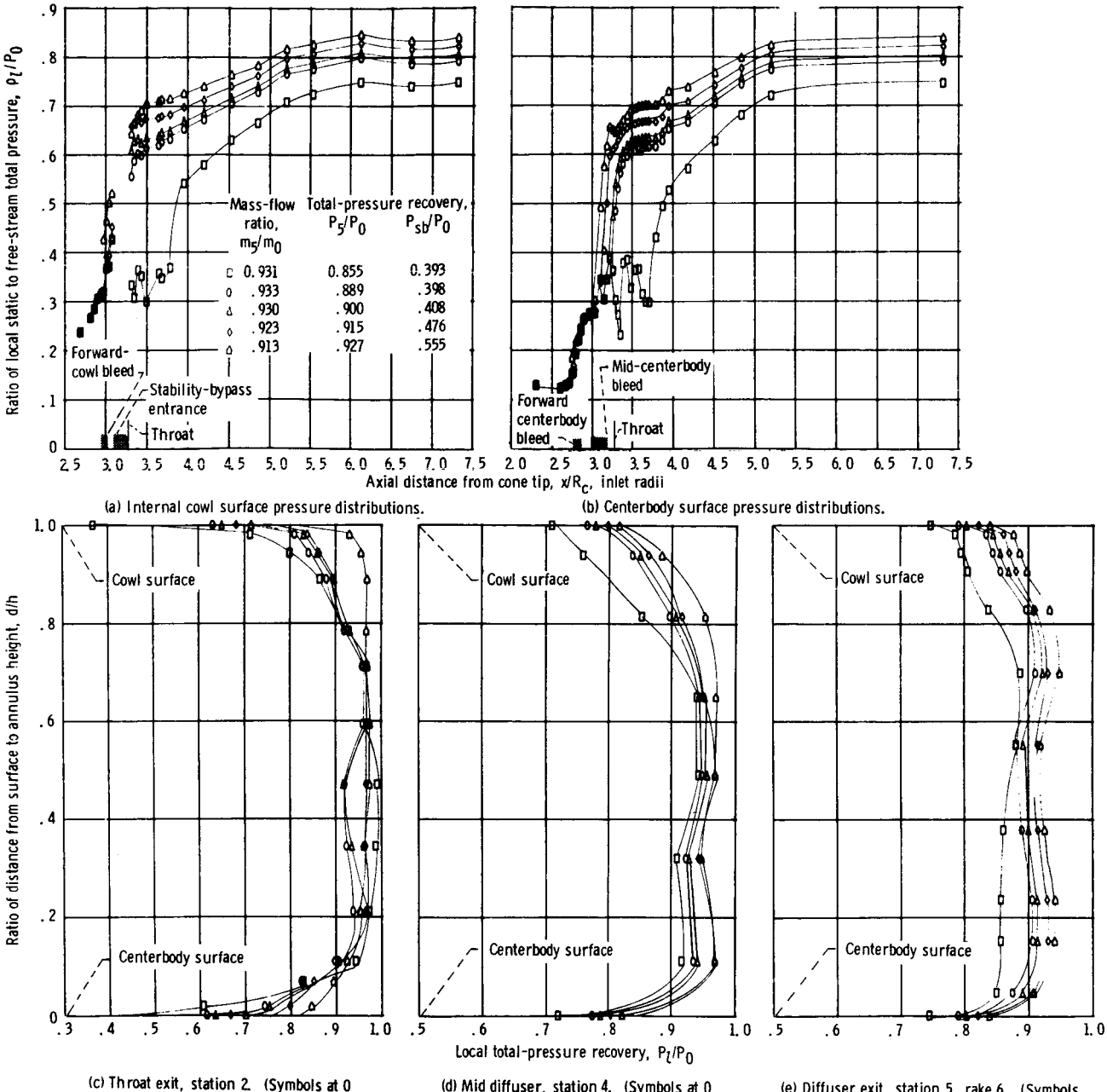

Figure 31. - Inlet diffuser and stability-bypass slot static- and total-pressure distributions obtained with fixed exit and forward-slanted-slot configuration.

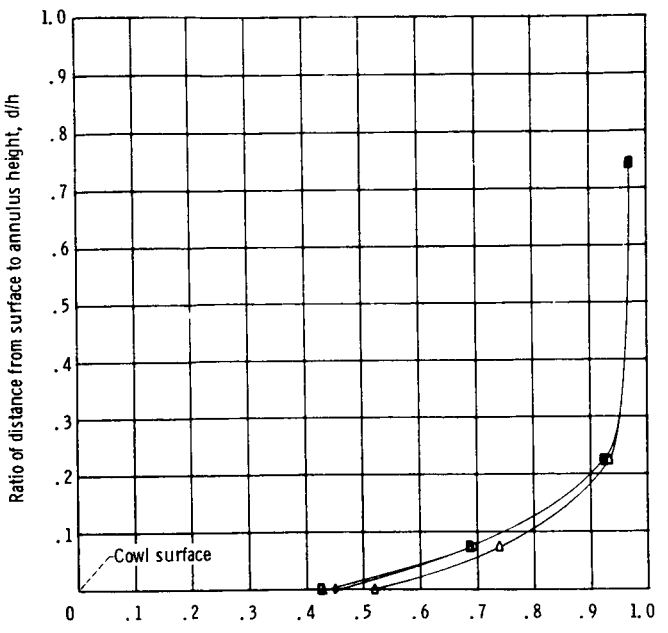

(f) Local total-pressure recovery for slot rake A. (Symbols at 0 d/h denote static pressures.)

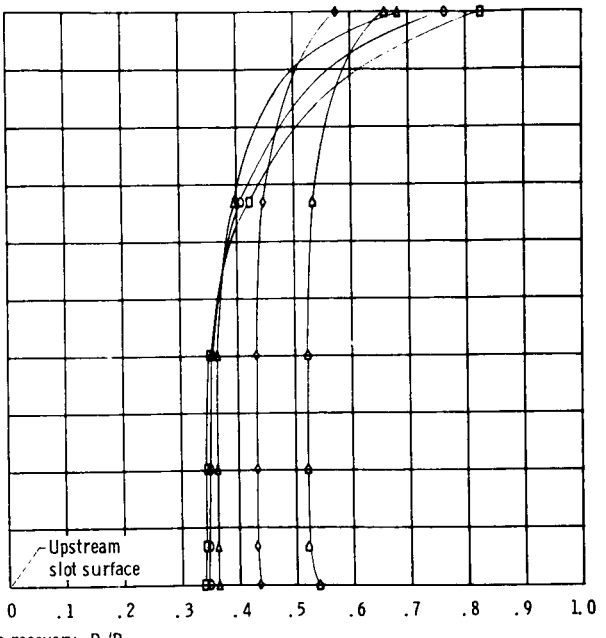

(g) Local total-pressure recovery for slot rake B. (Symbols at 0 d/h denote static pressures.)

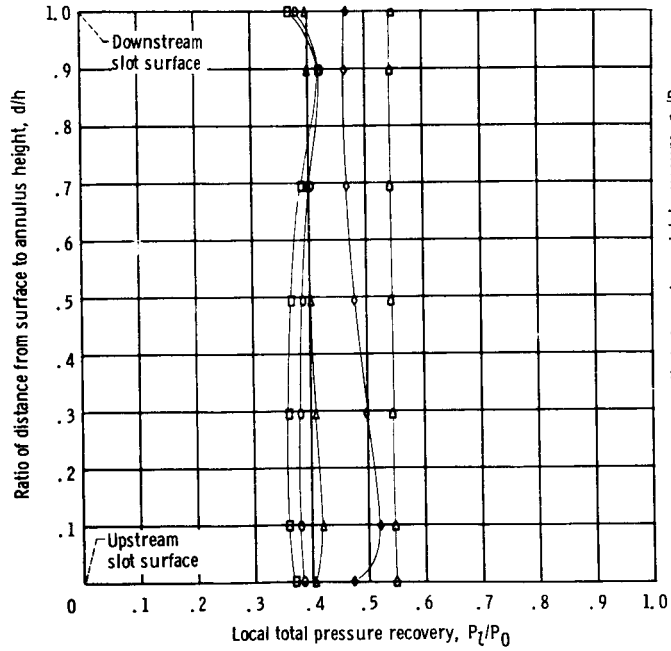

(h) Local total-pressure recovery for slot rake C. (Symbols at 0 and 1.0 d/h denote static pressures.)

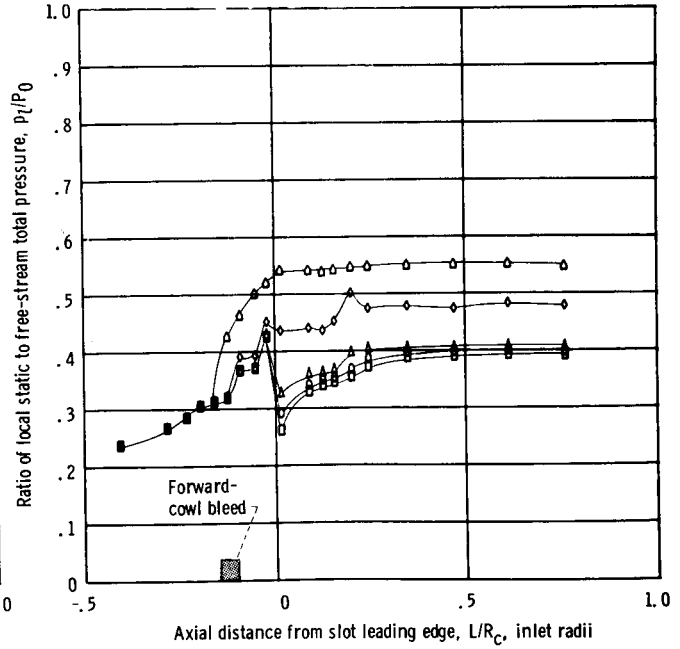

(i) Local pressure distributions on upstream surface of stability-bypass slot.

Figure 31. - Concluded.

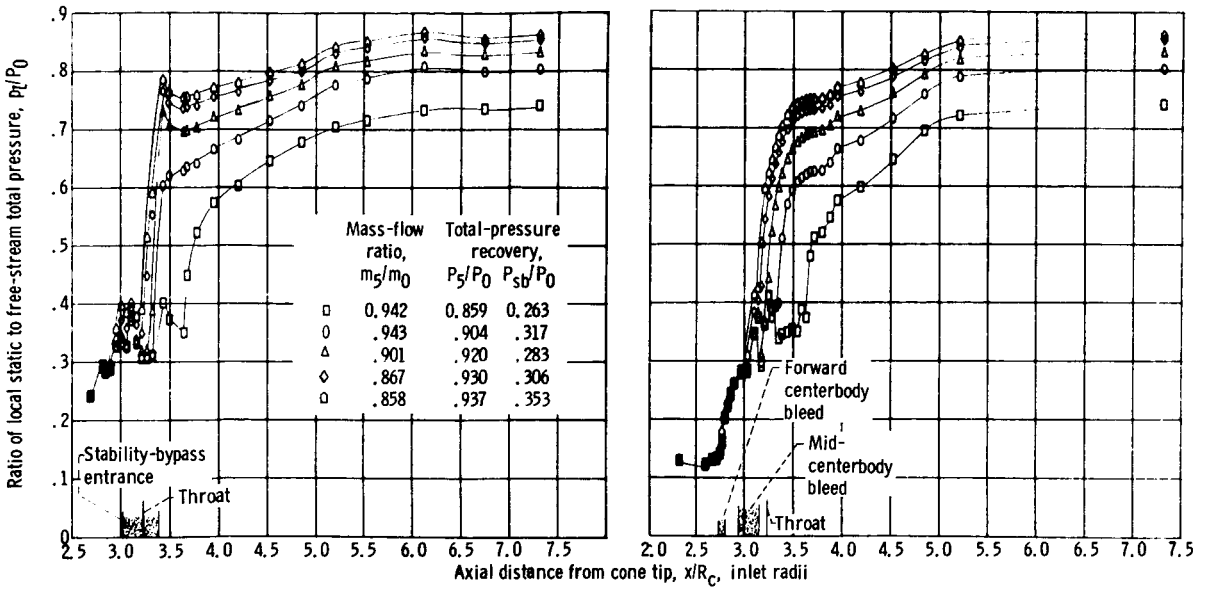

(a) Internal cowl surface pressure distributions.

(b) Centerbody surface pressure distributions.

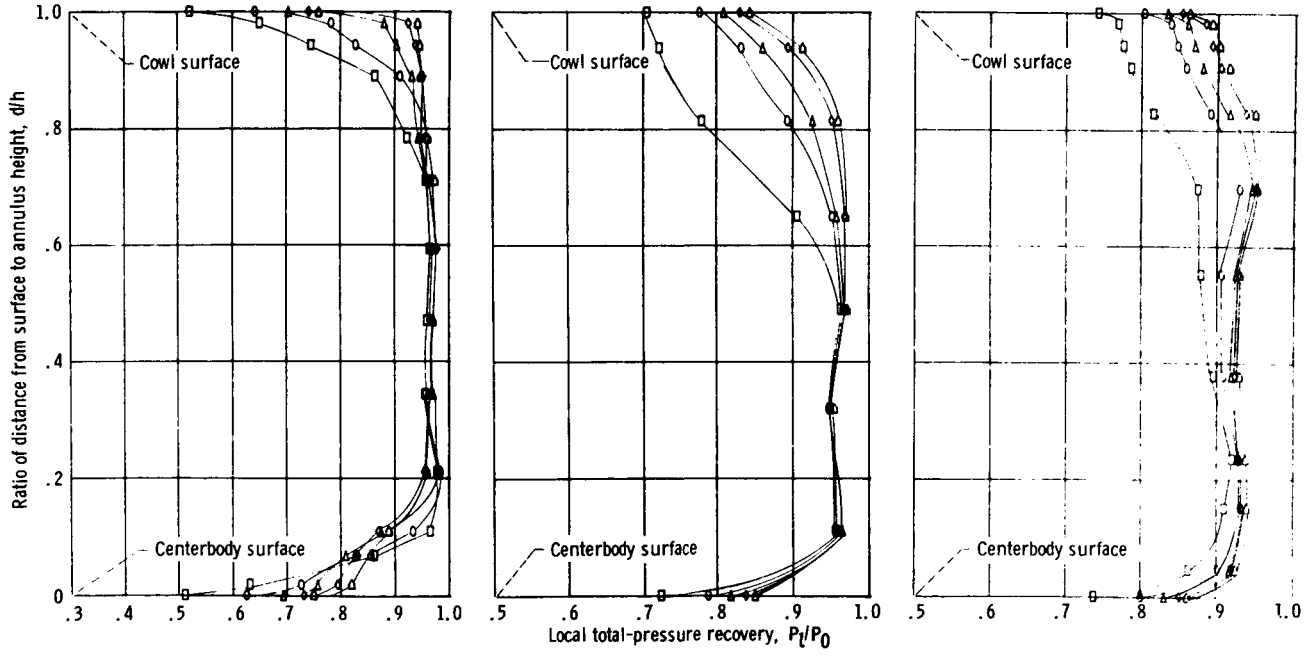

(c) Throat exit, station 2. (Symbols at 0 and 1.0 d/h denote static pressures.)

(d) Mid diffuser, station 4. (Symbols at 0 and 1.0 d/h denote static pressures.)

(e) Diffuser exit, station 5, rake 6. (Symbols at 0 and 1.0 d/h denote static pressures.)

Figure 32. - Diffuser static- and total-pressure distributions obtained with poppet valves and distributed educated configuration.

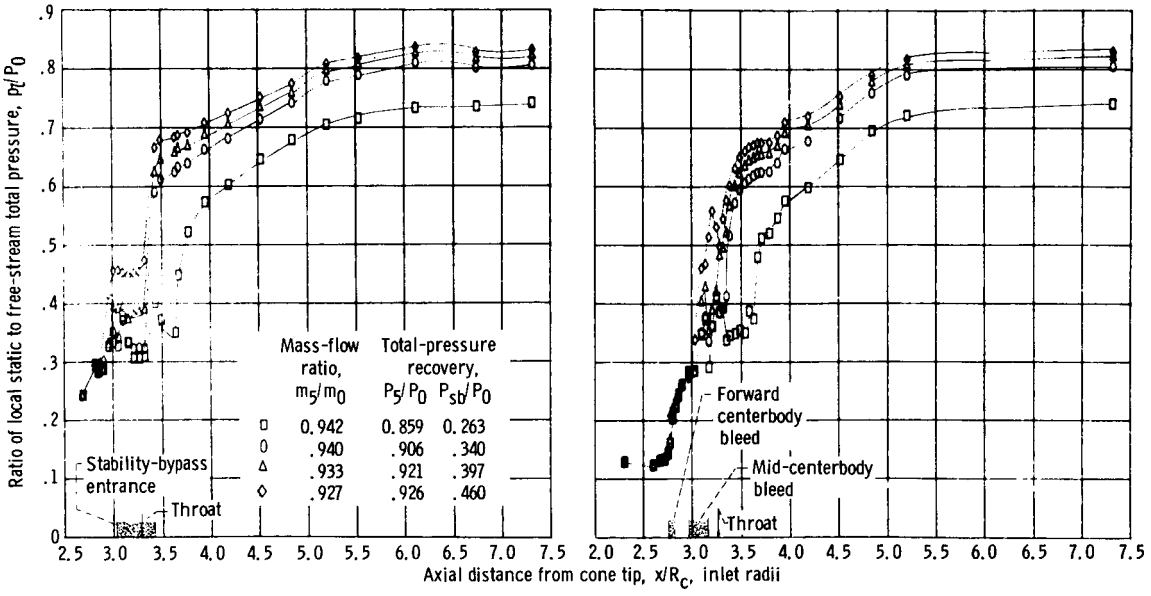

(a) Internal cowl surface pressure distributions.

(b) Centerbody surface pressure distributions.

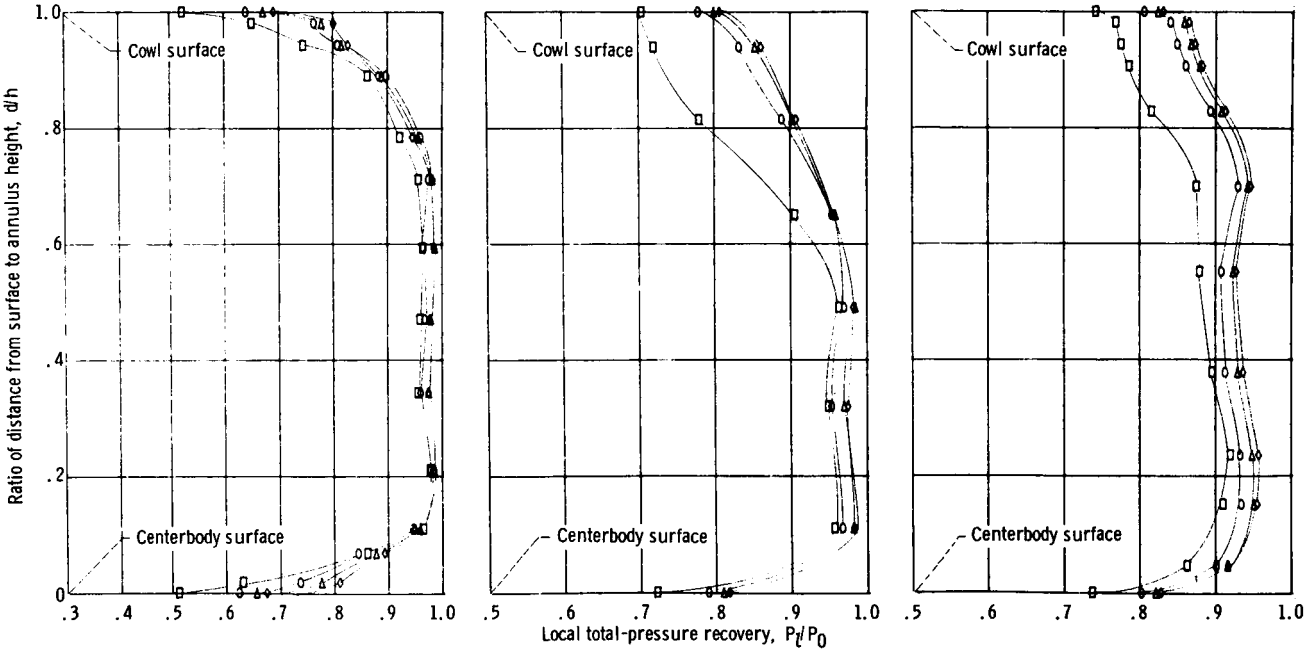

(c) Throat exit, station 2. (Symbols at 0 and 1.0 d/h denote static pressures.)

(d) Mid diffuser, station 4. (Symbols at 0 and 1.0 d/h denote static pressures.)

(e) Diffuser exit, station 5, rake 6. (Symbols at 0 and 1.0 d/h denote static pressures.)

Figure 33. - Diffuser static- and total-pressure distributions obtained with fixed exit and distributed educated configuration.

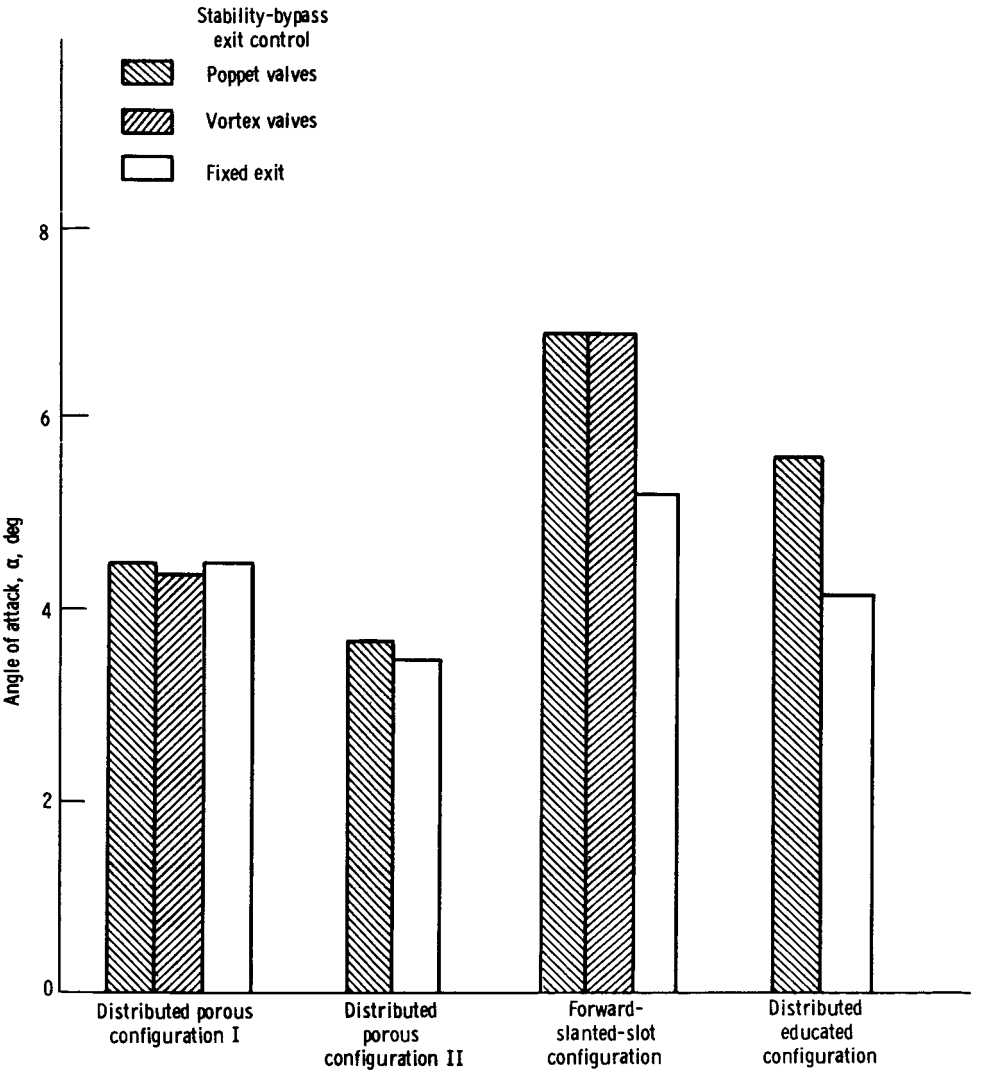

Figure 34. - Unstart angle of attack obtained with various stability-bypass exit controls and stability-bypass entrance configurations. Initial inlet total-pressure recovery, $P_5/P_0 \approx 0.90$.

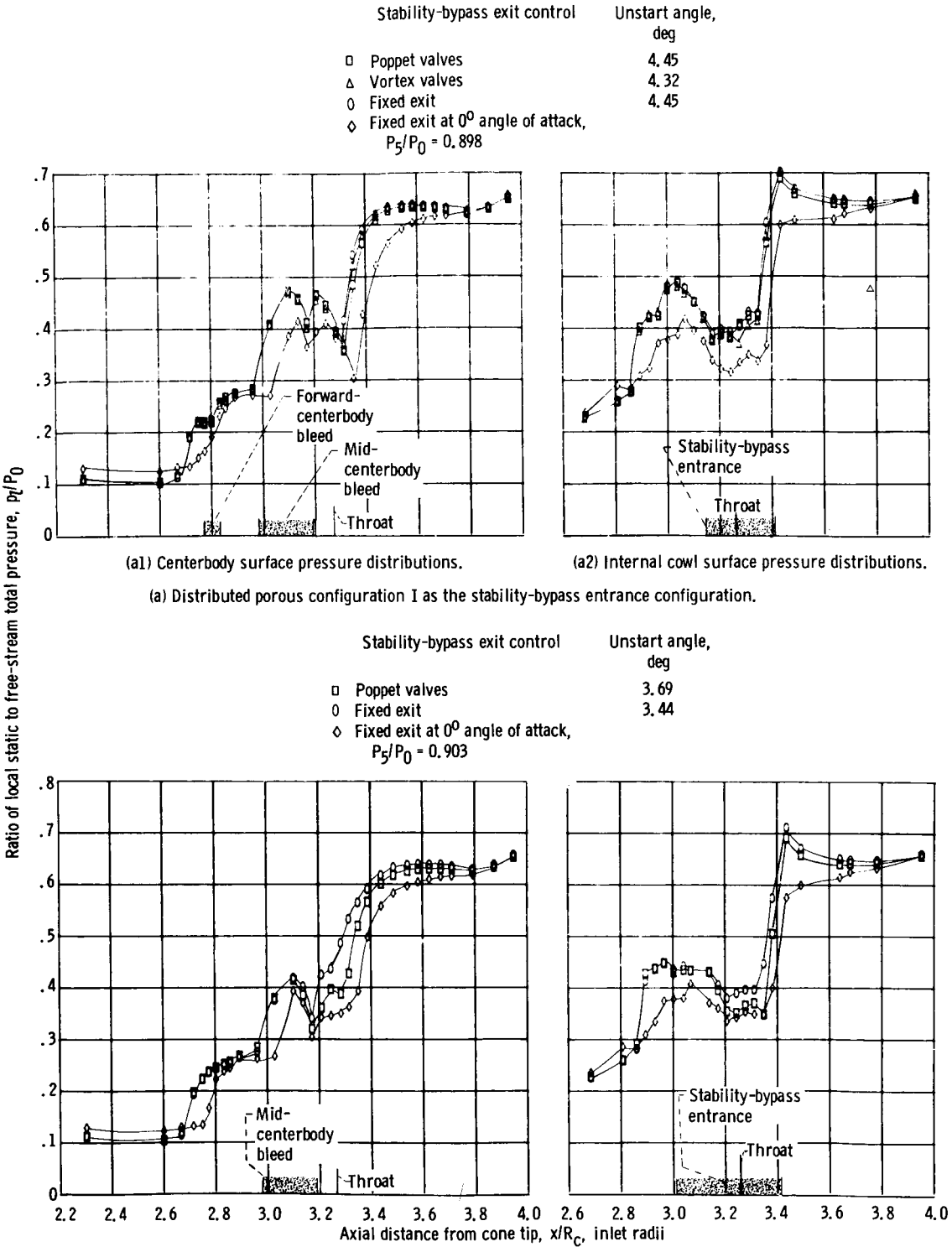

(a1) Centerbody surface pressure distributions. (a2) Internal cowl surface pressure distributions.

(a) Distributed porous configuration I as the stability-bypass entrance configuration.

(b1) Centerbody surface pressure distributions. (b2) Internal cowl surface pressure distributions.

(b) Distributed porous configuration II as the stability-bypass entrance configuration.

Figure 35. - Top centerline diffuser static-pressure distributions at unstart angles of attack.

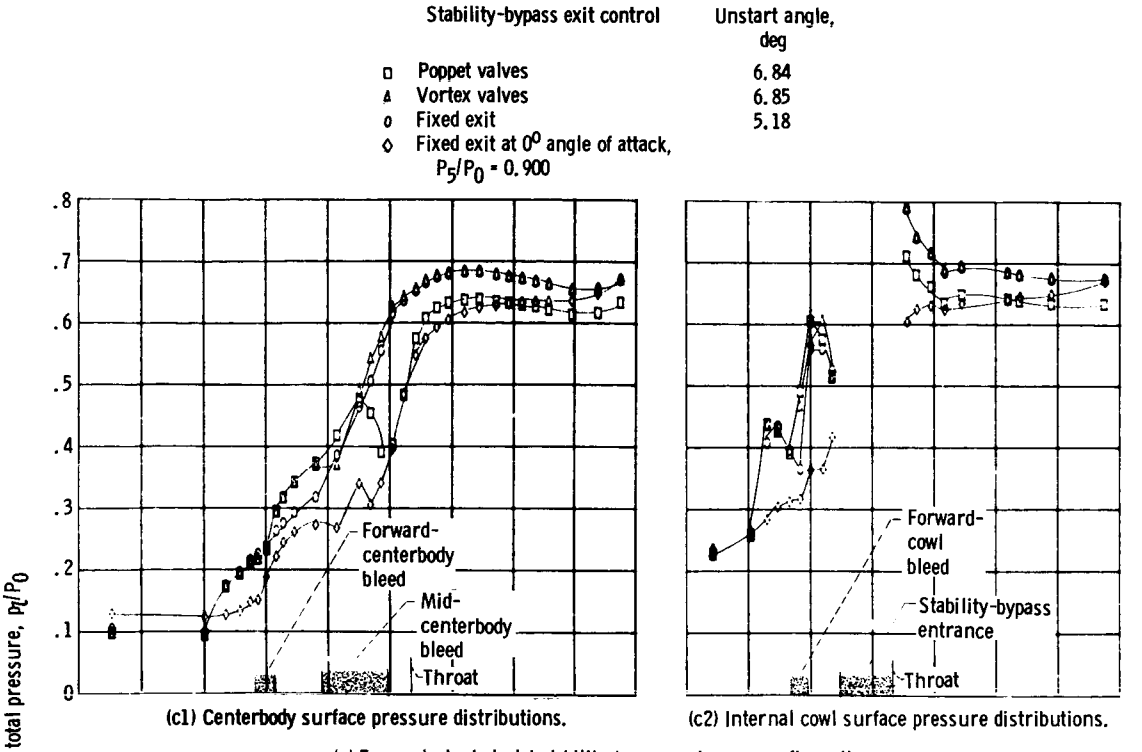

(c1) Centerbody surface pressure distributions. (c2) Internal cowl surface pressure distributions.

(c) Forward-slanted-slot stability-bypass entrance configuration.

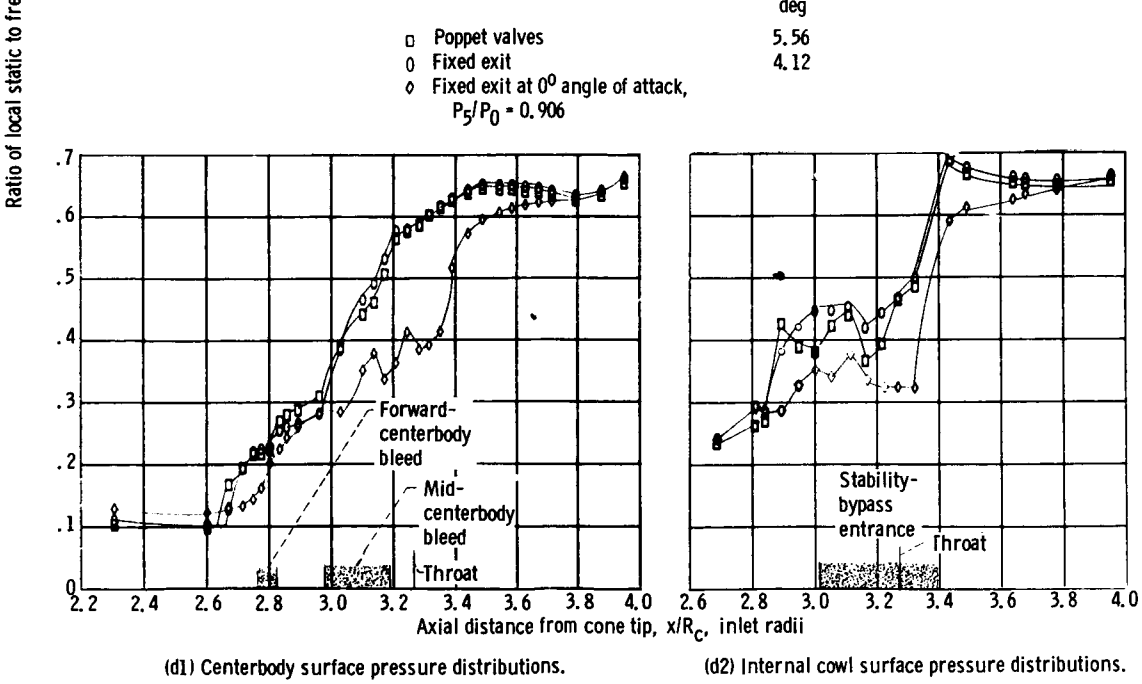

(d1) Centerbody surface pressure distributions. (d2) Internal cowl surface pressure distributions.

(d) Distributed educated stability-bypass entrance configuration.

Figure 35. - Concluded.

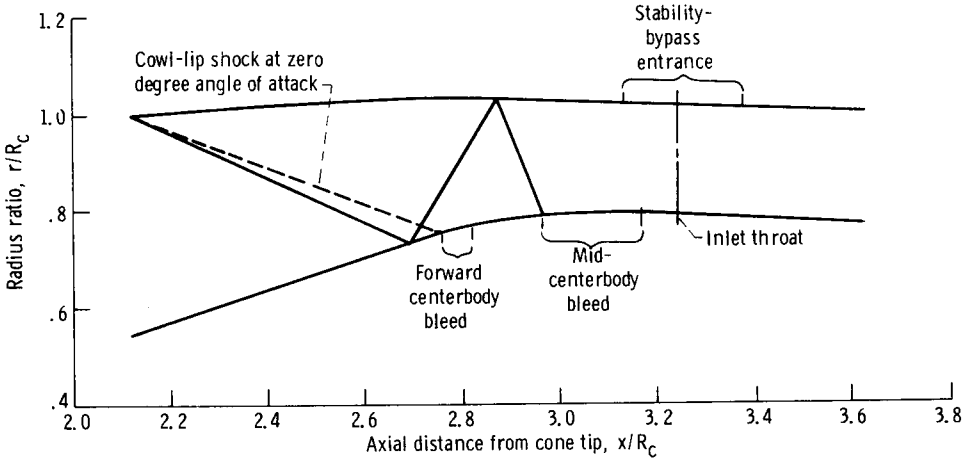

Figure 36. - Internal reflected shock structure on inlet top centerline at maximum unstart angle of attack. Distributed porous configuration I; unstart angle of attack, 4.45^0.

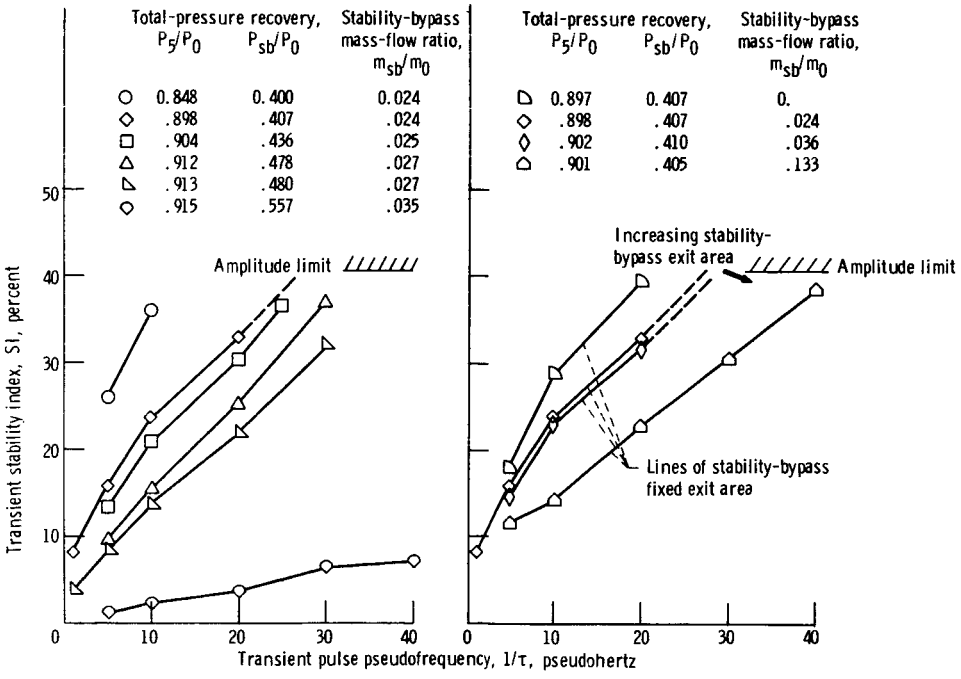

(a) Total-pressure recovery variation with fixed exit as the stability-bypass exit control.

(b) Stability-bypass exit area variation with constant total-pressure recovery.

Figure 37. - Effect of inlet operating point on transient unstart limits of inlet-coldpipe with forward-slanted-slot stability-bypass entrance configuration and large stability-bypass plenum volume (0.391 m^3).

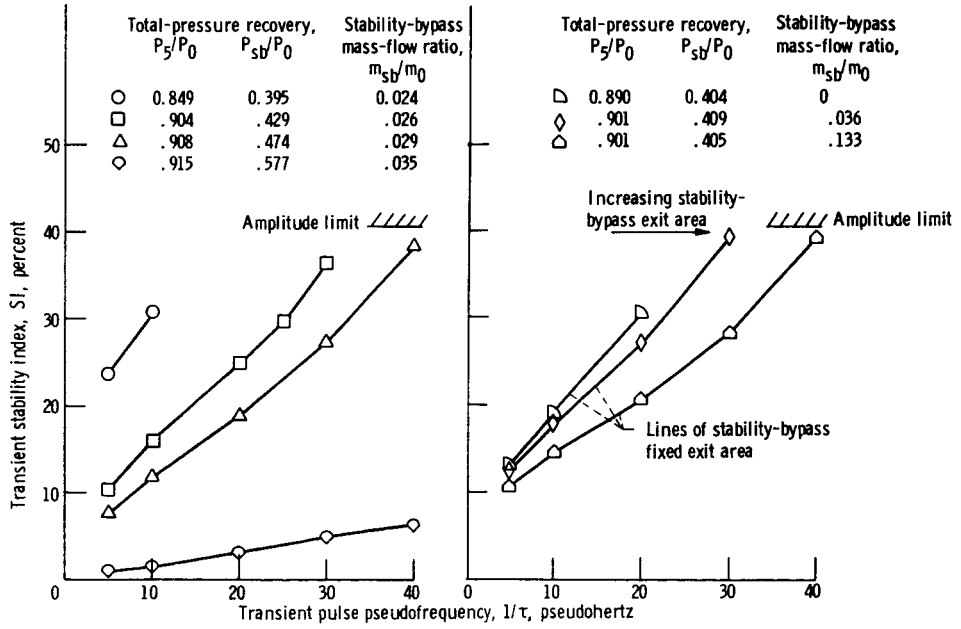

(a) Total-pressure recovery variation with fixed exit as the stability-bypass exit control.

(b) Stability-bypass exit area variation with constant total-pressure recovery.

Figure 38. - Effect of inlet operating point on transient unstart limits of inlet-coldpipe with forward-slanted-slot stability-bypass entrance configuration and medium stability bypass plenum volume (0.213 m^3).

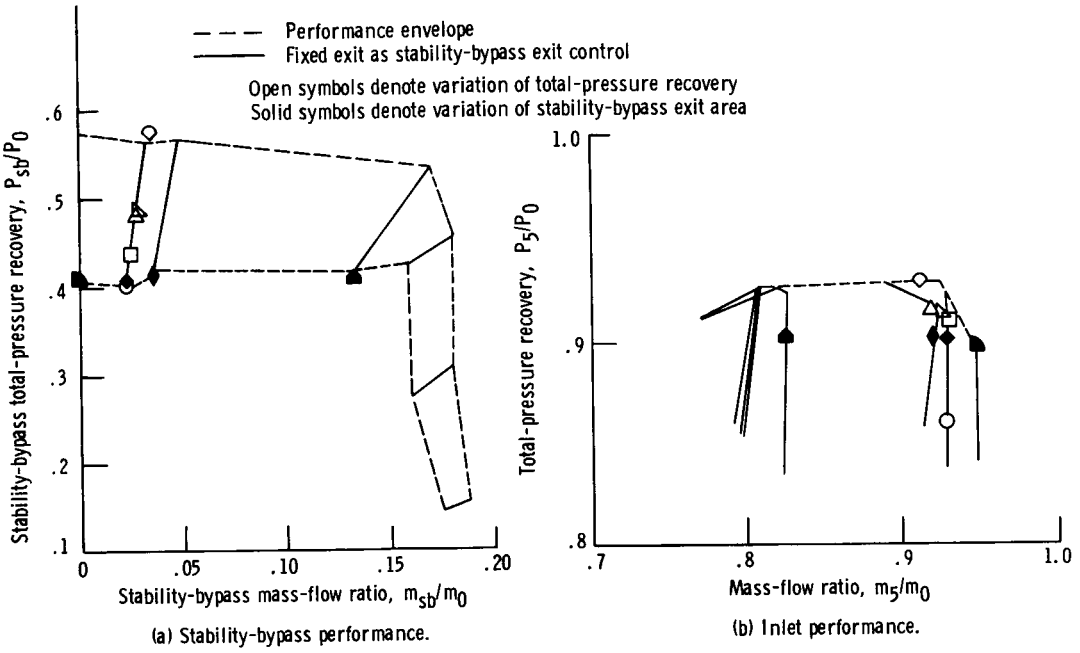

(a) Stability-bypass performance.

(b) Inlet performance.

Figure 39. - Performance of forward-slanted-slot stability-bypass entrance configuration (SB, ref. 4) showing steady-state operating points from which transients of figures 37 and 38 were initiated.

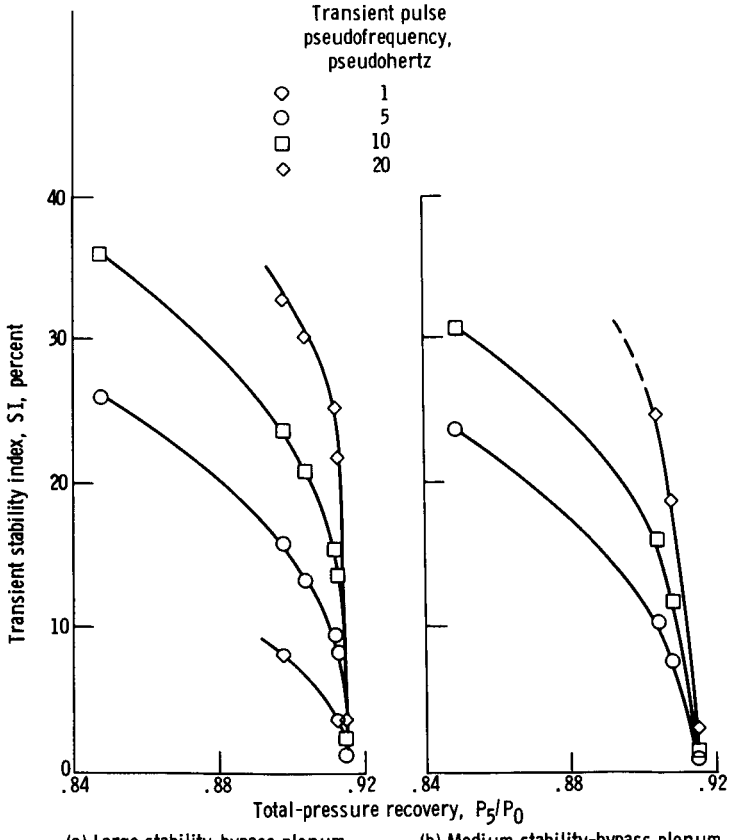

(a) Large stability-bypass plenum volume, 0.391 m^3.

(b) Medium stability-bypass plenum volume, 0.213 m^3.

Figure 40. - Variation of inlet-coldpipe transient unstart limits with diffuser total-pressure recovery, forward-slanted-slot stability-bypass entrance configuration, and fixed exit as the stability bypass exit control.

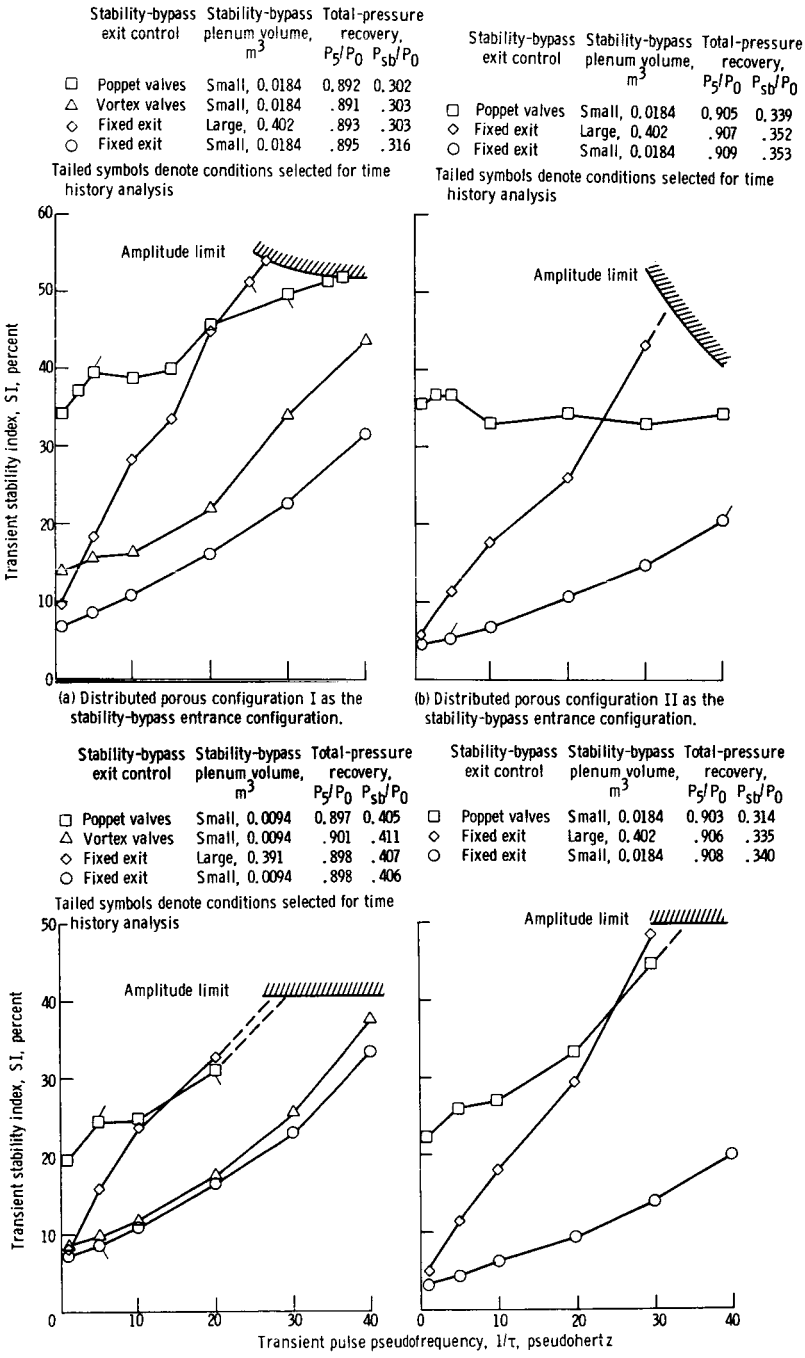

Figure 41. - Unstart limits of inlet-coldpipe combination utilizing a stability-bypass system when subjected to transient disturbances.

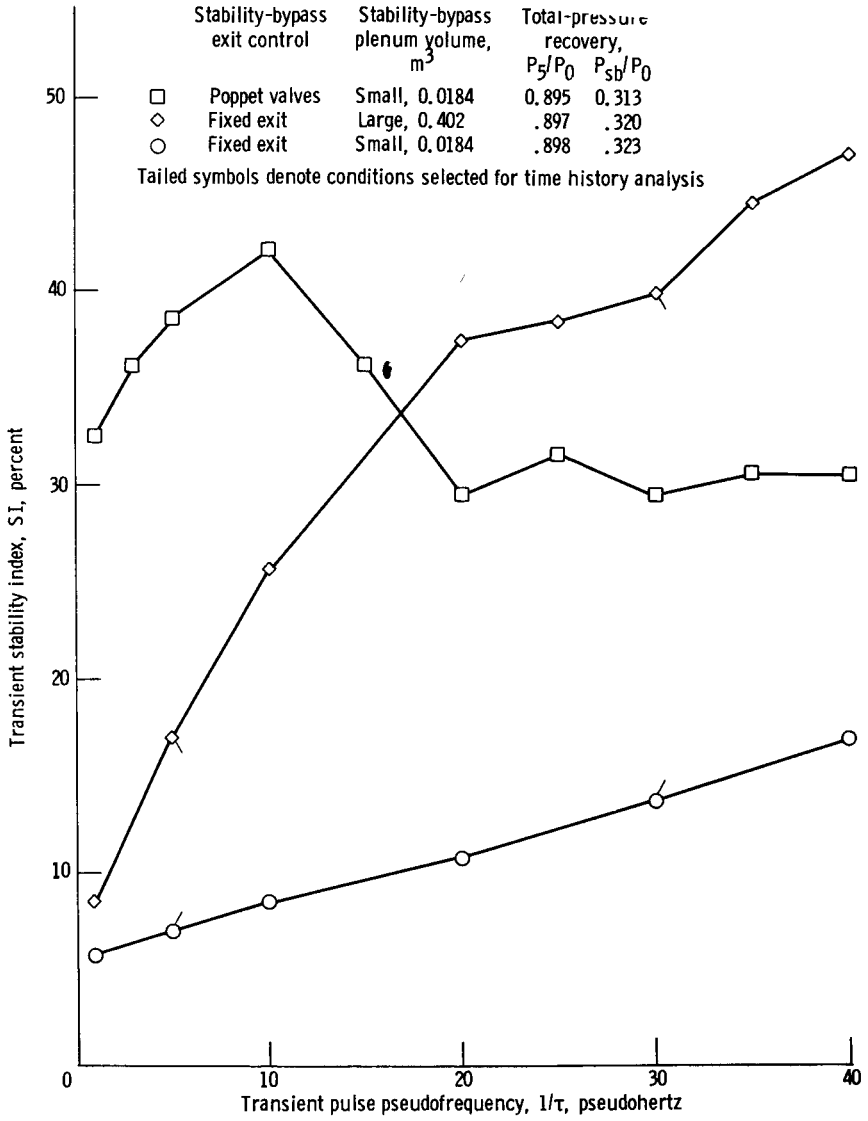

Figure 42. - Unstart limit of inlet with choke plate and distributed porous configuration I as the stability-bypass entrance configuration, when subjected to transient disturbances.

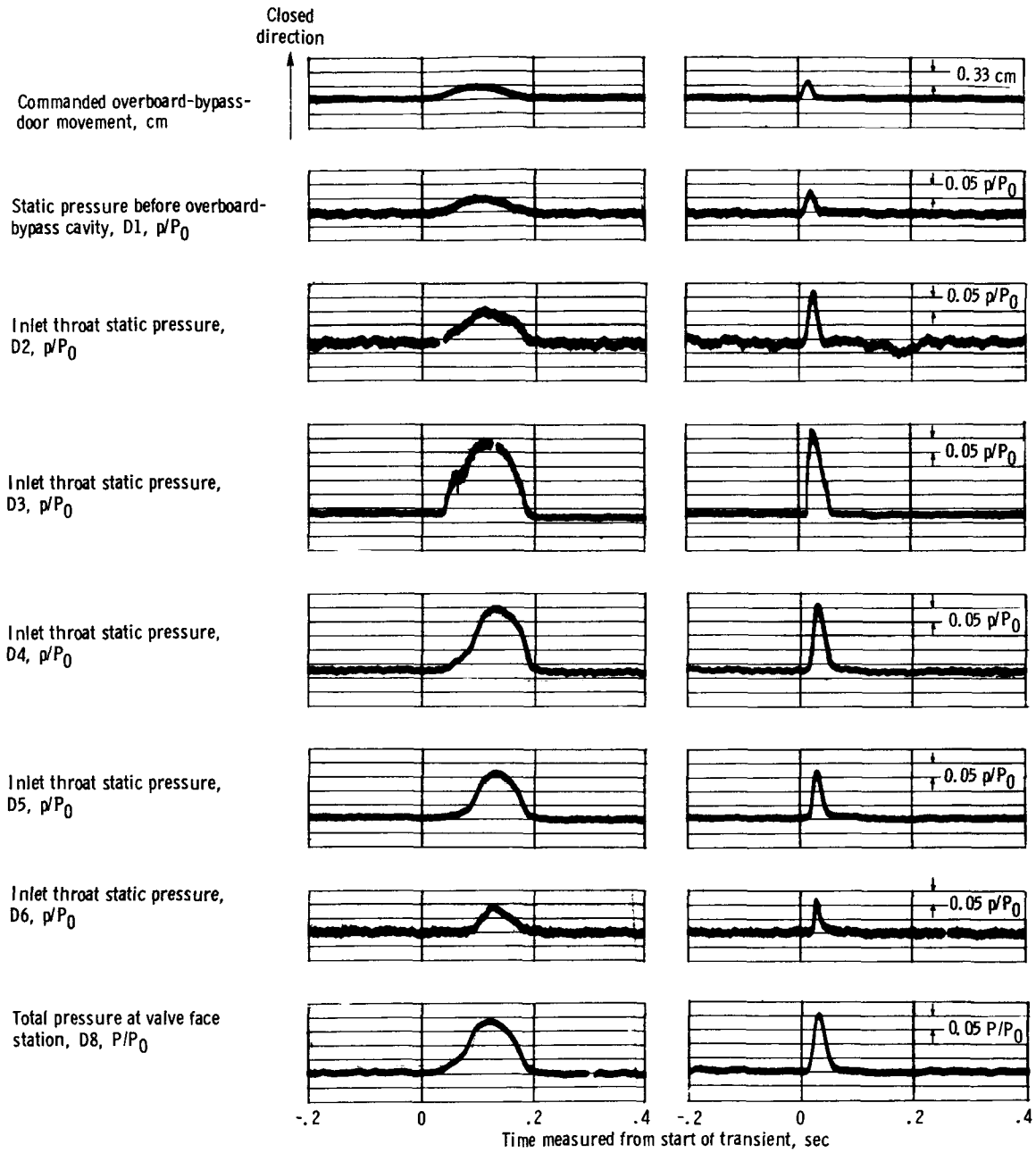

(a1) Transient pulse pseudofrequency, $1/\tau = 5$ pseudohertz.

(a2) Transient pulse pseudofrequency, $1/\tau = 30$ pseudohertz.

(a) Inlet with choke plate, distributed porous configuration I as the stability-bypass entrance configuration, fixed exit as the stability-bypass exit control, and small stability-bypass plenum volume.

Figure 43. - Time history of inlet parameters during internal transients.

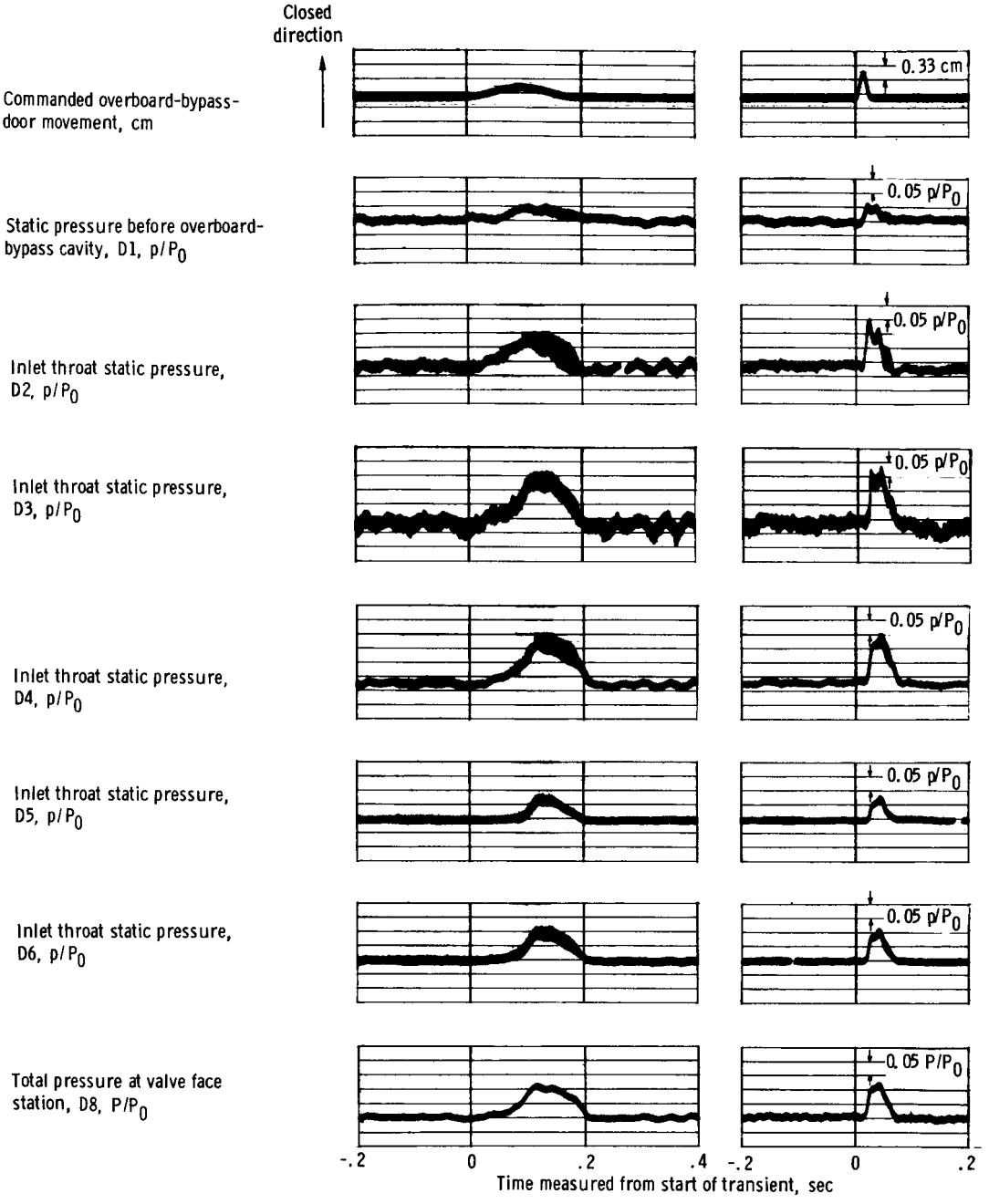

(b1) Transient pulse pseudofrequency, $1/\tau = 5$ pseudohertz.

(b2) Transient pulse pseudofrequency, $1/\tau = 40$ pseudohertz.

(b) Inlet-coldpipe combination, distributed porous configuration II as the stability-bypass entrance configuration, fixed exit as the stability-bypass exit control, and small stability-bypass plenum volume.

Figure 43. - Continued.

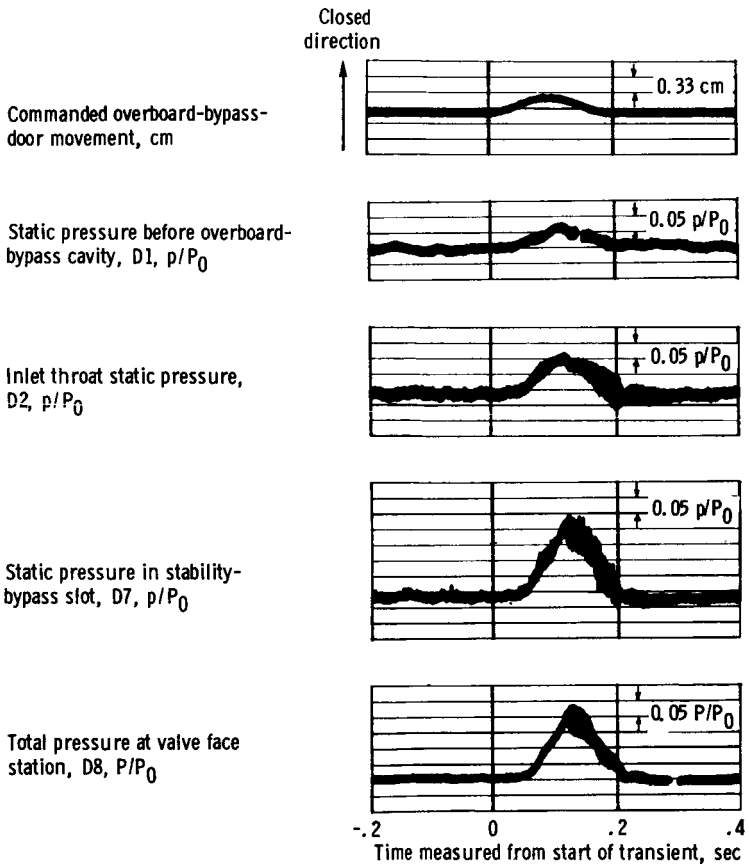

(c) Inlet-coldpipe combination; forward-slanted-slot configuration as the stability-bypass entrance configuration; fixed exit as the stability-bypass exit control; small stability-bypass plenum volume; and transient pulse pseudo-frequency, $1/\tau = 5$ pseudohertz.

Figure 43. - Continued.

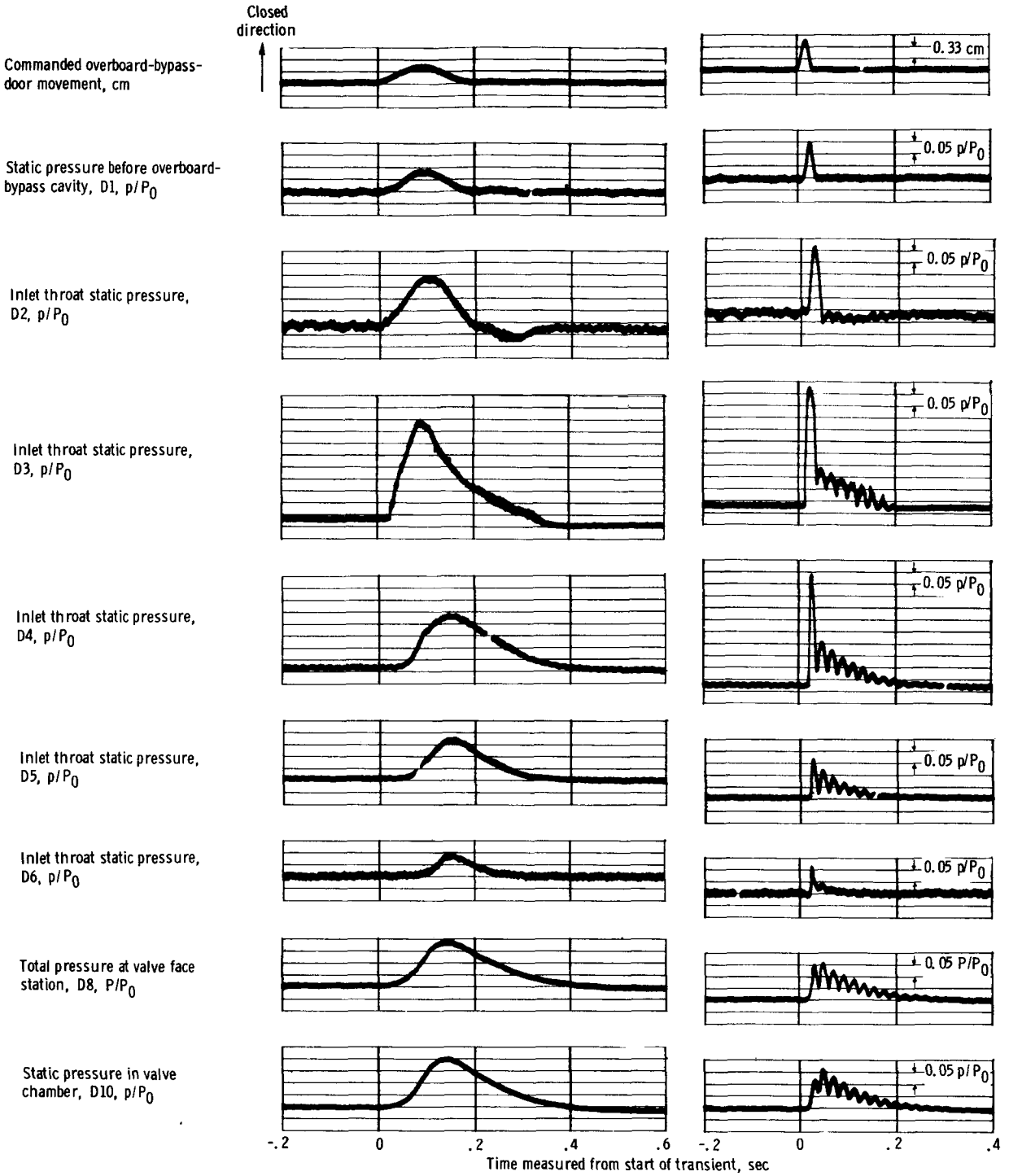

(d1) Transient pulse pseudofrequency, $1/\tau$ = 5 pseudohertz.

(d2) Transient pulse psuedofrequency, $1/\tau$ = 30 pseudohertz.

(d) Inlet with choke plate, distributed porous configuration I as the stability-bypass entrance configuration, fixed exit as the stability-bypass exit control, and large stability-bypass plenum volume.

Figure 43. - Continued.

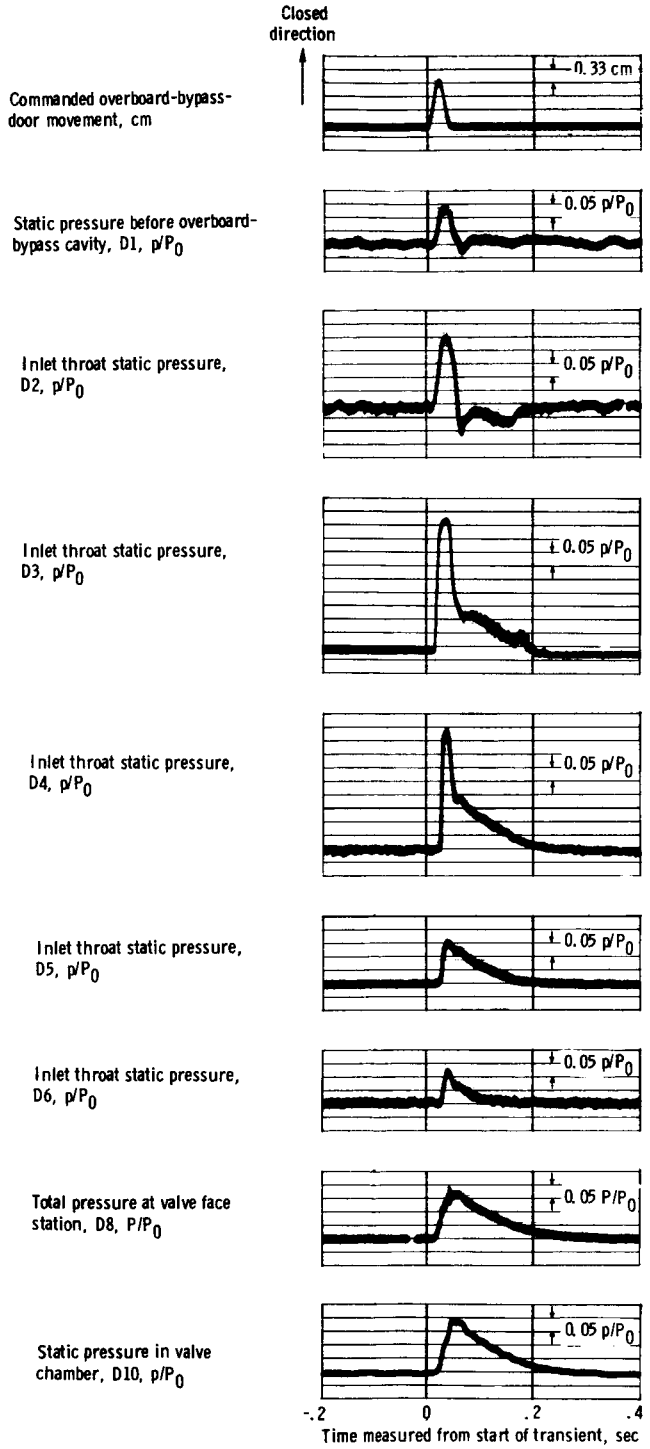

(e) Inlet-coldpipe combination; distributed porous configuration I as the stability-bypass entrance configuration; fixed exit as the stability-bypass exit control; large stability-bypass plenum volume; and transient pulse pseudofrequency, $1/\tau$ = 25 pseudohertz.

Figure 43. - Continued.

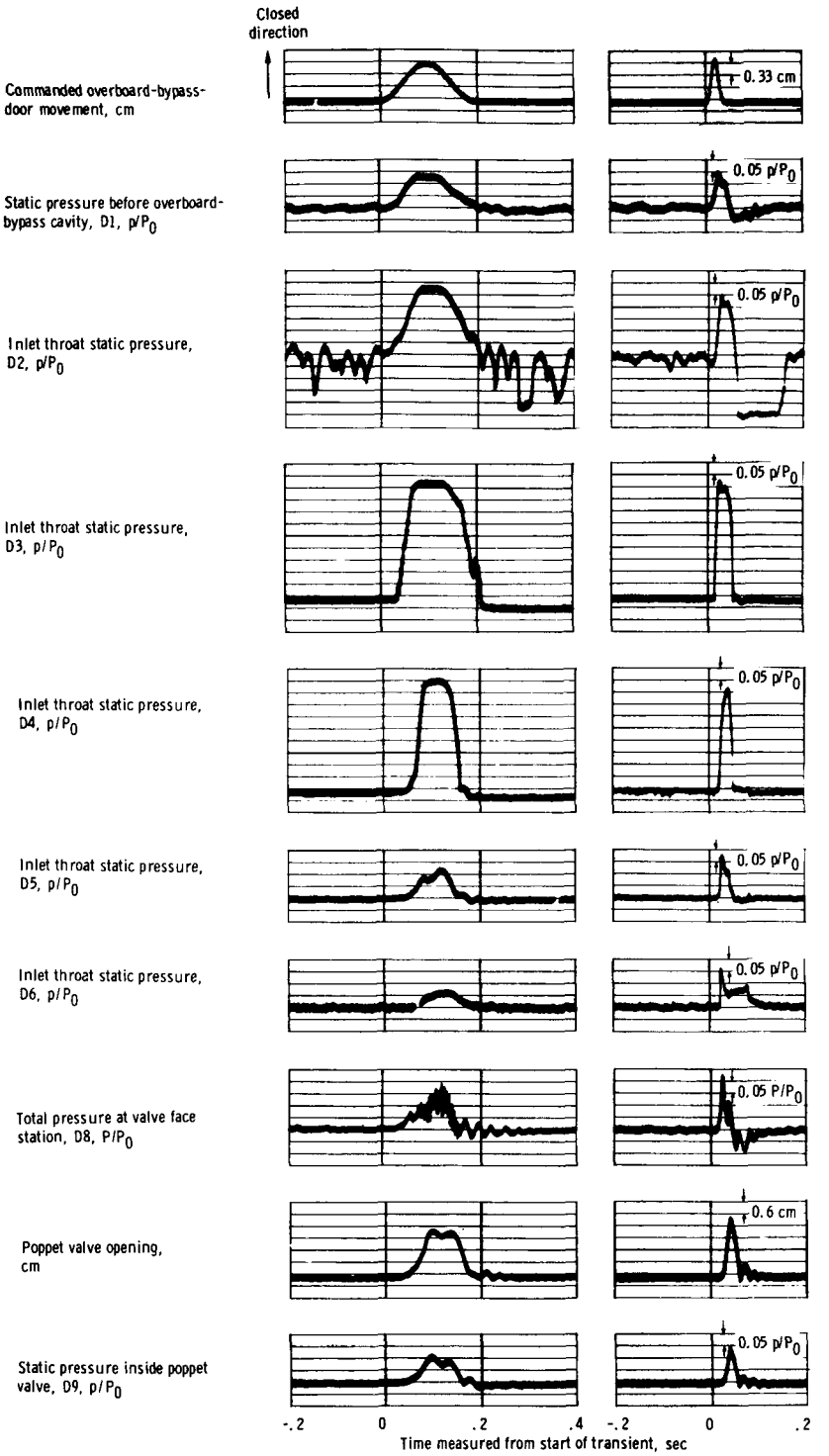

(f1) Transient pulse pseudofrequency, $1/\tau$ = 5 pseudohertz.

(f2) Transient pulse pseudofrequency, $1/\tau$ = 30 pseudohertz.

(f) Inlet-coldpipe combination, distributed porous configuration I as the stability-bypass entrance configuration, and poppet valves as the stability-bypass exit control.

Figure 43. - Continued.

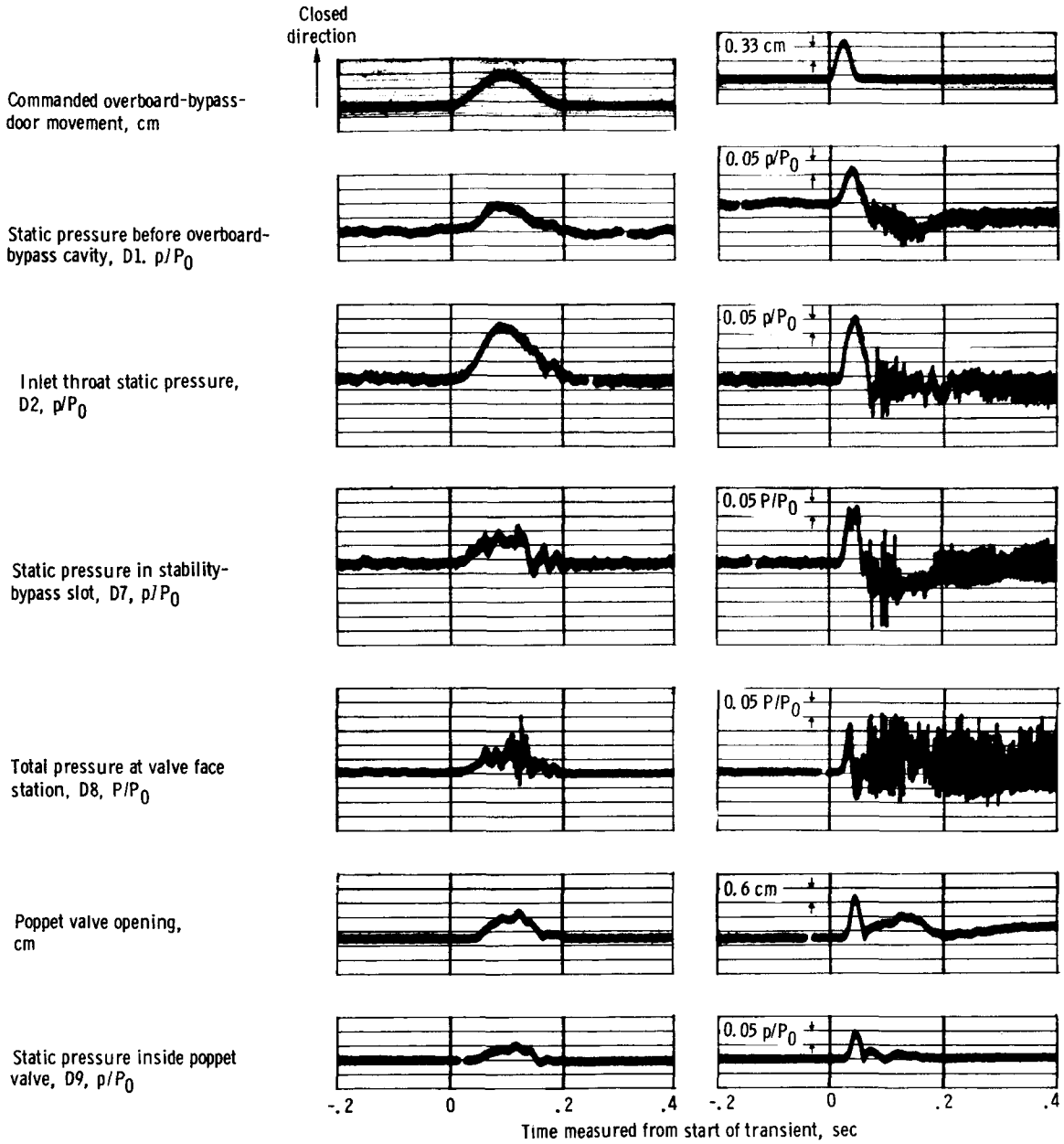

(g1) Transient pulse pseudofrequency, $1/\tau = 5$ pseudohertz.

(g2) Transient pulse pseudofrequency, $1/\tau = 20$ pseudohertz.

(g) Inlet-coldpipe combination, forward-slanted-slot configuration as the stability-bypass entrance configuration, and poppet valves as the stability-bypass exit control.

Figure 43. - Concluded.

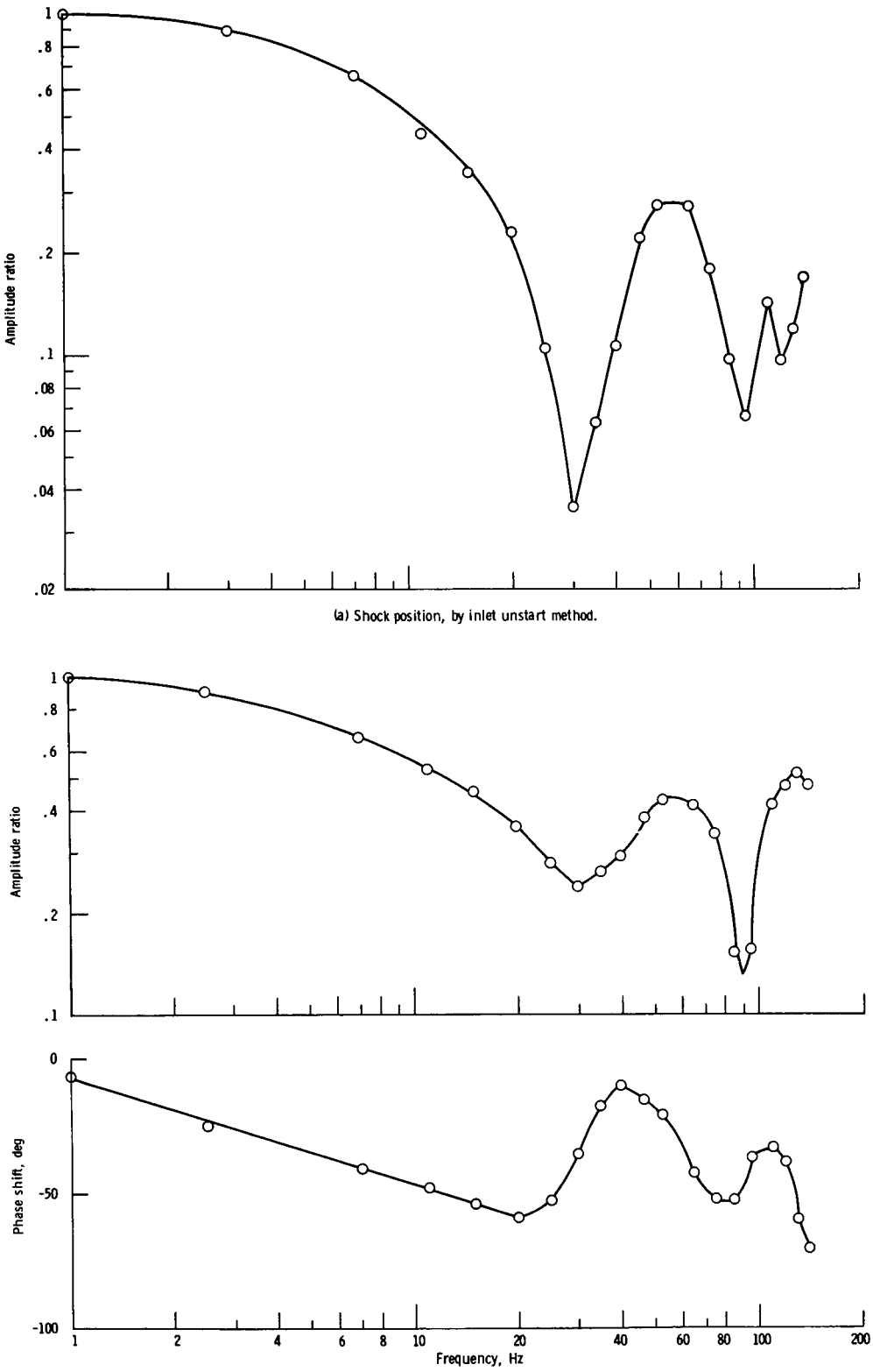

(a) Shock position, by inlet unstart method.

(b) Static pressure before overboard-bypass cavity, obtained during inlet unstart method.

Figure 44. - Dynamic response of inlet with coldpipe to internal disturbance. Distributed porous configuration I as the stability-bypass entrance configuration, fixed exit as the stability-bypass exit control, and small stability-bypass plenum volume ($m_{sb}/m_0 \approx 0.02$).

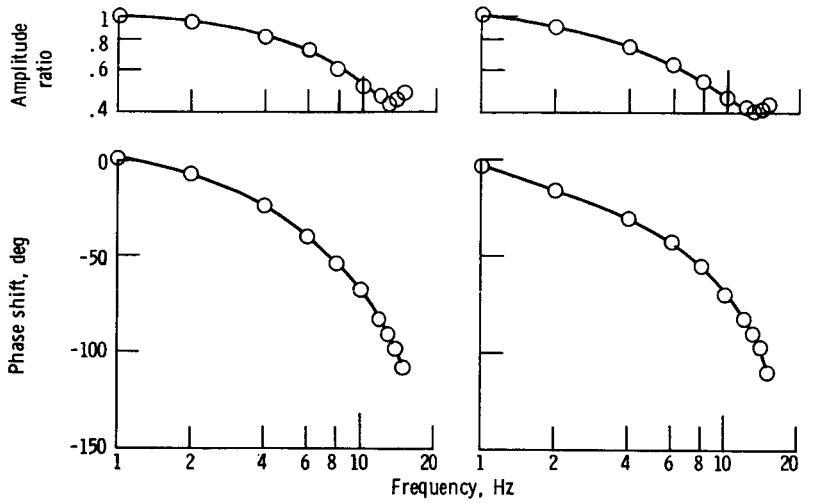

(a) Poppet valves as the stability-bypass exit control.

(b) Fixed exit as the stability-bypass exit control and large stability-bypass plenum volume.

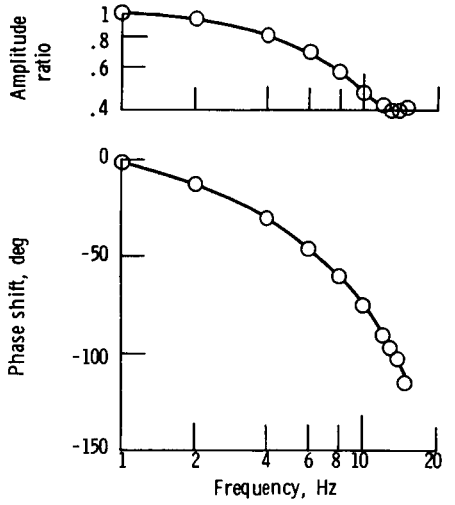

(c) Fixed exit as the stability-bypass exit control and small stability-bypass plenum volume.

Figure 45. - Dynamic response of inlet with coldpipe to external disturbance, as measured by static-pressure tap before overboard-bypass cavity. Distributed porous configuration I as the stability-bypass entrance configuration; initial stability-bypass airflow, $m_{sb}/m_0 \approx 0.02$; change in gust-plate angle of attack, 0^0 to -1^0.

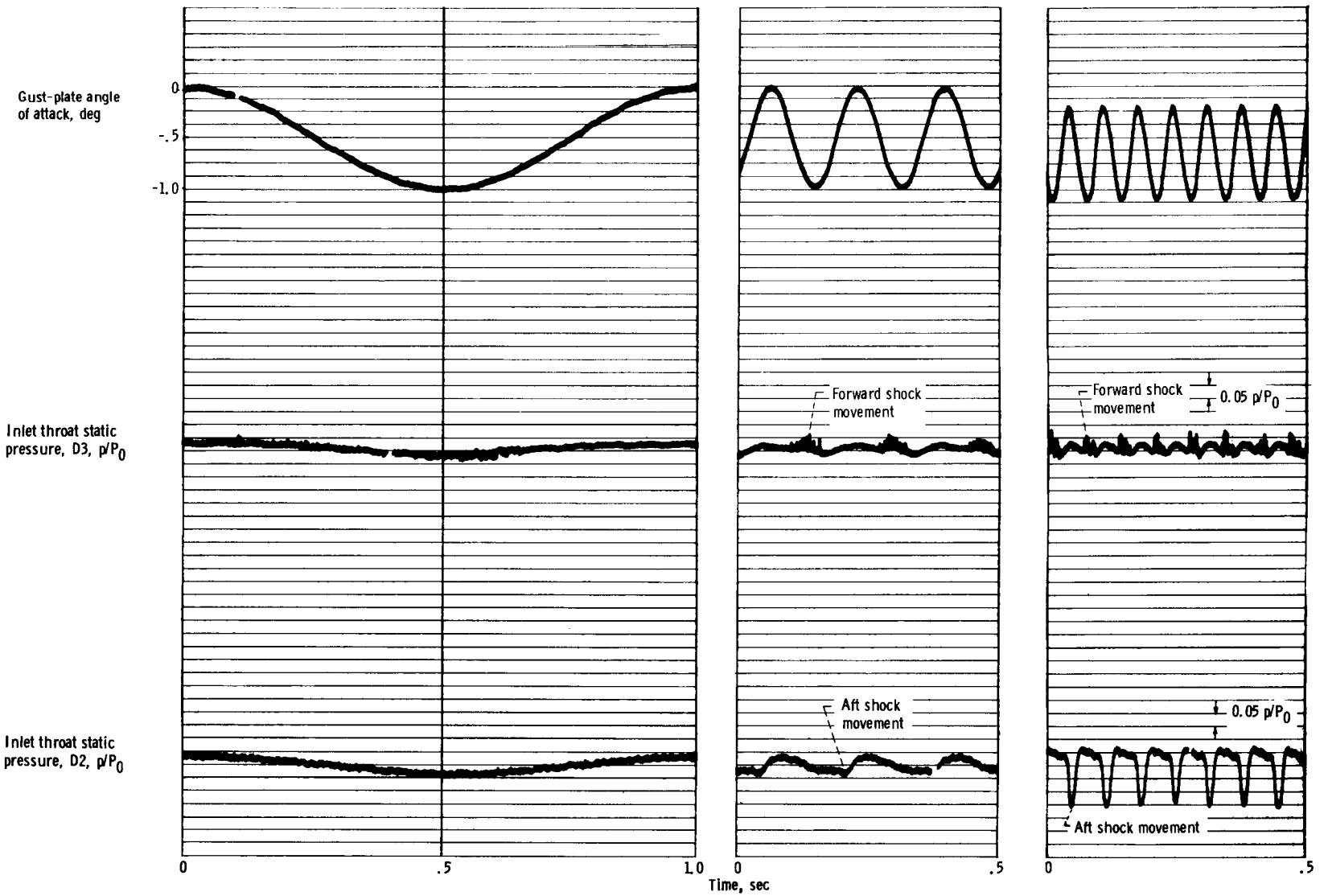

(a) Gust-plate oscillation frequency, 1 hertz.

(b) Gust-plate oscillation frequency, 6 hertz.

(c) Gust-plate oscillation frequency, 15 hertz.

Figure 46. - Dynamic response of inlet throat pressures to external disturbance. Inlet with coldpipe; distributed porous configuration I as the stability-bypass entrance configuration; initial stability-bypass airflow, $m_{sb}/m_0 \approx 0.02$, change in gust-plate angle of attack, 0^0 to -1^0.

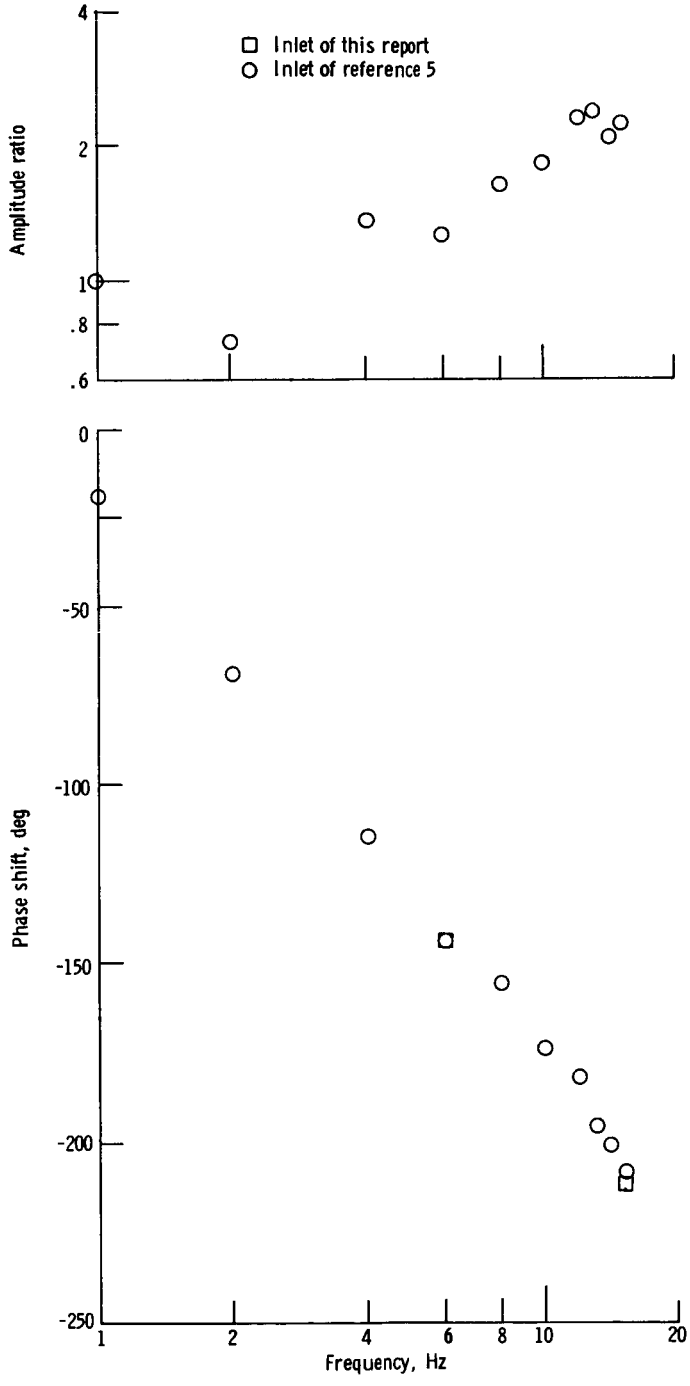

Figure 47. - Dynamic response of terminal shock position to external disturbance. Inlet with coldpipe; distributed porous configuration I as the stability-bypass entrance configuration; initial stability-bypass airflow, $m_{sb}/m_0 \approx 0.02$; change in gust-plate angle of attack, 0^0 to -1^0.

☆ U.S. GOVERNMENT PRINTING OFFICE: 1974—739-160/129